Sponsored by the Department of Science & Technology and GIZ

german cooperation
DEUTSCHE ZUSAMMENARBEIT

This journal is accredited by the South African Department of Higher Education and Training for university subsidy purposes. It is abstracted and indexed in Environment Abstract, Index to South African Periodicals, and the Nexus Database System.

The journal has also been selected into the Science Citation Index Expanded by Thomson Reuters, and coverage begins from Volume 19 No 1. It is also on the Scientific Electronic Library Online (SciELO) SA platform and is managed by the Academy of Science of South Africa (ASSAf).

Annual subscriptions (four issues)
Individuals (Africa): R160 (single copy R51)
Individuals (beyond Africa): US$109 (single copy US$39)
Corporate (Africa): R321 (single copy R103)
Corporate (beyond Africa): US$218 (single copy US$77)

Cost includes VAT and airmail postage.
Cheques should be made payable to the University of Cape Town and sent to the address given below.

Enquiries may be directed to:
The Editor, Journal of Energy in Southern Africa,
Energy Research Centre, University of Cape Town,
Private Bag, Rondebosch 7701, South Africa
Tel: +27 (021) 650 3894 Fax: +27 (021) 650 2830
E-mail: Richard.Drummond@uct.ac.za

Website: www.erc.uct.ac.za

It is the policy of the Journal to publish papers covering the technical, economic, policy, environmental and social aspects of energy research and development carried out in, or relevant to, Southern Africa. Only previously unpublished work will be accepted; conference papers delivered but not published elsewhere are also welcomed. Short comments, not exceeding 500 words, on articles appearing in the Journal are invited. Relevant items of general interest, news, statistics, technical notes, reviews and research results will also be included, as will announcements of recent publications, reviews, conferences, seminars and meetings.

Those wishing to submit contributions should refer to the guidelines given on the inside back cover.

JOURNAL OF ENERGY IN SOUTHERN AFRICA

Volume 24 Number 4 • November 2013

CONTENTS

A cost-benefit analysis of concentrator photovoltaic technology use in South Africa: A case study

Mario du Preez

Justin Beukes
Department of Economics, Nelson Mandela Metropolitan University

Ernest van Dyk
Department of Physics, Nelson Mandela Metropolitan University

Abstract
The South African Government currently faces the dual problems of climate change mitigation and the rollout of electricity provision to rural, previously disadvantaged communities. This paper investigates the economic efficiency of the implementation of concentrator photovoltaic (CPV) technology in the Tyefu area in the Eastern Cape, South Africa, as a means of addressing these problems. Two cost-benefit analyses (CBA) are carried out in the study, namely a private CBA and a social CBA. The private CBA investigates the desirability of the CPV project from a private energy investor's perspective, whilst the social CBA investigates the desirability of the CPV project from society's perspective. The social CBA found that the project was socially viable and was, thus, an efficient allocation of government resources. The private CBA, on the other hand, found that investing in a CPV project was not financially viable for a private investor. With respect to the incentive scheme currently offered to private energy investors, it is recommended that the maximum bidding price of R2.85/kWh be increased. A sensitivity analysis of the bidding price showed that an increase of 300% is required to attract private investors into electricity generation projects.

Keywords: Cost-benefit analysis, concentrator photovoltaic technology, social discount rate

1. Introduction

South Africa relies heavily on fossil fuels, particularly coal, to generate electricity (Department of Minerals and Energy, 2003). The use of fossil fuels, however, contributes to climate change, as it produces greenhouse gases (GHGs). Internationally, South Africa is the 31th highest emitter of CO_2 emissions with 9.2 metric tons per capita, whereas it is ranked 20th highest emitter of CO_2 emissions with 1.59 metric tons per GDP (World Bank, 2010). Coupled with the environmental consequences of fossil fuel use, South Africa has a further responsibility of addressing the inherited backlog of electricity provision to the mostly rural, previously disadvantaged communities. In an attempt to address these two problems, the government issued the White Paper on Renewable Energy. In this paper, renewable energy alternatives are proposed to replace a portion of traditional electricity generating methods.

Concentrator photovoltaic (CPV) energy generation is one such renewable option available to government. CPV is a form of active[1] solar-based renewable technologies that absorb energy from the sun into solar PV panels consisting of cells. The sunlight entering the cell is concentrated[2] through the use of mirrors or lenses that focus or concentrate sunlight onto PV material. The concentration of sunlight increases the intensity of the light, which allows the generation of more electricity. Owing to the light being concentrated, the cells in CPV use less semiconductor material, which makes them more efficient in comparison to conventional photovoltaic (PV) cells. The optical elements (such as lenses) multiply the sunlight intensity by factors that range from 2 (low concentration) to more than 1000 (high concentration). Figure 1 depicts the principle arrangement of a CPV concentrator.

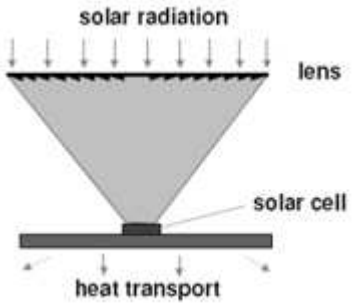

Figure 1: Principle arrangement of a CPV concentrator

Sunlight is concentrated by optical devices like lenses or mirrors thereby reducing the area of expensive solar cells and increasing their efficiency (PV Technology Research Advisory Council, 2007). The motive for applying this technology is to generate maximum electrical power with the minimum solar cell area, which in turn significantly lower the costs of photovoltaic generation (Daido, 2011a).

Both conventional PV and CPV systems can be used for grid-connected electricity generation and off-grid (stand-alone) generation. The latter is the most common application and where both photovoltaic technologies gain their advantage (Winkler, 2005). The useful life of a PV cell is a function of manufacturing methods and quality of the material used. Applications based on silicon material are often given a manufacturer's warranty of 25 years or more, although the expected useful life is much longer. CPV requires that the sun's orbit be tracked by moving the system accordingly, which also allows for a longer exposure time of the cells during the day (PV Technology Research Advisory Council, 2006).

CPV is a technology that operates well in regions with high solar radiation, utilising direct normal irradiance. As such, South Africa is particularly well suited for this technology, with average solar radiation levels ranging from 4.5 to 6.5kWh/m^2. CPV is also well suited for off-grid application, which addresses electricity demand in remote rural areas.

There is, however, a paucity of published studies that establish the economic rationale for the use of solar energy in South Africa. This study aims to fill this gap. To the authors' knowledge, this is the first formal attempt in South Africa to establish the economic efficiency of the use of CPV. The approach employed to achieve this aim is the cost benefit analysis (CBA) method. Two types of CBA are performed, namely a private CBA and a social CBA. The private CBA evaluates the CPV project from a private investor's perspective and the social CBA evaluates the CPV project from society's point of view. In terms of the social CBA, the current means of providing electricity can be viewed as the 'without scenario', while the CPV project is the 'with scenario'. The net benefit arising from the CPV project will simply be the difference between the 'with' and 'without' scenarios. In order to estimate the net benefit, an attempt is made to identify and estimate (where possible) the social benefits and social costs that will occur upon project execution. With respect to the private CBA, the private benefits of the CPV project are simply compared to the private costs.

The study area chosen for the implementation of the CPV project is the Tyefu rural[3] settlement located in the Eastern Cape, South Africa. The settlement is called Tyefu and consists of five villages, namely Ndlambe, Ndwayana, Glenmore, Pikoli and Kalikeni (Monde-Gweleta, van Averbeke, Ainslie, Ntshona, Fraser and Belete 1997). Tyefu falls under the Ngqushwa Local Municipality, which in turn falls under the jurisdiction of the Amathole District Municipality, Eastern Cape Province (Ngqushwa Local Municipality, 2011). The local communities in Tyefu are poor - the majority of households (66.8%) in the region earn less than R1500 per month (Ngqushwa Local Municipality, 2011). Most households depend on pensions and social grants as their main source of income. Tyefu was deemed ideal to serve as a case study due to four characteristics. First, Tyefu is a remote rural settlement at the end of the national grid. Second, the community is very poor and previously disadvantaged. Third, many households are without Eskom generated electricity. Last, the study area is located in an area with irradiance levels suitable for CPV. CPV technology requires direct normal irradiance (DNI) from the sun to generate electricity. The Tyefu area experiences annual average DNI levels of 5.27kWh/m^2 which are ideal for CPV systems (National Renewable Energy Laboratory, 2011).

2. The CPV project

The Ngqushwa Municipality identified 84 households in the Tyefu area as not having electricity. These households formed the sample on which the demand for electricity, and thus the CPV project, is based. Traditionally, unelectrified rural, households, such as those found in Tyefu, have obtained their energy from several sources, namely paraffin, candles, liquefied petroleum gas (LPG), dry-cell batteries, car batteries, wood, and diesel and petrol generators (Aitken, 2007). The amount of electricity required to replace some of the traditional energy sources is calculated below and was established by using Aitken's (2007) study results and personal correspondence (Purcell, 2011). Figure 2 provides the basic floor plan of a sample household for which a CPV system can provide electricity.

Figure 2 depicts a household which uses four fluorescent lamps, a television set, a radio and refrigerator. In order to provide an equivalent amount of energy[4] to light four rooms, run a television set, radio and refrigerator for one year, the typ-

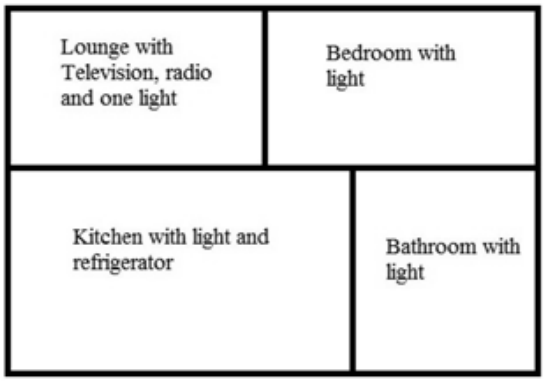

Figure 2: Sample household

ical Tyefu household requires:

- 6.39 litres of paraffin (lighting) at a cost of R639.24 per annum.
- 22 charges for a car battery (TV) at a cost of R333.44 per annum.
- 57 sets (4 batteries per set) of dry cell batteries (radio) at a cost of R902.26 per annum.
- 20.11 kilograms of LPG (fridge) at a cost of R854.77 per annum (Purcell, 2011).

In order to meet the electricity needs of the sample households identified, a CPV system will be installed and operated ('the CPV project') with an electricity generating capacity of 30kWp and an annual output of 30.3MWh per annum. The CPV modules that will be used are mounted on a dual-axis system in order to track the sun's movement. A battery bank will be used to store the energy produced for use at non-generating hours.

Either Eskom or independent power producers (IPPs) could implement the CPV project in the Tyefu area. This would align well with Eskom's attempts to mitigate grid instability issues, by investing in off-grid, distributed generation, co-generation and small-scale renewable projects (Eskom, 2011). If an IPP were to undertake the project, they would engage in the bidding process to supply the electricity generated by the system (Norton Rose, 2011). If the project were to be undertaken by Eskom, it would also be managed by them. On the other hand, if IPPs were to undertake the project, they would outsource management to a services engineering and managing company (Pardell, 2011). The installation of the CPV system could be carried out by a services engineering and management company regardless of whether Eskom or an IPP were to undertake the project. Installation of the 30kWp system would take approximately 2 months. Maintenance of the system could also be performed by a services engineering and management company. Basic maintenance can be performed by trained locals. However, more advanced technical maintenance would have to be undertaken by more highly trained individuals within the management company.

3. Cost benefit analysis

Cost benefit analysis (CBA) is a standard technique used to assess the desirability of an investment project (Watkins, 2010). More specifically, the costs and benefits of a project are determined and compared. The measured costs and benefits are weighed up against each other to establish criteria for decision-making. Normally, one or more of the following three decision-making criteria are used, namely the net present value (NPV), the internal rate of return (IRR) and the discounted benefit cost ratio (BCR) (Hanley and Spash, 1993). The NPV determines whether the sum of discounted benefits (B) exceeds the sum of discounted costs (C). The NPV can be formally expressed as follows:

$$NPV = \sum_{t=o}^{n} B_t(1+i)^t - \sum_{t=o}^{n} C_t(1+i)^t \quad (1)$$

where:
NPV = net present value B_t = benefit in year t
C_t = cost in year t
i = the discount rate
n = length of the project

A project is accepted if it generates a positive NPV. The IRR is the rate of interest that will produce a NPV of zero (if this interest rate is used as the discount rate). More formally:

$$\sum_{t=0}^{n} \frac{B_t - C_t}{(1+i)^t} = 0 \quad (2)$$

The IRR decision rule is that the project should proceed if the IRR exceeds the discount rate(i). The BCR is a different way of expressing the NPV (Hanley and Spash, 1993). More formally, the BCR can be expressed as follows:

$$BCR = \frac{\sum_{t=0}^{n} \frac{B_t}{(1+i)^t}}{\sum_{t=0}^{n} \frac{C_t}{(1+i)^t}} \quad (3)$$

If the BCR exceeds unity, then the project may proceed (Hanley and Spash, 1993).

There are four standard elements to CBA: time considerations, costs, benefits, and the discount rate. All of these are discussed below for the private CBA and the social CBA, respectively.

3.1 Private CBA

The private CBA employs costs and benefits valued at market prices (i.e. purely financial flows), and omit any potential effects the project may have on society.

3.1.1 Time considerations

All the estimated private cost and private benefit flows used in this analysis are captured in per annum periods and expressed at 2010 price levels.

Table 1: Derivation of the system cost

Cost component	*Euro/Wp (a)*	*Rand/Euro (b)*	*Rand/Wp (c) = (a) x (b)*	*System size (Wp) (d)*	*Local cost (R) (e) = (c) x (d)*
System	0.88	9.71	8.58	30 000	257 305.54

The project period or time horizon of the project was set at 25 years.

3.1.2 The private costs of the CPV project

Investment costs

The investment cost comprises initial capital costs on the system (500 times concentration CPV modules, trackers and inverters), the regulator, initial battery bank, transportation (foreign and local), installation and training. Of all the capital equipment, only the system is imported– the regulator and battery bank are acquired locally. The derivation of the system cost is shown in Table 1.

Local transport consists of a fee of R8 950 per container (one container is used) and a fuel surcharge of 5.3 percent. Insurance and freight cost for the private analysis includes customs duties (R80 306.85) and customs VAT (R93 691.36) among other charges imposed by both local and foreign ports (Emery, 2011). In addition to these costs, costs are also incurred for the installation of the system and the training of maintenance staff. Table 2 below gives the breakdown of the investment cost component.

Table 2: Private investment cost derivation
Source: Emery (2011); Pardell (2011)

Cost component	*Private cost (R)*
System	257 305.54
Regulator	40 000
Batteries (96 batteries)	96 000
Insurance and freight	206 915.57
Local transport	9 424.35
Installation	217 675.24
Training	10 000
Total	**837 320.69**

Operating and maintenance costs

Annual operating and maintenance costs consist of expenditures on labour (two unskilled labourers for routine tasks and one skilled labourer to manage the plant and to perform more advanced tasks), materials (spare parts and lubricants) and water (water cost is assumed to be zero since the amount used is considered negligible). In addition to the annual operating and maintenance costs, every four years the cost to replace the battery bank is added to the annual figure. The operating and maintenance costs (with battery cost) are displayed in Table 3.

Table 3: Cost components of operating and maintenance with battery cost
Source: Pardell (2011); Statistics South Africa (2007)

Operating and maintenance component	*Market price (R) per annum*
Skilled labour	80 478.22
Unskilled labour	47 553.60
Spare parts	41 968.18
Batteries	96 000[5]
Total	266 000

Decommissioning costs

Lastly, decommissioning costs (occurring in the final year) comprise of costs to dismantle the CPV plant. This cost equals R14 569.96 (Pardell, 2011).

3.1.3 The private benefits of the CPV project

The private benefits are the revenue earned by the private investor who initiates the project. This revenue is estimated as the product of the volume of electricity output and its unit value. The latter is the upper limit of the submitted price by the private investor during the bidding process (Norton Rose, 2011). The electricity output is expected to be 30 300kWh per year. Using the current upper limit for CPV in the bidding process of R2.85/kWh (Norton Rose, 2011), the expected revenue from the sale of electricity is R86 355 per annum.

Income from recycling the plant's components during decommissioning, and the recycling of the batteries every four years (Table 4), is also included in the private analysis. This amounted to R12 084.60.

Table 4: A breakdown of the income from recycling the CPV plant
Source: Goosen (2011)

Component	*Weight (kg)*	*R/kg*	*Private income (R)*
Glass	810	0.22	178.20
Aluminium	600	10.50	6 300
Steel	2190	2.56	5 606.40
Total			12 084.60

3.1.4 The private discount rate

The private discount rate was estimated as the difference between the prime lending rate and the inflation rate. Table 5 shows the data used for this calculation.

Table 5: Data for the derivation of private discount rate
Source: SARB (2010)

Year	Prime overdraft rate %	Inflation rate %
2006	11.17	3.1
2007	13.17	5
2008	15.13	11.5
2009	11.71	6.4
2010	9.83	2.9

The private discount rate was calculated to be 6.42 percent per annum.

3.2 Social CBA

The costs and benefits used in the private CBA are amended (via shadow pricing) for the purposes of the social CBA to reflect their underlying opportunity costs. Externalities (secondary effects) are identified and classified under the appropriate cost or benefit category.

3.2.1 Time considerations

All estimated social cost and social benefit flows derived in this analysis are captured in per annum periods and expressed at 2010 price levels. A distributional weighting of one was used for all cross-sectional costs and benefits over the full project period. This weighting assumes that a Rand benefit is worth the same to all members of the population affected by the project. The project period for the project was set at 25 years.

3.2.2 The social costs of the CPV project

Investment costs

As mentioned before, of all the capital equipment, only the system is imported. The social cost for the imported system is the sum of its fob price plus the c.i.f. (European Union, 2008). The social cost of the system was calculated to be R290 222.90 (i.e. R257 305.54 + R32 917.36). The social cost of the system is considerably lower than its private cost since taxes (i.e. customs duties and customs VAT amounting to R173 998.21) are excluded from the former.

The market prices of locally acquired capital components (regulator and batteries), local transport, installation, and training were transformed into shadow prices by applying a standard conversion factor of 0.88 as recommended by Mullins et al. (2007). These conversions are shown in Table 6.

The components of the total economic investment cost are shown in Table 7.

Operating and maintenance costs

Of all the operating and maintenance costs identified in section 3.1.2, the following ones require transformation into economic costs: salaries and wages, battery replacement, spare parts and lubricants (as mentioned before, water costs are assumed to be zero). This is carried out by applying the relevant conversion factors as recommended by Mullins *et al.* (2007).

Table 6: Derivation of shadow prices for investment cost components

Cost component[6]	*Market price (R)*	*Conversion factor*	*Economic cost (R)*
Regulator	40 000	0.88	35 087.72
Batteries[7 7]	96 000	0.88	84 210.53
Local transport	9 424.35	0.88	8 266.97
Installation	217 675.24	0.88	190 943.19
Training	10 000	0.88	8 771.93
Total	373 099.59	0.88	327280.34

Table 7: Total economic investment cost

Economic cost component	*R*
System (CIF)	290 222.90
Regulator	35 087.72
Batteries	84 210.53
Local transport	8 266.97
Installation	190 943.19
Training	8 771.93
Total	617 503.24

Table 8: Economic cost derivation of operating and maintenance with battery cost
Source: Pardell (2011); Statistics South Africa (2007). Mullins et al. (2007)

Operating and maintenance component	*Market price (R) p.a.*	*Conversion factor*	*Economic cost (R) p.a.*
One skilled labourer	80 478.22	1	80 478.22
Two unskilled labourers	47 553.60	0.46	21 874.66
Spare parts and lubricants	41 968.18	0.88	36 814.19
Batteries	96 000	0.88	84 210.53
Total	266 000		223 377.60

Decommissioning costs

These costs are the same type of costs as those mentioned for the financial costs. However, a conversion factor of 0.88 is applied to arrive at the economic cost. The economic decommissioning cost amounts to R12 780.67 (R14 569.96 0.88).

Secondary (externality) costs

A secondary cost is that the landscape may be negatively affected, aesthetically and in terms of lost area available for other uses such as agriculture. CPV, however, has a minimal optical impact on the

ground. The ground beneath the CPV panel receives enough sunlight so that it may be used for agricultural purposes. The visual impact on the site location is minimal (Daido, 2011b).

3.2.3 The social benefits of the CPV project

Primary benefits

The social benefits of CPV are based on the 'with or without' principle. Without CPV, the Tyefu community would incur costs in obtaining energy for themselves. With CPV, the community avoids these costs. These avoided costs are the economic benefits of CPV in the study.[8] The savings of recurring energy costs relative to the existing situation for 84 households amounted to R201 137.04 per annum (Purcell, 2011). The disaggregated cost savings are shown in Table 9.

Table 9: Disaggregated cost savings
Source: Purcell (2011)

Component	*Cost per household p.a. (R) (a)*	*No. of households (b)*	*Total (R) (c) = (a) x (b)*
Paraffin	639.24	84	53 696.43
Car battery	333.44	84	28 008.95
Dry cell batteries	902.26	84	75 790.14
LPG	854.77	84	71 800.71
Total	2 729.72		229 296.20

The total cost savings amount was converted into an economic benefit by applying the standard conversion factor (R229 296.20 0.88 = R201 137).

Income from recycling the plant's components during decommissioning, and the recycling of the batteries every four years, is also considered in the social analysis. The economic benefit from recycling the glass, aluminium and steel of the CPV plant is calculated to be R10 600.53 (R156.32 + R5 526.32 + R4917.89). The income from the recycling of batteries every four years is R48 661.05. Table 10 shows the income from recycling.

Secondary benefits

CPV systems do not emit any GHGs during power generation. This benefit is insignificant, given the size of the study area, and is thus not included in the analysis (SolFocus, 2011b).

3.2.4 The social discount rate

The social discount rate used is a composite rate made up of the social opportunity cost of capital (SOCC) and the social time preference rate of consumption (STPR).

The composite social discount rate can be estimated as follows:

$$i = (1 - f)t[(1 - s)(x_1 - p) + (s)(x_2 - p)] + (1 - f)(1 - t)(x_3 - p) + f\,(x_4 - p) \quad (4)$$

where:

- f = proportion of foreign funding of total;
- t = proportion of government expenditure funded through taxes paid;
- $1 - t$ = proportion of government expenditure funded through borrowing;
- s = proportion of people's disposable ncome that is saved;
- $1 - s$ = proportion of disposable income consumed;
- x_1 = average of the predominant overdraft rate on current accounts and the term lending base rate;
- x_2 = average of dividend yield and the capital growth of all listed shares on the Johannesburg Stock Exchange;
- x_3 = average of the government loan stock yield and the Eskom bond rate;
- x_4 = interest rate cost of foreign funding;
- p = consumer price index (inflation) (Du Preez, 2004).

Data was gathered for these mentioned variables for the period 2006 to 2010. Table 11 shows the cost of government borrowing, the cost of household consumption borrowing, the return on savings and the annual inflation rate for the period (2006 to 2010). Table 12 shows the calculation of weights t and $1 - t$ and Table 13 shows the calculation of weights s and $1 - s$.

Using the above equation and the data provided in Tables 11, 12 and 13, the real social discount rate was estimated at 5.97 percent per annum.

Table 10: Income from recycling the CPV plant and batteries

Component	*Weight (kg)*	*R/kg*	*Private income (R)*	*Conversion factor*	*Economic income (R)*
Glass	810	0.22	178.20	0.88	156.32
Aluminium	600	10.50	6 300	0.88	5 526.32
Steel	2190	2.56	5 606.40	0.88	4 917.89
Battery	12 192	4.55	55 473.60	0.88	48 661.05

Table 11: Cost of government borrowing, cost of household consumption borrowing, the return on savings and the annual inflation rate (2006-2010)

Source: SARB (2010)

Cost of government borrowing				*Cost of household consumption borrowing*			*Return on savings*			
Year	*Government stock - yields on loan stock traded on the bond exchange (10 years and over), %, (a)*	*Eskom Bond Yield, %, (b)*	*Average yield, %, $\frac{(a)+(b)}{2}$, X3*	*Predominant overdraft rate on current accounts, (c)*	*Long-term lending base rate (Hire-purchase credit), %, (d)*	*Average rate, %, $\frac{(c)+(d)}{2}$, X1*	*Dividend Yield, (e)*	*Capital growth %, (f)*	*Average rate, %, $\frac{(e)+(f)}{2}$, X2*	*Average annual inflation rate as measured by consumer price index, %*
2006	7.81	8.91	8.36	13.76	11.12	12.44	2.41	35.6	19.01	3.1
2007	8.29	11.48	9.98	14.96	12.78	13,87	2.29	21.5	11.90	5
2008	7.82	11.45	9.64	15.16	14.53	14.85	3.16	-33.4	-15.12	11.5
2009	9.03	9.49	9.26	13.78	11.95	12.86	3.3	24.8	14.05	6.4
2010	8.38	8.99	8.69	10.75	10.18	10.47	2.16	14.4	8.28	2.9

Table 12: The calculation of discount rate weights *t* and *1 – t*

Source: SARB (2010)

Year	*Government borrowing requirement R millions (a)*	*Government revenue R millions (b)*	*Total R millions (c) = (a) + (b)*	*Borrowing proportion (a)/(b) (1 – t)*	*Tax revenue proportion (b)/(c) (t)*
2006	6 868	402 463	409 331	0.017	0.983
2007	-6 049	470 168	464 119	-0.013	1.013
2008	-16 584	547 977	531 393	-0.031	1.031
2009	13 065	595 972	609 037	0.021	0.979
2010	132 233	570 565	702 798	0.188	0.812

Table 13: The calculation of discount rate weights *s* and 1 – *s*

Source: SARB (2010)

Year	*Final consumptionexpenditure R millions (a)*	*Gross savings R millions (b)*	*Gross national disposable income (c) = (a) + (b)*	*Final consumption expenditure proportion (a)/(b) (1 – s)*	*Gross savings proportion (b)/(c) (s)*
2006	1 116 315	254 196	1 370 511	0.815	0.185
2007	1 264 726	287 680	1 552 406	0.815	0.185
2008	1 398 236	350 846	1 749 082	0.799	0.201
2009	1 456 089	372 826	1 828 915	0.796	0.203
2010	1 575 420	438 094	2 013 514	0.782	0.218

4. Summary results of applying the decision-making criteria

4.1 Private CBA

The mentioned costs and benefits along with the private discount rate were used to estimate the NPV, IRR and BCR of the private project. These results are summarised in Table 14.

Table 14: Summary results of private CBA decision criteria

CBA criteria (at private discount rate of 6.42%)		
NPV (R)	*IRR (%)*	*BCR*
-2 046 629.01	Undefined	0.365

The private CBA shows unfavourable results – the NPV is R-2 046 629.01, the IRR is undefined (this is due to no sign change being present in the cost benefit profile), and BCR is less than unity (0.365).

4.2 Social CBA

The above mentioned costs and benefits along with the social discount rate were used to estimate the NPV, IRR and BCR of the social project. These results are summarised in Table 15.

Table 15: Summary results of social CBA decision criteria

CBA criteria (at social discount rate of 5.97%)		
NPV (R)	*IRR (%)*	*BCR*
125 616.64	*8*	*1.045*

The social CBA yielded positive results, with a NPV of R125 616.64, an IRR of 8 percent (which exceeds the social discount rate of 5.97 %), and a BCR of 1.045.

5. Sensitivity analysis

5.1 Private CBA

A sensitivity analysis is applied to the private CBA to test the results found by altering the discount rate and the bidding price.

5.1.1 The private discount rate

The derived private discount rate of 6.42 percent was revised upwards and downwards by 2 percent and 4 percent. The results are shown in Table 16.

Table 16: Sensitivity analysis – discount rate

CBA decision-making criteria		
Discount rate (%)	NPV (R)	BCR
2.42 (-4%)	- 2 640 006.58	0.423
4.42(-2%)	- 2 297 030.96	0.404
6.42	-2 046 629.01	0.365
8.42(+2%)	- 1 860 022.39	0.369
10.42(+4%)	- 1 718 182.17	0.353

The changes in the discount rate do not significantly change the decision-making criteria. All results remain negative.

5.1.2 The bidding price

The revenue earned by the Tyefu electrification project is dependent on the bidding price given during the tender process. A sensitivity analysis was conducted by varying the upper limit of the bidding price, namely R2.85/kWh (Norton Rose, 2011). The price was increased by 200 percent, 250 percent, and 300 percent. The results of the sensitivity analyses are shown in Table 17.

All three decision criteria become favourable when the bidding price is increased by 300 percent (R8.55/kWh).

5.2 Social CBA

A sensitivity analysis is applied to the social CBA to test the results by altering the discount rate.

The derived social discount rate of 5.97 percent was revised upwards and downwards by 2 percent and 4 percent, respectively. The results are shown in Table 18.

Table 18: Sensitivity analysis – discount rate

CBA decision-making criteria[9]		
Discount rate	*NPV (R)*	*BCR*
1.97 (-4%)	482 910.19	1.092
3.97% (-2%)	276 209.70	1.061
5.97%	125 616.64	1.045
7.97% (+2%)	13 618.10	0.993
9.97% (+4%)	-71 349.59	0.958

In terms of the NPV, the project becomes socially undesirable for an upward revision of 4 percent in the social discount rate.

Table 17: Sensitivity analysis – bidding price change

		CBA decision-making criteria		
Bidding price (per kWh)	*Revenue (pa) (R)*	*NPV (R)*	*IRR(%)*	*BCR*
R5.70 (200%)	172710	-913 476.78	Undefined	0.726
R7.13 (250%)	215887.5	-346 900.66	1%	0.896
R8.55 (300%)	259065	219 675.45	9%	1.066

6. Conclusion and recommendations

The purpose of this study was to evaluate the economic feasibility of a concentrator photovoltaic project in a non-electrified, rural, previously disadvantaged community. The study area chosen for the case study was a settlement, named Tyefu, consisting of five villages in the Eastern Cape province of South Africa. Two cost benefit analyses (CBAs) were carried out: a private CBA to investigate the project's feasibility from a private energy investor's point of view, and a social CBA to investigate the project's desirability from society's perspective.

The main results were favourable in terms of the social CBA, but unfavourable for the private CBA. More specifically, the social CBA yielded a NPV of R125 616.64, an IRR of 8 percent (which exceeds the social discount rate of 5.97%) and a BCR of 1.045, whereas the private CBA yielded a NPV of R-2 046 629.01 and a BCR of 0.365 (the IRR could not be calculated as there was no sign change in the cost benefit profile – all net benefits were negative).

It can thus be deduced that CPV rollout appears to be economically efficient on a small scale according to the social CBA, but not according to the private CBA. The benefit (income received per kWh) in the private CBA is too small to outweigh the costs of implementing and running a CPV plant in Tyefu. Currently the maximum revenue investors can earn from CPV is R2.85/kWh (Norton Rose, 2011). For a small plant of Tyefu's size, this amount is not high enough to attract private energy investors into undertaking a project of this kind. A sensitivity analysis showed that the current upper limit must be increased by up to 300% to make a project of this magnitude financially viable.

Notes

1. Passive solar energy refers to the design of buildings for harnessing the sun's energy.
2. Conventional solar PV systems make use of non-concentrated sunlight.
3. An anonymous referee made the valid point that normal PV prices have fallen since 2010. Therefore small scale CPV which is more maintenance intensive, may be difficult to justify in remote rural areas.
4. These costs were calculated using an energy conversion table where the useful energy is determined per traditional fuel (Purcell, 2011).
5. The battery cost is only incurred every four years.
6. All cost components relate to a system size of 30 000 Wp.
7. 96 batteries are required for electricity storage.
8. An anonymous referee made the valid point that if electricity was generated for income generation (productive use), then both the social and private perspectives would change in a positive direction.
9. The IRR is not reported here, as a change in the discount rate does not affect it. The IRR is independent of the discount rate, and remains at 8%.

Acknowledgements

The authors wish to thank two anonymous referees for their valuable comments as well as an anonymous referee from the ERSA for additional comments and recommendations.

References

Aitken, R. (2007). Household Energy Use: A Comparison of Household Energy Consumption and Expenditure across Three Provinces. *Journal of Energy in Southern Africa*, 18(1): 20-28.

Daido. (2011a). *What is CPV and Why It is Important?* Online. http://www.daido.co.jp/en/products/cpv/whats.html. (Accessed 16 March 2011).

Daido. (2011b). *Double Use of Land*. Online. http://www.daido.co.jp/en/products/cpv/space.html. (Accessed 21 May 2011).

Department of Minerals and Energy. (2003). *White Paper on Renewable Energy*. Online. http://www.info.gov.za/view/DownloadFileAction?id=68765. (Accessed 14 October 2009).

Du Preez, M. (2004). The Discount Rate for Public Sector Conservation Projects in South Africa. *African Development Review.* 16: 456-471.

Emery, J. (2011). Personal Correspondence. DB Shenker. Port Elizabeth.

Eskom. (2011). *Guide to Independent Power Producer (IPP) Processes*. Online. http://www.eskom.co.za/live/content.php?Item_ID=14324. (Accessed 19 May 2011).

Goosen, J. (2011). Personal Correspondence. RECLAM. Port Elizabeth.

Hanley, N. and Spash, C.L. (1993). *Cost-Benefit Analysis and the Environment*. Vermont: Edward Elgar.

Monde-Gweleta, N.N., van Averbeke, W., Ainslie, A., Ntshona, Z.M., Fraser, G.C.G., and Belete, A. (1997). Agriculture and Rural Livelihood in North-West Peddie district. *Agrekom*.36: 616-625.

Mullins, D., Mosaka, D.D., Green, A.B., Downing, R. and Mapekula, P.G. (2007). *A Manual for Cost Benefit Analysis in South Africa with Specific Reference to Water Resource Development*. Water Research Commission, Report No. TT 305.07. 2nd ed. South Africa: Conningarth Economists.

National Renewable Energy Laboratory. (2011). *Climatological Solar Radiation (CSR) Model.* Online. http://www.nrel.gov/gis/solar_map_development.html. (Accessed 29 January 2010).

Ngqushwa Local Municipality. (2011). *Integrated Development Plan (IDP)*. Online. http://www.ngqushwamun.gov.za/INTEGRATED-FEVELOPMENT-PLAN. (Accessed 20 June 2011).

Norton Rose, (2011). *South Africa Renewable Energy IPP Request for Proposals*. Online: http://www.nortonrose.com/knowledge/publications/54959/south-africa-renewable-energy-ipp-request-for-pro-

posals. (Accessed 15 August 2011).
Pardell, R. (2011). Personal Correspondence. Valldoreix Greenpower. Valldoreix, Spain.
Purcell, C. (2011). Personal Correspondence. Energy and Development Group (EDG). Port Elizabeth.
PV Technology Research Advisory Council. (2006). *A Strategic Research Agenda for Photovoltaic Solar Energy Conversion Technology.* Online. http://www.eurec.be/en/. (Accessed 29 January 2010).
PV Technology Research Advisory Council. (2007). *A Strategic Research Agenda for Photovoltaic Solar Energy Conversion Technology.* Online. http://www.eurec.be/en/. (Accessed 29 January 2010).
South African Reserve Bank. (2010). Official Website. Online. http://www.reservebank.co.za. (Accessed 4 March 2010).
SolFocus. 2011b. *Sustainability*. Online. http://www.solfocus.com/en/sustainability/. (Accessed 22 March 2011).
Statistics South Africa. (2007). *Labour Force Survey*. Online: http://www.statssa.gov.za/publications/P0210/P0210March2007.pdf. (Accessed 23 January 2011).
The World Bank (2010). Database. http://data.worldbank.org/indicator/EN.ATM.CO2E.PC?order=wbapi_data_value_2010+wbapi_data_value+wbapi_data_value-last&sort=desc. (Accessed 31 October 2013).
Watkins, T. (2010). *An Introduction to Cost Benefit Analysis*. Online. http://www.sjsu.edu/faculty/watkins/cba.htm. (Accessed 22 April 2010).
Winkler, H. (2005). Renewable Energy Policy in South Africa: Policy Options for Renewable Electricity. *Energy Policy*. 33: 27-38.

Received 3 July 2012; revised 4 November 2013

A possible design and justification for a biogas plant at Nyazura Adventist High School, Rusape, Zimbabwe

Patrick Mukumba
Physics Department, University of Fort Hare, South Africa

Golden Makaka
Physics Department, University of Fort Hare, South Africa

Sampson Mamphweli
Institute of Technology, University of Fort Hare, South Africa

Sherpherd Misi
Department of Civil Engineering, Faculty of Engineering, University of Zimbabwe, Zimbabwe

Abstract
The research study was carried out to assess the biogas potential at Nyazura Adventist High School, Rusape, Zimbabwe, a co-educational school with a total enrolment of 700 boarders. The school is connected to the national grid electricity. The electricity is in short supply due to long hours of load shedding. Firewood to be used for heating and cooking purposes is in short supply. The main objective of the study was to make an assessment of biogas potential at the school. The energy demand for the whole school was calculated and it was found to be 2 710 kWh per day. The biogas yields for the feedstocks at the school were estimated. The total biogas yield that could be obtained from the feedstocks was 50 m3 per day. The digesters volume for the feedstocks was estimated and the material requirements for the digesters were also determined. The techno-economic analysis of the proposed project was done. The results suggested that the proposed project was feasible, and it was concluded that the school is capable of producing enough biogas from its feedstocks to support a feasible project. The daily 50 m3 biogas yield is adequate to supply enough electricity for lighting purposes during the load shedding periods.

Keywords: biogas potential, techno-economic analysis, biogas digesters

1. Introduction

Biogas refers to a gas produced by anaerobic fermentation of organic matter in the absence of oxygen in airtight containers called biogas digesters (Walekwa et al., 2009; Sibisi and Green, 2005). The composition of biogas varies depending on the raw materials, the organic load applied, the retention period and temperature. The gas consists mainly of methane, which is generally between 55%-80% (Jemmett, 2006). Biogas contains about 9 kWh/m3 of available energy (Thouars, 2006).

Biogas is about 20% lighter than air and has an ignition temperature in the range of 650-750 °C (Deublein & Steinhauser, 2008). It is an odourless and colourless gas that burns with a blue flame similar to that of liquid petroleum gas (Sathianathan, 1975).The biogas anaerobic process is divided into four steps as follows: hydrolysis, fermentation (acidogenesis), anaerobic oxidation (acetogenesis) and methanization (Davidsson, 2007; Goswami & Kreith, 2008; Leksell, 2005). Figure 1 shows the degradation pathways to produce methane.

Biogas technology can be viewed as a vehicle to reduce rural poverty and leads to rural development. Biogas can be an energy substitute for animal waste, fire wood, agricultural residues, diesel, paraffin, petrol and electricity. In addition, eutrophication and air pollution are minimized (Lantz *et al.*, 2007). Furthermore, it eliminates the daily task of fire wood gathering (Mwakaje, 2007). Biogas can be regarded as an eco-friendly fuel and can be used as a substitute for compressed natural gas.

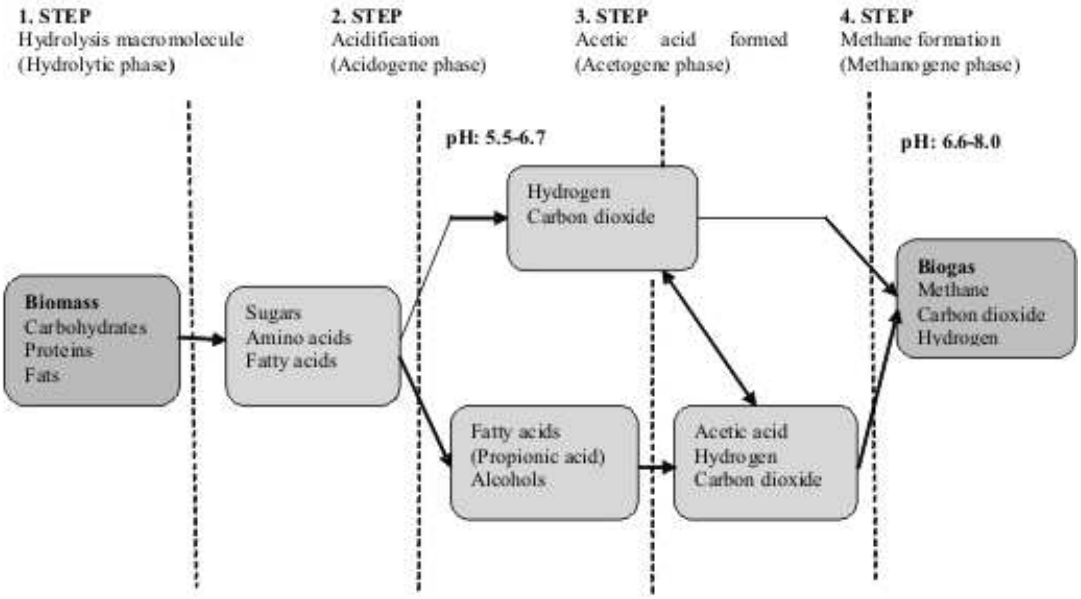

Figure 1: Four steps of anaerobic digestion (Gerardi, 2003)

Zimbabwe is endowed with plenty of anaerobic digestion feedstocks but the technology is not optimally applied in the conversion of these feedstocks (Jingura & Matengaifa, 2009). Zimbabwe is heavily dependent on fossil fuel imported from the Middle East. To worsen the situation, the country has a shortage of foreign currency for importing fossil fuel.

There are a number of biogas digesters producing biogas in Zimbabwe, at Glen View Firle and Crowborough sewage treatment works in Harare. However, the biogas from the primary biogas digesters is carried to biogas tanks and burnt in air without being utilised (Mukumba, 2007). The biogas digesters were installed at these activated sewage treatment plants as a way to treat sewage but not to produce biogas for utilisation. These digesters are producing biogas that has enough energy to drive several other industrial operations that require large amounts of power. There are some biogas digesters that were installed in Chishawasha, Harare and Kushinga Agricultural College. However, these digesters are not operational due to lack of knowledge for operating these digesters.

The main objective of this paper is to assess daily biogas potential for Nyazura Adventist High School and use the information to design the biogas digesters for the mission high school.

2. Description of the study area

The study was carried out at Nyazura Adventist High School. The school is 1200 m above sea level and was established in 1910. It is located closer to the Harare-Mutare highway and is 33 kilometres from Rusape town and 63 kilometres from the city of Mutare. It is a co-educational boarding school with a total enrolment of 700 students.

The school is located at the foot of Mount Matukashiri. The school area is covered with stable rocks. These rocks are granitic in nature. The area is free from earthquakes and earth tremors due to good rock stability and therefore, building a biogas digester is advantageous to the school since rock stability prevents cracking of digesters thereby preventing gas leakages through the digester walls. In addition, the school area has sandy soils that are suitable for growing of crops such as tobacco. Figure 2 shows Nyazura Adventist High School.

2.1 The school's energy requirements

The boarding school is connected to the national power utility grid. However, like most other consumers in Zimbabwe, it suffers from electricity supply interruptions due to recurring load shedding. To relieve the situation, a 60kVA diesel generator was installed to supply electricity during load shedding. However, the rising costs make it impractical to run the generator for long hours as operating costs become very high and unaffordable. The other two generators (100 kVA and 80 kVA) donated by the Reserve Bank are not in use. The water for the school comes from a nearby school dam. Before the water is harnessed, high-powered centrifugal pumps first pump it into reservoirs. These pumps are powered with electricity. The school bus, a Mazda T35 truck, tractors, generator set and diesel pumps use diesel as fuel.

Eutrophication is a process in which bodies of water such as lakes, ponds, and rivers receive excess nutrients for example nitrogen and phosphorous that stimulates excessive growth of algae.

Firewood is now a popular fuel at the school because grid electricity is no longer reliable. The

firewood is used for cooking and heating purposes especially during load shedding periods that can last up to 15 hours. This paper seeks to assess biogas potential at the school so as to minimise energy problems at the school by using biogas as an alternative fuel for mainly lighting the whole school. The study came as result of current energy related problems the school is facing such as shortage of water due to long hours of load shedding and shortage of firewood. To worsen the situation, the copper cables supplying the electricity to the school are often vandalised. The most recent vandalisation of copper cables was in November, 2011. This adversely affected students' reading hours especially Upper Sixth and Form Four students. Due to the current price of diesel, the generator set is operated only for few hours a day.

However, the school has plenty of biogas substrates, namely, cow dung, human excreta and vegetable wastes. The importance of the waste materials in meeting the needs of the school is not being realised. These substrates when fed into the digester produce biogas and the digester sludge is ploughed back into the fields thereby improving soil fertility. The biogas from this waste material can be used by the school as a source of cheap energy.

3. Methodology

3.1. Biogas feedstocks

The study examined the total gas yield of the following feedstocks at the school; human excreta, cow dung, and chicken manure. This involved physical counting of learners, teaching and non-teaching staff, chicken and cattle at the school. Total biogas for all the feedstocks was then estimated.

3.2. Energy requirements

Premises at Nyazura High School that consume electricity were identified and these were: the school library, school church, administration block, computer laboratory, classrooms, boys' dormitories, girls' dormitories, dining halls, workshop and tuckshop, staff houses, pumps (7.5 hp and 10 hp), and the home economics department. Table 1 is an example of how total energy demand for dining halls was obtained.

3.3. Biogas digester sizing

The volumes of the digesters were calculated from the following equations (Shonhiwa, 2005):

$$V_d = S_d \times R_t \quad (1)$$

where:
V_d = volume of the digester in cubic meters
S_d = amount of substrate in kilograms
R_t = retention time in days

Therefore,

$$V_d = (B + W)R_t \quad (2)$$

where:
B = Biomass (kg)
W = Water (litres)

Biogas production was calculated using equation 3.

$$G = V_s \times G_y \quad (3)$$

where:
V_s = weight of feedstock available per day in kilograms
G_y = Gas yield in cubic meters
G = biogas production in cubic meters

Gas production rate was calculated using equation 4.

Table 1: Energy requirements for dining halls

Load (Devices)	*Number of each device*	*Power rating [W]*	*Power rating [kW]*	*Operating tim e [h]*	*Total energy [kWh/ day]*
Dining hall (F1-4)	24	40	0.040	4	4
Dining hall (F1-4)	3	60	0.060	4	1
'A' Level dining hall					
14	40	0.040	4	2	
'A' Level dining hall	14				
	60	0.060	4	2	
Cookers	6	2 000	2	12	
	144				
Refrigerator	1	41 500	41.5	24	
	996				
Oven	1	25 000	25	12	
	300				
Total					1449

$$G_p = G/V_d \quad (4)$$

where:
G_P = gas production rate in cubic metres per day
G = biogas production in cubic metres
V_d = digester volume in cubic meters

Recalling equation (3), equation (4) can be written as:

$$G_p = G\,V_d = V_S G_Y \quad (5)$$

Figure 2 shows the fixed dome digester design for the cow dung, chicken manure and human excreta. Fixed dome plants were chosen because they can last for over fifty years and they are easily insulated and scum formation is less due to the digester slurry that is displaced (pushed out) by incoming feed (influent). A fixed dome digester is an underground biogas digester lined with brick, with a dome-shaped cover made from concrete. The cover is fixed and held in place with earth piled over the top to resist the pressure of the gas inside. A second pit, the slurry reservoir, is built above and to the side of the digester. As the gas is given off by slurry, it collects in the dome and displaces some of the slurry into the reservoir. As the gas is used, the slurry flows back into the digester to replace it.

The digester presented in Figure 2 would be modified to include a heating system for optimum biogas production. Figure 3 shows the heating system proposed. The heating system would involve

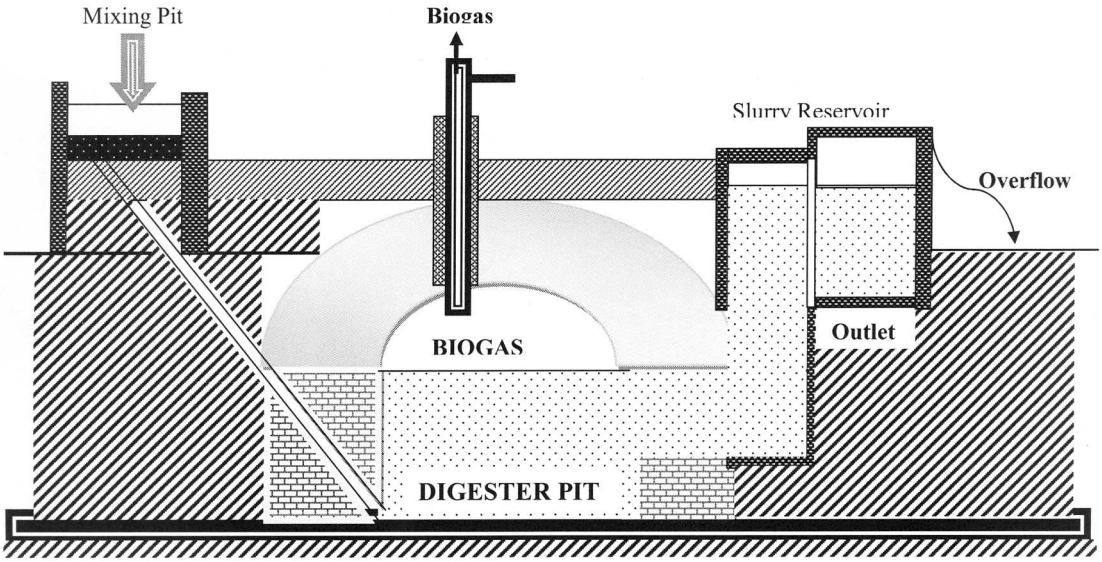

Figure 2: Fixed dome digester for the substrates
(Adapted from Fulford, 2001)

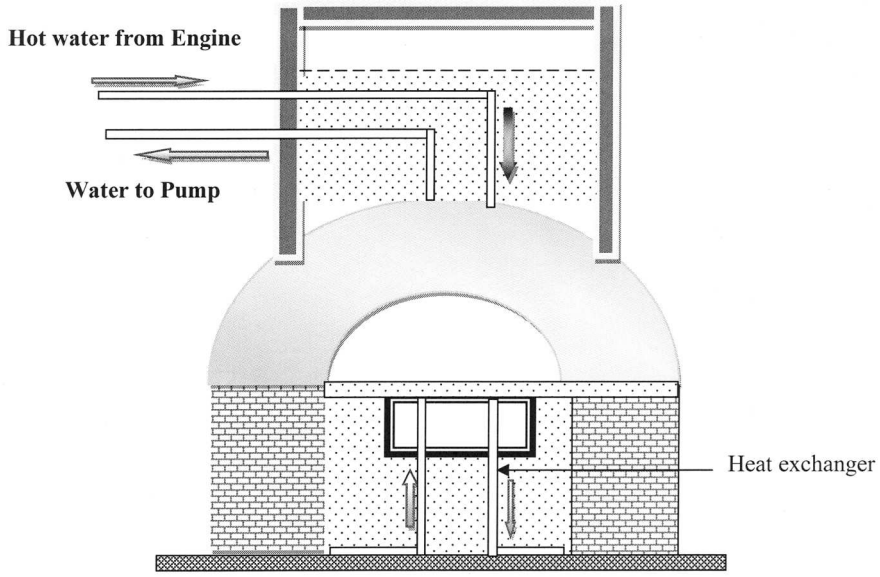

Figure 3: Biogas digester with heat exchanger (own design)

the use of the engine cooling water, which would be at 65°C. This water would be transported from the engine to the digester by means of copper tubes. The tubes would be placed at the bottom of the digester. The heat would flow from the tubes to the slurry thereby maintaining desirable temperature for maximum biogas production.

3.4. Material requirements for the digester

The material requirements for the biogas digester construction were estimated, such as cement, steel, wire mesh, paint, aggregate, sand, bricks and labour costs.

3.5. Economic analysis methods

The techno-economic analysis for the project was used to evaluate the favourability and profitability of the biogas investment project. The economic indicators considered were the investment costs, the liquidation yield, the total operational costs, total income and revenues, cost comparison, cost annuity comparison, profitability, static Pay Back Period (PBP), Net Present Value (NPV) and Internal Rate of Return (IRR).

3.5.1. Procedure for financial evaluation

The procedure for financial evaluation is determined by Finck and Oelert (1985).

3.5.1.1. Cost annuity comparison, A_k

Cost annuity is the annual total cost of the biogas digester

$$A_K = K_0 + (1_0 - L) \times R_F(i,t) + L \times i) \quad (6)$$

where:
A_K = cost annuity (US $)
K_0 = the operating costs per unit of time (US $)
I_0 = investment costs (US $)
L = liquidation yield (years)
R_F = recovery period (years) and is a function of assumed interest rate and the project duration
i = assumed interest rate (%)
t = the project duration (years)

3.5.1.2. Profitability

Profitability or return on investment (ROI) is the average profit per time interval on an investment project or the profit of the plant per annum.

$$ROI = \frac{N_p}{K_A} \times 100 \quad (7)$$

where:
ROI = return on investment [US $]
N_P = average net profit per time interval
K_A = average capital invested

3.5.1.3. Pay-back period

Pay-back period is the time at which the capital invested in an investment project will be recovered by the annual returns.

$$n = \frac{\text{capital investment}}{\text{annual return}} \quad (8)$$

where:
n = payback period (years)

3.5.1.4. Net present value

Net present value (NPV) of an investment project is the sum of the present values of all the cash inflows and outflows linked to the investment.

$$NPV = -I_0 = (R \times PF) + L_T \times q^{-T} \quad (9)$$

where:
NPV = Net present balue (US $)
I_0 = investment costs (US $)
PF = present value factor (years)
R = annual returns (US $)
L_T = liquidation yield at the end of service life (years)
q^{-T} = discount factor (years)

3.5.1.5. Internal rate of return

Internal rate of return of an investment project is the achievable interest tied-up in the investment.

$$IRR = i_1 - NPV_1\left(\frac{i_2 - i_2}{NPV_2 - NPV_1}\right) \quad (10)$$

where:
IRR = Internal rate of return
NPV_1 = Net present value 1
NPV_2 = Net present value 2
i_1 and i_2 are discount rates

3.5.1.6. Annuity method

The annuity is the constant annual payment for an investment.

$$A = NP \times RF\ (iT) \quad (11)$$

where:
A = annuity
T = a known planning period in years
i = discount rate

3.5.1.7. Present value factor

$$PF = \frac{q^t - 1}{q^t\,(q - 1)} \quad (12)$$

$$q = 1 + \frac{i^*}{100} \quad (13)$$

where:
i* = market interest rate
t = time of payment (years)

$$i = \left(\frac{1 + i^*}{1 + f} \right) - 1 \quad (14)$$

where:
f = inflation rate

Liquidation yield is the estimated value of a plant at the end of its useful life or fixed service life.

Recovery period is the designated period for depreciation of a plant.

An annual return (R) from an investment of a project is the difference between total incomes and operating costs (Finck & Oelert, 1985).

Present value factor (PF) is a factor used to calculate present value of money on a future period.

NPV of an investment project is the sum of present value of money moving into or out of an investment project.

Market interest rate (i*) is the interest rate for external or internal financing (Finck & Oelert, 1985).

3.6. Sizing of the electric generators

For the sizing of the electric generators, the following equation was used:

$$P_{(kW)} = S_{(kVA)} \times Pf \quad (15)$$

Where;
$P_{(kW)}$ = power in kilowatts
S (kVA) = generator size in kVA
Pf = power factor

The power factor (Pf) for each electric biogas generator was assumed to be 0.8 and the average electric efficiency of each biogas generator was assumed to be 40% due to lower heating of biogas. Furthermore, it was assumed that 1 m^3 would produce energy equivalent to 9 kWh.

4. Results and discussions

4.1. Electricity requirements

The total electricity requirements for Nyazura Adventist High School are shown in Table 2.

The highest proportion of energy is consumed by activities in the dining halls. The school has a total energy requirement of 2 751 kWh/ day. The total energy requirements for the two dining halls are 1449 kWh/day. Dining halls are consuming 53% of the electricity supplied to the school because they have the following devices that consume large amounts of electricity; cold room (996 kWh/day), one oven (300 kWh/day) and six cookers (144 kWh/day). The electricity supplied to the boarding school is used mainly for water heating, cooking, lighting, welding and water pumping.

Table 2: Electricity needs for the whole school

Energy demand areas	Total energy (kWh/day)
Computer laboratory	32
Classrooms	39
Administration	14
School library	4
Boys' dormitories	37
Girls' dormitories	33
Dining halls	1449
Workshop and Tuck-shop	93
Pumps (10 Hp and 7.5 Hp)	403
Staff houses	600
School church	7
Home economics department	40
Total	2 751

4.2. Total gas yield per feedstock

The dung produced by cattle per day per animal is 10 kg, and 1 kg dung of cattle produces 0.036 m^3 of biogas (Nijaguna, 2002). Since the cattle are not pastured, it was assumed that collectable waste per day was 5 kg. In addition, 1 kg chicken manure and 1 kg human waste produce 0.062 m^3 and 0.070 m^3 per day respectively. Table 3 shows the estimated gas yield per feedstock available at the school.

It is clear from Table 3 that the total biogas yield for the feedstocks is 50 m^3/day. Human waste had a total gas potential of 27 m^3 /day, chicken manure a total gas yield of 4 m^3/day and cow dung a total gas yield of 18 m^3. Assuming that 1m^3 of gas produces 9 kWh of energy, the 50 m^3 of biogas could produce 450 kWh/day of energy. The school is capable of producing energy of 13 500 kWh from its waste material per month. The installation of the

Table 3: Total estimated gas yield per feedstock

Feedstock Type	Total number of animals	Gas yield m^3/kg	Manure per animal per day (kg)	Gas yield per day (m^3)	Total gas yield per day (m^3)
Cattle dung	100	0.036	5.00	0.18	18
Chicken manure	500	0.062	0.18	0.011	4
Human waste	960 (secondary school learners & families)	0.070	0.40	0.028	27
Human waste	50 [primary school pupils]	0.070	0.10	0.007	1
Total					50

digesters at the school can therefore reduce the energy shortage in the school. The total daily biogas produced at the school would meet 16% of the total energy demand. The quantity of daily biogas production would be increased by increasing the number of cattle and chicken kept at the school. Since the demand for biogas would be low during school holidays, the school would pump excess biogas by means of biogas pumps into the bio-bags for storage.

4.3. Digester volume for each feedstock

Table 4 shows the calculations results of digester volume for cattle dung, chicken manure and human waste. Equations 1 and 2 were used to calculate the digester volume. The mixing ratio of the biomass (cow dung) to water was 1: 1 and the retention time was 50 days. In addition, the mixing ratio of the biomass (chicken manure) to water was 1: 5 at a retention time of 50 days and furthermore, the mixing ratio of the biomass (human excreta) to water was 1: 1, 5 at a retention time of 40 days.

Table 4: Digester volume for each feedstock type

Feedstock type	Volume of the digester (m^3)
Cattle dung	50
Chicken manure	27
Human waste	37

The volume of the digester for cattle dung was 50 m^3, and for chicken manure was 27 m^3 and finally, for human waste was 37 m^3. The school would build three fixed dome biogas digesters for the feedstocks so that the digesters would be used concurrently and in addition, when one digester is under maintenance the other digesters would be producing biogas. Furthermore, it would be expensive to have one biogas digester that would use a mixture of cow dung, human waste and chicken manure since this would involve carrying some feedstocks from longer distances to the digester. Therefore, the chicken manure digester would be closer to the chicken broilers and cattle dung digester could be constructed in the cattle pastures.

4.4. Construction materials for the digesters

Table 5 shows the construction materials for the biogas digesters and these include cement, steel bars mesh wire, oil paint, aggregate, sand and bricks. In calculation of the material requirements for the biogas digesters, the gas production rate was calculated first from equation 3. For the equation, the value for biogas yield in m^3/kg for each feedstock was obtained from Table 3 and in addition, the weight of dung available per day (kg/day) was also obtained from the same table. For example for cow dung, $G = 500 \times 0.04 = 20\ m^3$, where 500 represents weight of cattle dung (kg) available per day and 0.04 was the estimated biogas yield of cattle per kg (Table 3).

Tractors at the school could be used to transport cement, bricks and sand to the construction sites. Farm bricks would be used for the construction because they are cheap and locally available. The permanently employed mission workers would be involved in the construction of the digesters. These workers included builders, welders, farm brick moulders, carpenters, drivers and groundsmen.

4.5. Calculation of the electric biogas generator sizes

Equation 15 was used to size the three electric biogas generators for cow dung, chicken manure and human waste. The assumptions made in the calculations are in section 3.6. For the cow dung having a biogas yield of 18 m^3, the size of the electric generator would be 80 kVA, and for the 4 m^3 biogas yield from chicken manure a 20 kVA generator set would be used. Lastly, the 28 m^3 biogas yield from human waste would require 120 kVA generator set. Therefore, the three generators at the high school would be used to harness the biogas for the electricity generation.

4.6. Biogas production and distribution

Figure 4 shows a schematic diagram for the biogas production and distribution system. Sewage from the school community would be carried by means of pipes to the sewage sump. The sewage sump gate directs the sewage either into the sewage pond or mixing pit. When sump gate A is open while gate B is closed, the sewage gets into the sewage pond. When gate A is closed while gate B is open, the sludge gets into the mixing pit. In the mixing pit, water is continuously added to the sludge until a correct sludge water-mixing ratio is obtained. A homogeneous mixture of water and slurry in the mixing pit is maintained by using a mechanical stir-

Table 5: Material estimates for the digesters
(Nijaguna, 2002)

Feedstock	*G (m^3)*	*Cement bags*	*Bricks No*	*Sand (m^3)*	*Aggregate (m^3)*	*Steel (kg)*	*Mason (days)*	*Mesh wire (kg)*	*Labour (days)*	*Paint (L)*
Cattle dung	20	91	10 184	10.85	3.89	221	33	66	148	7.0
Chicken manure	6	40	5 121	5.05	1.29	74	16	31	68	3.0
Human waste	27	115	13 239	13.0	5.06	276	41	85	192	9.0

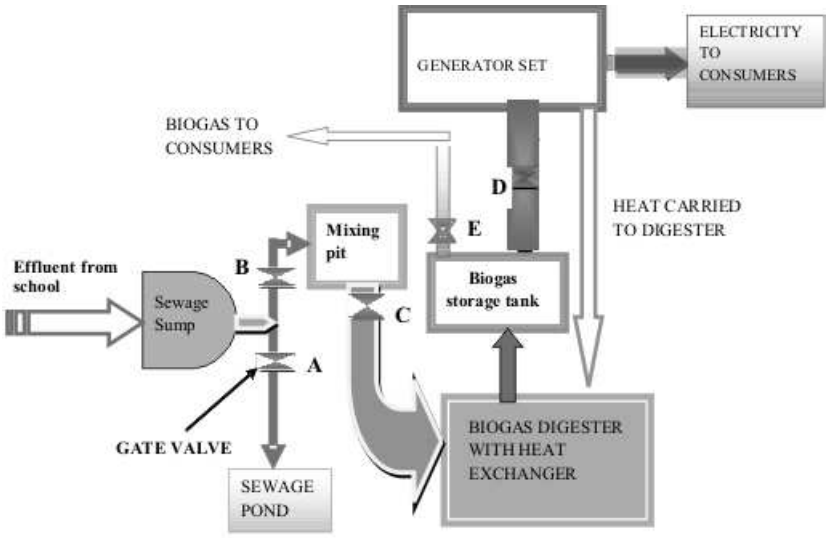

Figure 4: Schematic diagram showing biogas production and distribution

rer. When the desired mixture is obtained, gate C is opened, and the sludge then enters the dome digester. The biogas is produced in the biogas digester by anaerobic digestion process.

The heat exchanger system at the bottom would provide suitable temperature around 35°C, for anaerobic digestion. The mechanical stirrers distribute heat evenly in the biogas digester. From the digester the biogas is collected in the storage tank. When valve D is open biogas would flow to the generator set. The generator would use the biogas to produce electricity. The electrical energy from the biogas generator would be used for lighting and heating purposes at the school. When biogas is used as fuel for the diesel generator, the modification required for the generator would be replacing the diesel injector by a spark plug. The electricity from the generator set would be mainly used for lighting classrooms, dormitories, houses and for cooking. In addition, biogas can also be utilized directly from the biogas storage tank to fuel gas stoves, gas heaters and gas refrigerators.

Table 6: Total investment costs

Description	Quantity	Unit price (US$)	Total (US$)
50 kg cement	230	7.00	1,610
Bricks	27 000	0.01888	510
6m length of 27 mm gas pipes	10	30.00	300
4 m length asbestos pipes-110 mm	15	35.00	525
Steel (kg)	552	2.00	1 104
Mesh wire (m^2)	82	1.00	82
6 m length of copper tubes-25 mm	6	30.00	180
Sand (m^3)	26	19.00	500
Aggregate (m^3)	10	30.00	300
Paint (litres)	18	10.00	180
Generator modifications	2	1,200	2 400
Heat exchangers	1	600	600
Others			666
Labour			1 000
Total			9 957

4.7. Economic analysis of the biogas project

The investment costs for the digesters were calculated and the results are summarized in Table 6. From Table 6, the total investment costs for the biogas digesters are US$ 6957.

Table 7 shows the techno-economic analysis data for the investment project. The calculated values on Table 7 were obtained through equations 6 to 14 on procedures for the financial evaluation.

Table 7: Techno-economic analysis data for the investment project

Parameter	*Calculated value (US$)*
Investment costs	9 957
Operating costs	58 334
Manpower costs	1 500
Repair and maintenance costs	2 000
Energy related costs	300
Revenues	1 152
Other income and subsidies	8 000
Total income	9 152
Returns	5 485
Cost comparison, K	6 857
Cost annuity	6 845
Profitability (ROI)	87%
Payback period	2 years
NPV	22 435
Annuity	5,048
Dynamic payback period	2 years

From Table 7, the repair and maintenance costs were US$ 2 000, the energy related costs were US$ 300.00 and the cost comparison was US$ 6 857. The cost annuity was US$ 6845 and the Net Present Value was US$ 22 435. The dynamic payback period was one year.

The economic analysis of the biogas project showed that the project is financially feasible. The Net Present Value is high and positive showing the feasibility of the investment on the project. The payback period was short implying that the project pays itself off within the service life or within a set payback limit, which must be shorter than the technical service period of 5 years.

5. Conclusion and recommendations

The total energy requirement for the school is 2 710 kWh per day and the total energy from biogas of the feedstocks was 450 kWh/day. Therefore, the biogas would contribute to 16% of the total energy needs of the school. The total energy for lighting was 135 kWh/per day. It can be concluded that lighting for the whole school takes only 30% of electricity that is generated from the biogas. Therefore, the other 60% of electricity from biogas would be enough for all electricity requirements in the following; computer laboratory, classrooms, administration block, school library, boys and girls laboratories. The remainder 10% of electricity from biogas would add to the cooking needs supported by the electricity from the grid. The calculated annuity, the dynamic payback period and the net present value (NPV) are high. This can be concluded that the project is favourable, profitable and worth undertaking.

Technical problems of the digesters include a lack of trained operators, poor equipment design and failure to feed the digester regularly. It can be recommended that operators require induction courses for the digesters to be operated more efficiently. The school should have ready information on operation of digesters and in addition operators should be kept updated with relevant information on biogas digesters. Furthermore, the opening and closing of the gas outlet and main gate valves must not be cumbersome and the feedstock should be fed into the digester when correct amount of water is mixed with it. The most favourable total solids (TS) value desired for better biogas production is 8% (Ituen *et al.,* 2007). The pH changes in the digester would affect methane formation process and therefore, pH fluctuation would be controlled by the addition of wooden ash at zero cost. However, temperature fluctuations in the digesters would be minimal since the digesters would be constructed underground.

References

Davidsson, Å. (2007). Increase of biogas production at waste water treatment plant- Addition of urban organic waste and pre-treatment of sludge, Water and Environmental Engineering, Sweden: Department of Chemical Engineering, Lund University. Available at: www.dissertations.se/dissertation/a80f88cc0e/ (Accessed on 24 August 2012).

Deublein, D. and Steinhauser, A. (2008). Biogas from Waste and Renewable Resources. An Introduction, Weinheim: WILEY-VCH Verlag GmbH & Co. KGaA,

Finck, H. and Oelert, G. (1985). A guide to the financial evaluation of investment projects in energy supply, Germany: GTZ.

Fulford, D. (2001). Running a Biogas Programme. United Kingdom: ITDG Publishing.

Gerardi, M.H. (2003). The Microbiology of Anaerobic Digesters, Hoboken Jersey: John, Wiley & Sons, Inc.

Goswami, Y.D. and Kreith, F. (2008). Energy conversion, London New York: CRC press, Taylor and Francis Group, Boca Raton.

Ituen, E.E., John, N.M. and Bassey, B.E. (2007). Biogas production from organic waste in Akwa Ibom State of Nigeria. Appropriate Technologies for Environmental Protection in the Developing World, 207, pp. 17-19.

Jemmett, R., (2006). Methane, biogas, production guide, United Kingdom, Available at: www.small-farm-permaculture-and-sustainable-living.com/support-files/methane. (Accessed on 13 August 2006).

Jingura R.M. and Matengaifa, R. (2009). Optimization of biogas production by anaerobic digestion for sustainable energy development in Zimbabwe, Renewable and Sustainable Energy Reviews, 13 (5), pp.1116-1120.

Lantz, M., Mattias, S. and Börjesson, L. (2007). The prospects for an expansion of biogas systems in Sweden- Incentives, barriers and potentials, *Energy Policy* (35), pp. 1830-1843.

Leksell, N. (2005). Present and future digestion capacity of Käppala waste treatment plant a study in a laboratory scale, Master thesis, Master of Science program in aquatic and Environmental Engineering, Uppsa University, Sweden.

Mukumba, P. (2007). Industrial attachment report with Firle Sewage Treatment Works, Harare, Zimbabwe.

Mwakaje, A.G. (2007). Dairy farming and biogas use in Rungwe district, South-West Tanzania; a study of opportunities and constraints, Renewable and Sustainable Energy Reviews 12 (8), pp. 2240-2252.

Nijaguna, B.T. (2002). Biogas Technology. New Delhi: New Age International (P) Limited, Publishers.

Sathianathan, M.A. (1975). Biogas achievements and challenges, New Delhi: Association of Voluntary Agencies for Rural Development.

Shonhiwa, S. (2005). Renewable Energy Programme (REP) lectures notes, University of Zimbabwe, Faculty of Engineering, Department of Mechanical Engineering, Harare, Zimbabwe.

Sibisi N.T. and Green J.M. (2005). A floating dome biogas digester: perceptions of energizing a rural school in Maphephetheni, KwaZulu-Natal, *Journal of Energy in Southern Africa* 16 (2), pp. 45-52.

Thouars, A .P. (2007). Optimization of biogas production at Kappala wastewater treatment plant: thicken-

ing sludge and biogas potential measurement in a laboratory scale. Master of Science thesis, Sweden.
Walekwa, P.N., Mugisha, J. and Drake, L. 2009. Biogas energy from family-sized digesters in Uganda: Critical factors and policy implications, *Energy Policy* 37, pp. 2754-2762.

Received 15 May 2012; revised 30 October 2013

Critical factors to be considered when planning the implementation of environmental improvements and energy saving

Juliane Barbosa dos Santos

Charbel José Chiappetta Jabbour
UNESP – Sao Paulo State University, Brazil

Abstract
To identify the critical success factors in the adoption of energy efficiency actions in Brazilian hospitals and describe their behaviour are the objectives of this paper. In order to achieve these goals, a literature review was performed on green management and energy efficiency. This was the basis to define the questions of the interview script applied to two hospitals located in the state of São Paulo, Brazil. The interview script application was complemented by secondary data and direct observation. The results showed that: a) the studied hospitals are embracing environmental management actions more often and, whenever possible, energy efficiency actions are taken as well; and b) in the cases analysed top management support, commitment with the environment, green process design and employee empowerment were some of the most relevant critical success factors to the accomplishment of energy efficiency actions. These findings may be of interest to emerging countries, including BRICS (Brazil, Russia, India, China and South Africa).
Keywords: Brazil; energy efficiency; critical success factors; sustainability; green management; hospitals

1. Introduction

An essential green management strategy, energy efficiency has been suggested as a road towards sustainable development, which is in turn, considers the best way to harmonize the economy, the environment and the society of today and tomorrow (Wu *et al*., 2012). Nevertheless, the majority of studies (Rohdin, 2007; Sardianou, 2008; Van Berkel, 2007; Walsh and Thornley, 2012) on energy efficiency discuss the reality of the developed countries and of the manufacturing sector (Taghizadeh and Pourrabbi, 2013; Fleiter *et al*., 2011; Garcia, *et al.,* 2007). Thus, there is a literature gap, that is, a lack of research on developing countries – such as Brazil – on service sectors – such as hospitals – in the energy efficiency state-of-the-art body of knowledge.

Therefore, the analytical focus of this paper is on energy efficiency in Brazilian hospitals, due to the energy-saving opportunities found on the premises (heating, hot water, lighting and other related consumptions) and due to the fact that hospitals are supposed to provide patients with top comfortable facilities, by means of modern technology or management strategies which will assure power cost reduction (Congradac *et al.*, 2012).

After the literature review of satisfactory experiences from energy efficiency practices in hospitals (Santamouris *et al*., 1994; Szklo *et al*., 2004; Bizzarri and Morini, 2006; Bujak, 2010; Saidur *et al*., 2010; Sanz-Calcedo *et al*., 2011; Vanhoudt *et al*., 2011; Congradac *et al*., 2012; Çakir *et al*., 2012), it was verified that the Brazilian scenario – Latin America's most economically significant country and BRIC member – is not properly assessed.

Based on existing gaps, the objective of this study is to identify the critical success factors in the adoption of green management and energy efficiency actions in Brazilian hospitals. Because this research topic is still exploratory, it is qualitative research, using a two-case study strategy in order to achieve its proposed goal.

2. Conceptual background

2.1 Green management and energy efficiency in Brazil

Green management can be defined as an organizational process outlined to reach environmental sustainability, reduce waste, obtain corporate social responsibility and competitive advantage by fostering green goals and strategies totally integrated with

the company's objectives and strategies (Jabbour *et al*., 2012).

Many green management studies are focused on industrial organizations, because their activities have a greater visible environmental impact. The service companies – known as the 'silent destroyers of the environment' – are given much less attention (Molina-Azorín *et al.*, 2009).

However, even service companies can adopt three types of green management practices (González-Benito and González-Benito, 2006):

- Organizational and planning practices, related with the Environmental Management
- System (EMS) development and implementation, as well as other organizational aspects which are important to the environmental management;
- Communication practices, related with the communication on developed environmental actions; and
- Operational practices, related with the operational changes performed in the production system and in the operations, which are important to the environmental issues.

Pursuant to the World Business Council for Sustainable Development (WBCSD) (2012), the principle of eco-efficiency, which is related with operational environmental practices (González-Benito and González-Benito, 2006) – is achieved by delivering goods and services at competitive prices, meeting the human needs and providing quality of life, while progressively diminishing the ecological impacts and the resource intensity along its life cycle, creating more value and reducing the impact.

The eco-efficiency has three main dimensions (WBCSD, 2012):

- Reduction of the resource consumption: includes the minimization of the use of energy, materials, water and earth; recycling increase and product durability;
- Reduction of the impact on the environment: includes the minimization of air emissions, water discharges, waste elimination and dispersion of toxic substances, as well as the promotion of the sustainable use of renewable resources;
- Enhancement of product/service value, meaning the offer of greater benefits to clients by the functionality, flexibility and modularity of the product, enabling the achievement of the same functional need by the client with less materials and resources.

Some organizations have a fourth dimension: the EMS implementation (WBCSD, 2012). There are many eco-efficiency actions, such as the reduction in the consumption of water or energy (Van Berkel, 2007). Energy efficiency is a powerful and cost-effective way to supply the sustainable development requirements against the dependence on fossil fuels (Al-Mansour, 2011). In Brazil, the energy efficiency activities started in 1984 with the establishment of Inmetro (National Institute of Metrology, Quality and Technology), currently responsible for the Brazilian Labelling Program on Energy Efficiency (Bodach and Hamhaber, 2010). In 1985, the Brazilian National Program of Electric Energy Conservation (PROCEL) was devised in order to promote the conservation of electric energy according to the supply and demand, so that the investment costs in the electricity generation sector could be curtailed (Bodach and Hamhaber, 2010).

After the 2001 energy crisis, the National Policy for Conservation and Rational Use of Energy, Law No. 10.295, from October 17, 2001 was established, with a focus on elaborating the consumption limits or the minimum requirements to the energy efficiency of power-consuming machines or devices (Bodach and Hamhaber, 2010). On December 11, 2002 the 4.508 decree was set up, becoming a further step in the voluntary process of energy efficiency improvement (Garcia et al., 2007).

The 'Procel Edifica' action plan was approved in September 2006. It performs the voluntary labelling of the energy efficiency levels in public, commercial and service buildings (Carlo and Lamberts, 2008). The Brazilian Energy Plan estimates to 2030 that the energy efficiency actions in the electric sector may avoid the consumption of 53 TWh of energy (Sheinbaum et al., 2011).

2.2 Critical success factors of energy efficiency in hospitals

The Critical Success Factors (CSF) are intended to clarify the important areas that influence the organizational success (Eni, 1989), especially useful to the performance management and organizational excellence measurement (Xu *et al*., 2011).

The literature review on green management critical success factors (Daily and Huang, 2001; Babakri *et al*., 2003; Zutshi and Sohal, 2004; Chavan, 2005; Wee and Quazi, 2005; Zutshi *et al*., 2008; Sambasivan and Fei, 2008) enabled the identification of the factors shown in Table 1.

Hospitals are major power consumers, since they are supposed to provide patients with top comfortable facilities and may save a great deal of energy efficiency (Congradac *et al.*, 2012).

Hospitals as central health care providers can minimize the negative side effects from their activities to the environment by applying the sustainability concept in green building projects, energy efficiency improvement or environmental management systems (Weisz *et al*., 2011).

2.3 Conceptual framework of the study

A conceptual framework was set up to relate the most relevant concepts from this research, thus proposing a mutual relationship, for posterior verification that such framework is adherent or not to the

Table 1: Systematization of the critical success factors related with green management

Environmental management CSF	*Concepts*	*Research*
Top management support	Communication of the policy, plan and further worker-related information; Leadership, management and support; Reluctance in providing the needed resources; Top management commitment; Provision of basic training.	Daily and Huang (2001); Zutshi and Sohal (2004); Chavan (2005); Wee and Quazi (2005); Zutshi *et al*. (2008); Sambasivan and Fei (2008)
Commitment with the environment	Increasing pressure from clients, government and other parties interested in demonstrating environmental commitment.	Sambasivan and Fei (2008)
Green process design	Procedures and activities in the green process factor area.	Wee and Quazi (2005)
Employee empowerment	The skilled employees have autonomy and decision power, being more inclined to get involved in the environmental improvement; The responsibility increase may cause the employees to oppose the EMS.	Daily and Huang (2001); Chavan (2005)
EMS	Time, effort and high EMS implementation cost; The EMS integration may allow the organizations for being more competitive in business; Long-term initiatives in the EMS adoption.	Babakri *et al*. (2003); Zutshi and Sohal (2004); Zutshi *et al*. (2008)
Supplier management	All involved parties in the environmental management – enclosing suppliers, clients and employees.	Wee and Quazi (2005)
Information management	Information share among the organizations may help in finding solutions.	Wee and Quazi (2005)
Advanced environmental management practices	Life Cycle Analysis (LCA); Design for Disassembly (DFD); Industrial ecology.	Zutshi and Sohal (2004)
Rewards	Reinforce the empowerment and the decision-making process; Motivation to continue with the good environmental practices.;	Daily and Huang (2001)
Review and improvement	Belief that there is no need for constant review and improvement; To a continuous, adequate and effective management.	Chavan (2005); Sambasivan and Fei (2008);
Teamwork	The contribution of each individual to the organizational well-being is important to an accomplished EMS; Creation of green teams to implement the environmental projects; Organizations committed with the environment are inclined to reinforce teamwork and loyalty.	Daily and Huang (2001); Wee and Quazi (2005); Sambasivan and Fei (2008)
Environmental training	Preparation of employees to new environmental operations, helping in corrective action efforts; The employees need to be aware of the importance of their operations to the organization and the environmental impact; The training length may originate various outcomes.	Daily and Huang (2001); Zutshi and Sohal (2004); Zutshi *et al*. (2008)

analysed cases (Figure 1). The green practices proposed by González-Benito and González-Benito (2006) with the energy efficiency and its dimensions allocated into the operational practices are presented in this framework. The research focus is on energy efficiency in hospitals, trying to discover which most relevant critical success factors facing the constant demands from the reduction of the energy consumption (Szklo *et al*., 2004).

3. Research methodology

This study is devoted to understand the energy efficiency CSF in Brazilian hospitals. According to a search made from the ISI Web of Science and Scopus, studies with this analytical focus were not located during 2011 and 2012 (using the keywords of this paper). This way, the topic can be regarded as exploratory. In this context, qualitative research is the most appropriate one, with an option for the case study strategy (two cases) (Voss *et al*., 2002).

The data to this research comes from two hospitals in the state of São Paulo, Brazil. After the agreement, interview date and time, direct observation and document analysis for data was established. This phase took place in 2012, in Hospitals 1 and 2, according to Table 2.

4. Results

Hospital 1 refers to a large Philanthropic hospital, with about 230 beds. Hospital 1 presents the fol-

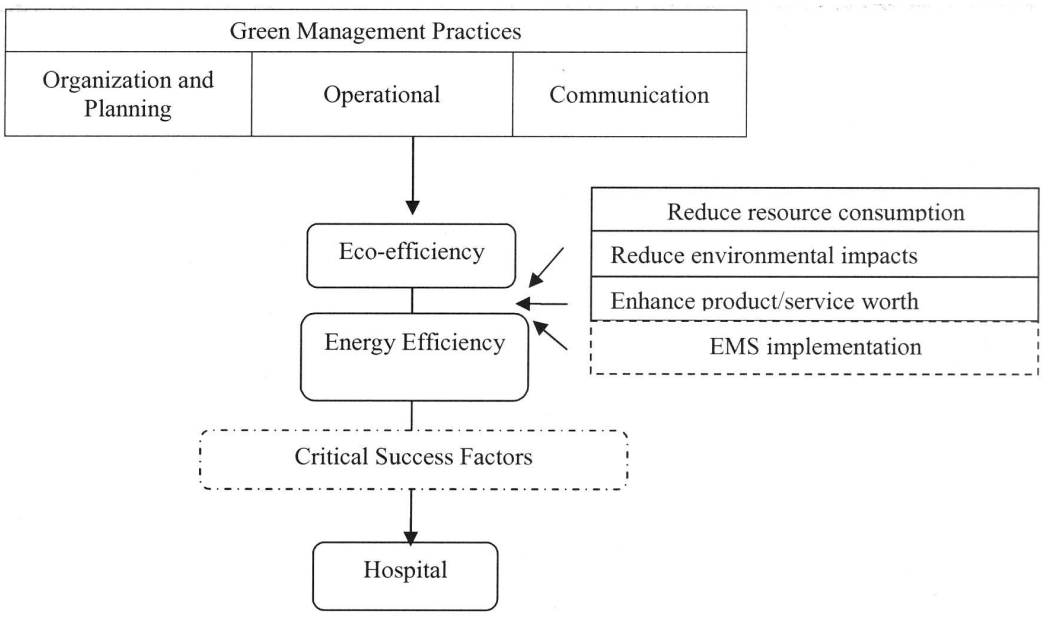

Figure 1: Framework with the green management critical success factors focusing on energy eco-efficiency

Table 2: Data collection procedures summary

		Data collection dynamics	
Hospital	*Type*	*Interviewee*	*Documents*
1.	General Hospital / Philanthropic Hospital	Infrastructure and Project Manager	Documents available in the Unit website. Documents on the Unit history and data.
2	Specialized Hospital / Public Hospital	Maintenance Engineer	Documents available in the Unit website. ocuments on the Unit history and data.

lowing green practices: Healthcare Waste Management Plan, a campaign against disposable cups, campaign for imaging examination material collection, own water collection and storage system, substitution of bulbs and air-conditioning device use control.

Hospital 2 refers to a medium-sized public hospital. It has 91 beds. Hospital 2 presents the following green practices: Healthcare Waste Management Plan**,** Water Conservation Program, proper battery and bulb disposal, substitution of bulbs, correct use of the air-conditioning device, Plan for the Rational Use of Energy and an implementing project on individual energy control.

Hospitals 1 and 2 present similarities in the critical success factors regarding green management. These similarities can be observed based on each CSF adopted by this research and described further.

4.1 Top management support

To Daily and Huang (2001), Zutshi and Sohal (2004), Chavan (2005), Wee and Quazi (2005), Zutshi *et al*., (2008) and Sambasivan and Fei (2008), an environmentally aware top management enables an open and participative employee management. Both hospitals have top management support as a critical success factor. According to the interviewee from Hospital 1, there is both support and pressure for green issues. In Hospital 2, such a critical factor is highlighted by the support for green trainings and release of budgetary resources.

4.2 Commitment to the environment

The commitment with the green responsibilities is listed by Sambasivan e Fei (2008) as a critical success factor. In both studied hospitals, one can find support and incentive in the sustainability-related issues as well as pressures originated from the surrounding community.

4.3 Green process design

Wee and Quazi (2005) developed and validated a set of green management critical success factors based on bibliographic research and interviews with environmental managers, thus establishing the green process design as a core critical factor.

The green process design critical factor corresponds in Hospital 1 to the Healthcare Waste Management Plan, campaign against disposable cups, campaign for imaging examination material collection, own water collection and storage system, substitution of bulbs and air-conditioning device use control.

In Hospital 2, the green process design critical

factor corresponds to the Healthcare Waste Management Plan, Water Conservation Program, proper battery and bulb disposal, substitution of bulbs, correct use of the air-conditioning device, Plan for the Rational Use of Energy and an implementing project on individual energy control.

4.4 Employee empowerment

To Daily and Huang (2001), motivated and engaged employees are more participative when involved in advanced green management practices. The employee empowerment can be realized in Hospital 1 due to the fact that the interviewee – infrastructure and project manager – has proposed and led green management-related ideas, such as the feasibility study on the replacement of fluorescent bulbs with LED bulbs. In the second case, the interviewee – a maintenance engineer – has autonomy to accomplish a feasibility study, such as to study energy sectorial sub-metering, so that expenses can be better controlled.

4.5 Environmental management systems

The critical factor related to Environmental Management System (EMS) implementation is important to Babakri *et al*., (2003), Zutshi and Sohal (2004) and Zutshi *et al*., (2008), because they enable corporate competitiveness. Both hospitals lack the EMS, and to date there is no intention recorded to implement it.

4.6 Supplier management

The supplier management critical success factor is inclusive of clients, suppliers and employees, and all must be involved in the green management, a relevant item to Wee and Quazi (2005). The supplier management critical success factor in the green management area was not found in both hospitals.

4.7 Information management

According to Wee and Quazi (2005), the share of information among organizations can lead to solutions. At first, the share of information among organizations in order to solve problems was not detected in both cases. Information shared via the web in the first case and internally in the second case solely informs the public on projects or news already consolidated.

4.8 Adoption of advanced green management practices

The adoption of green management practices are inserted in major critical success factor categories presented by Zutshi and Sohal (2004), and they can be used in any organization, regardless of its size, business nature or sector. On advanced green management practices focusing on energy efficiency, it is highlighted in the second case the Plan for the Rational Use of Energy. The substitution of bulbs and the correct use of the air conditioning device are the directed practices, among others. In the first case, the energy efficiency measurements are limited to substitution of bulbs and the use of the air conditioning device only in areas of great need.

4.9 Employees rewards

A reinforcement to continuously motivate the commitment of the employees with the green issues is an important factor to Daily and Huang (2001). The reward critical success factor was not attested with factors related with the environmental issues in none of the cases studied. Thus, there are no bonuses for energy saving in the studied hospitals.

4.10 Review and improvement

According to Chavan (2005) constant reviews and improvement are needed in order to have a continuous, adequate and effective management (Sambasivan and Fei, 2008). The review and improvement critical success factor was not identified in the first case, but it can be observed in the second case, when the interviewee states that in the 2002 energy crisis ('the 2002 Brazilian blackout'), the employees revised the energy saving related project, and a new awareness arose.

4.11 Teamwork

The contribution of each individual, combining competences in the organization is important to a successful green management (Daily and Huang, 2001). In the first case, the teamwork critical success factor is related with several actions, among them the total employee adherence to the disposable cup campaign, as well to the non-use of air conditioning devices in unnecessary areas and also to trivial actions such as turning off the light when leaving a place. According to Wee and Quazi's conception (2005), the creation of green teams is needed to the implementation of the environmental projects. In the second case, the main difficulty is maintaining the employee awareness; as time goes by such awareness undergoes a common relaxation. The employee awareness is the main obstacle in the adoption of green practices.

4.12 Environmental training

The environmental training prepares the employees to new green operations and helps in the corrective action efforts (Daily and Huang, 2001). In the first case, there is no specific environmental training but a general week training performed to the new employees, in which some orientations are transmitted, among them the environmental-related ones. In the second case, when the eco-efficiency programs were installed, there was training in mid-1997. As the employees need to be aware of their organizational operations and their environmental impact (Zutshi and Sohal, 2004), a new training

was again reinforced during the energy crisis, known as the '2002 Brazilian blackout'.

5. Discussing the adherence between the proposed framework and reality of Hospitals 1 and 2 cases

In Figure 2, an empirical framework refining the conceptual framework (Figure 1) was presented to relate the environmental management critical success factors with a focus on the energy efficiency. From the four dimensions based on the WBCSD (2012), both hospitals have three of them (reduction in the resource consumption, reduction of the nature impact and enhancement of the service value). The fourth dimension constituted by the implementation of an EMS does not take place in the two hospital units. Also there is no intention to date to implement the EMS.

In both cases, the 'reduction of the resource consumption' is the central issue. Searching for further green actions, both hospitals attempt to accomplish projects aiming at saving energy, basically. The energy efficient practices seemed to be related with one another:

- To Hospital 1, one can highlight the employee empowerment, commitment with the environment, green management practices, green process design, top management support, teamwork and environmental training;
- To Hospital 2, it is highlighted the employee empowerment, commitment with the environment, green management practices, green process design, top management support, teamwork, environmental training and review and improvement;
- In an exploratory way, it was possible in addition to spot critical factors not yet met, that is, barriers that should be overcome, both for Hospital 1 (financial and lack of sub-metering) and for Hospital 2 (human organizational factors and lack of sub-metering).

This way the conceptual framework is adequate to offer understanding on energy efficiency CSF in Hospitals 1 and 2, also suggesting that the topic 'barriers to energy efficiency' should be incorporated to the empirical framework, refining the conceptual framework. Further, the EMS is lacking in reality.

6. Conclusion

The aim of this study is to identify the critical success factors in the adoption of energy eco-efficiency programs in some Brazilian hospitals. In order to achieve this goal, a literature review on the topic was held and a case study was conducted using evidence from two hospitals located in the state of São Paulo, Brazil. The two cases were analysed regarding a brief hospital characterization, green management characterization and finally the energy efficiency and CSF characterization.

In Hospital 1, the critical success factors are the top management support, the commitment with the environment, green process design, employee empowerment, advanced environmental management practices, environmental training and teamwork.

In Hospital 2, the critical success factors are top management support, commitment with the environment, green process design, employee empowerment, advanced environmental management practices, review and improvement, environmental training and teamwork.

Table 3 shows the two studied cases relating the critical success factors and the main barriers found. Therefore, the objective proposed by this study was achieved.

Table 3: Systematization of the opportunities and barriers found in the studied cases

Critical success factors	
Hospital 1	*Hospital 2*
top management support;	top management support;
commitment with the environment;	commitment with the environment;
green process design;	green process design;
employee empowerment;	employee empowerment;
advanced environmental management practices;	advanced environmental management practices;
environmental training;	review and improvement;
teamwork.	environmental training;
	teamwork.

According to this context, this study shares its contribution with two cases in hospitals from the state of São Paulo. As a suggestion, a future study should analyse the support from specialized consultancy on energy efficiency to Hospitals' sustainability, exploring critical barriers and factors of success

.

References

Al-Mansour F. (2011). 'Energy efficiency trends and policy in Slovenia', *Energy*, Vol. 36, pp.1868–1877.

Babakri, K.A, Bennett R.A, and Franchetti M. (2003). 'Critical factors for implementing ISO 14001 standard in united states industrial companies', *Journal of Cleaner Production*, vol. 11, pp.749-752.

Bizzarri G., and Morini G. L. (2006). 'New technologies for an effective energy retrofit of hospitals', *Applied Thermal Engineering*, Vol. 26, pp.161-169.

Bodach S, and Hamhaber J. (2010). 'Energy efficiency in social housing: Opportunities and barriers from a case study in Brazil', *Energy Policy*, Vol. 12, pp. 7898-7910.

Bujak J. (2010). 'Heat consumption for preparing domestic hot water in hospitals', *Energy and Building*, Vol. 42, pp. 1047-1055.

Çakir U, Çomakli K., and Yuksel F. (2012). 'The role of cogeneration systems in sustainability of energy', *Energy Conversion and Management*, (in press).

Carlo J., and Lamberts R. (2008). 'Development of envelope efficiency labels for commercial buildings: Effect of different variables on electricity consumption', *Energy and Buildings,* vol.40, pp. 2002-2008.

Chavan M. (2005). 'An appraisal of environment management systems: A competitive advantage for small businesses', *Management of Environmental Quality: An International Journal*, Vol. 16, pp. 444-463.

Congradac V, Prebiracevic B, Jorgovanovic N, and Stanisic D (2012). 'Assessing the energy consumption for heating and cooling in hospitals', *Energy and Buildings*, Vol. 48, pp. 146-154.

Daily B.F, and Huang S. (2001). 'Achieving sustainability through attention to human resource factors in environmental management', *International Journal of Operations & Production Management*, vol. 21, pp. 1539-1552.

Eni G.O. (1989). 'The concept of critical success factors (CSFs) as a planning tool for healthcare managers', *Health Management Forum*, Vol.2, pp. 12-17.

Fleiter T, Worrell E., and Eichhammer W. (2011). 'Barriers to energy efficiency in industrial bottom-up energy demand models – a review', *Renewable and Sustainable Energy Reviews*, Vol. 6, pp. 3099-3111.

Garcia A.G.P, Szklo A.S, Schaeffer R., and Mcneil M A. (2007). 'Energy-efficiency standards for electric motors in Brazilian industry', *Energy Policy*, Vol. 35, pp. 3424-3439.

González-Benito J, and González-Benito O. (2006). 'A review of determinant factors of environmental proactivity', *Business Strategy and the Environment*, Vol.15, pp. 87-102.

Jabbour C.J.C., Silva E.M, Paiva E.L., and Santos F.C.A. (2012) 'Environmental management in Brazil: is it a completely competitive priority?' *Journal of Cleaner Production*, Vol. 21, pp. 11-22.

Molina-Azorín J.F, Claver-Cortés E, Pereira-Moliner J., and Tarí J.J. (2009). 'Environmental practices and firm performance: an empirical analysis in the Spanish hotel industry', *Journal of Cleaner Production*, Vol.17, pp. 516-524.

Rohdin P, Thollander P, and Solding P. (2007). 'Barriers to and drivers for energy efficiency in the Swedish foundry industry', *Energy Policy*, Vol. 35, pp. 672-677.

Saidur R, Hasanuzzaman M, Yogeswaran S, Mohammed H A, and Hossain M S. (2010). 'An end-use energy analysis in a Malaysian public hospital', *Energy*, Vol. 35, pp. 4780-4785.

Sambasivan M. and Fei N.Y. (2008). 'Evaluation of critical success factors of implementation of ISO 14001 using analytic hierarchy process (AHP): a case study from Malaysia', *Journal of Cleaner Production*, Vol.16, pp.1424-1433.

Sardianou E. (2008). 'Barriers to industrial energy efficiency investments in Greece', *Journal of Cleaner Production,* Vol. 16, pp.1416-1423.

Santamouris M., Dascalaki E, Balaras C, Argiriou A., and Gaglia A. (1994) 'Energy performance and energy conservation in health care buildings in Hellas', *Energy Conversion Management*, vol.35, pp. 293-305.

Sanz-Calcedo J G, Blázquez F C, Rodríguez F.L, Ruiz-Celma A. (2011). 'Influence of the number of users on the energy efficiency of health centres', *Energy and Buildings*, Vol. 43, pp. 1544-1548.

Sheinbaum C, Ruíz B.J, and Ozawa L. (2011). 'Energy consumption and related CO_2 emissions in five Latin American countries: Changes from 1990 to 2006 and perspectives', *Energy*, Vol.36, pp. 3629-3638.

Szklo A S, Soares J.B, and Tolmasquim M.T. (2004). 'Energy consumption indicators and CHP technical potential in the Brazilian hospital sector', *Energy Conversion and Management*, Vol. 45, pp. 2075-2091.

Taghizadeh, H., and Pourrabbi, M.V. (2013). 'Energy cost versus production as a performance benchmark for analysis of companies', *Journal of Energy in Southern Africa*, Vol.24, pp. 2-8.

Voss, C, Tsikriktsis, N, and Frohlich, M. (2002). 'Case research in operations management', *International Journal of Operations & Production Management*, Vol. 2, pp.195-219.

Vanhoudt D, Desmedt J, Van Bael J, Robeyn N, and Hoes H. (2011). 'An aquifer thermal storage system in a Belgian hospital: Long-term experimental evaluation of energy and cost savings', *Energy and Buildings*, Vol. 43, pp. 3657-3665.

Van Berkel R. (2007). 'Eco-efficiency in primary metals production: Context, perspectives and methods', *Resources, Conservation and Recycling*, Vol. 51, pp.511-540.

Walsh C, and Thornley P. (2012). 'Barriers to improving energy efficiency within the process industries with a focus on low grade heat utilization', *Journal of Cleaner Production*, Vol. 23, pp. 138-146.

World Business Council for Sustainable Development – WBCSD. (2012). *'Corporate social responsibility: making good business sense'*, WBCSD, 2000. Available at: http://www. wbcsd. Org, Access: May 2012.

Wee Y S, and Quazi H A. (2005). 'Development and validation of critical factors of environmental management', *Industrial Management & Data Systems*, Vol.105, pp. 96-114.

Weisz U, Hass W, Pelikan J M, and Schmied H. (2011). 'Sustainable hospitals: A socio-ecological approach', *Gaia*, Vol.20, pp. 191-198.

Wu J, Wu Z, and Holländer R. (2012). 'The application of Positive Matrix Factorization (PMF) to eco-efficiency analysis', *Journal of Environmental Management*, Vol.98, pp. 11-14.

Xu P., Chan E.W, and Qian Q.K. (2011). 'Success factors of energy performance contracting (EPC) for sustainable building energy efficiency retrofit (BEER) of hotel buildings in China', *Energy Policy*, Vol.39, pp. 7389-7398.

Zutshi A., and Sohal A S. (2004). 'Adoption and maintenance of environmental management systems: Critical success factors', *Management of*

Environmental Quality: An International Journal, Vol.15, pp. 399-419.

Zutshi A., Sohal A.S, and Adams C. (2008). 'Environmental management system adoption by government departments/agencies', *International Journal of Public Sector Management*, Vol. 21, pp. 525-539.

Received 23 February 2013; revised 22 November 2013

Emissions analysis from combustion of eco-fuel briquettes for domestic applications

Tsietsi J Pilusa
Department of Mechanical Engineering Science, University of Johannesburg

Robert Huberts
Department of Chemical Engineering Technology, University of Johannesburg

Edison Muzenda
Department of Chemical Engineering Technology, University of Johannesburg

Abstract
In this study, flue gas emissions from combustion of eco-fuel briquettes in a ceramic lined stove were investigated. The eco-fuel briquettes were made of biomass such as spent coffee beans, mielie husks, saw dust, paper pulp and coal fines using a hand operated screw press. A combustion set-up consisting of digital weightometer, a ceramic lined stove and a complete chimney system was used. The emissions from the combustion process were measured using a Testo 350 gas analyser linked to the chimney system. The eco-fuel briquettes made from a mixture of biomass and coal fines burnt within the acceptable exposure limits as set out by the Occupational Safety and Health Agency (OSHA). The flue gas emissions from the combustion of eco-fuel briquettes were found to contain 74 parts per million (ppm) carbon monoxide (CO), 4.32 ppm hydrogen sulphide (H2S), 1.34ppm nitrogen oxides (NOx) and 3.67 ppm sulphur oxides (SOx). The measured gross calorific value was 18.9MJ/kg, with a burning rate of 2g/min. These properties make eco-fuel briquettes suitable for domestic applications. A survey conducted as part of this study also revealed a significant demand for eco-fuel briquettes in many informal settlements in Gauteng Province, South Africa, at a competitive selling price of R2.60/kg.

Keywords: biomass fuel, coffee grounds, clean air, eco-fuel, emissions, flue gas quality

1. Introduction

1.1 Eco-fuel briquettes

Due to the rising costs and historical lack of access to electricity, heat energy for cooking and heating in most townships of Gauteng Province in South Africa is obtained from the combustion of paraffin, fuel wood and coal. A recent survey conducted as part of this study has indicated that each household in these townships could use up to 200 kg of coal and 20 kg wood per month in addition to electricity for lighting and other applications in the winter season. Combustion of these fuels contributes significantly to air pollution resulting in potential risks to human health. 1 cubic meter of fuel wood emits 61-73 kg of carbon dioxide (CO_2) equivalents as well as other toxic and greenhouse gasses over its life cycle. Prolonged exposure to these, the toxic emissions such as carbon monoxide (CO), Sulphur Oxides (SOx) and Nitrogen oxide (NOx) may cause human health complications (Raymer, 2006).

Briquetting of biomass is a densification process which improves its handling characteristics, enhances its volumetric calorific value, reduces transportation cost and produces a uniform, clean, stable fuel or an input for further refining processes (Granada *et al.,* 2002). Fuel briquettes are bonded by the random alignment of fibers, generated when plant fibres and shredded waste paper are soaked in water. The process occurs at ambient temperature at a pressure of 1.5 to 3.0 MPa. To a large degree, the bonding force in the fuel briquette is mechanical, not chemical. Because of this, retaining fibre integrity and the right degree of plasticity in the mixture is crucial to the quality of the fuel briquette (Husain *et al.*, 2002).

Fuel briquettes made from corn stover, which is a major biomass stream in the United States of America, comprised roughly of 75% of total agri-

Figure 1: Production of briquettes using a manually operated screw press

cultural residues with an average bulk density of 42 kg/m^3. These briquettes are produced using a hydraulic piston and cylinder press at pressures of 5-15 Mega Pascal (MPa), (Mani *et al.*, 2006). Other fuel briquettes are made from palm shell and residue and are available in 40 mm, 50 mm and 60 mm diameters. They are also made using a hydraulic press at pressures of 5-13.5 MPa but have a higher density of 1200 kg/m^3 when compared with other briquettes, (Husain *et al.*, 2002).

The eco-fuel briquettes shown in Figure 1 were made from a mixture containing 32% spent coffee grounds, 23% coal fines, 11% saw dust, 18% mielie husks, 10% waste paper and 6% paper pulp contaminated water, using a very low pressure, of about 0.87MPa, hand operated screw press. All briquettes had an outer diameter of 100 mm, inner diameter of 35 mm and were 50 mm long. There was no need for a chemical binder; the material components underwent natural binding by interlocking themselves by means of partially decomposed plant fibres. They are not as compact as corn stover and Palm shell briquettes but yet have longer burning times and higher gross calorific values (Yaman *et al.*, 2001).

1.2 Flue gas emissions

Flue gas emissions from biomass combustion refer to the gas product resulting from burning of biomass solid fuel. Household solid fuels are mostly burnt with ambient air as opposed to combustion with pure oxygen. Since ambient air contains about 79 volume percent gaseous nitrogen, which is essentially non-combustible, the largest part of the flue gas from most fossil fuel combustion is inert nitrogen, (Demirbas and Sahin, 1998). The next largest part of the flue gas is carbon dioxide which can be as much as 10 to 15 volume percent. This is closely followed in volume by water vapour created by the combustion of the hydrogen in the fuel with atmospheric oxygen.

A typical flue gas from the combustion of fossil fuels will also contain some very small amounts of nitrogen oxides (NO_x), hydrogen sulphide (H_2S), sulphur oxides (SO_x) and particulate matter (Debdoubri *et al.,* 2005). The nitrogen oxides are derived from a very small fraction of the nitrogen in the ambient air as well as from any nitrogen-containing compounds in the fossil fuel. The sulphur dioxide is derived from any sulphur-containing compounds in the fuels.

1.3 Toxicity of combustion emissions

The potential health hazard to humans from exposure to combustion emissions depends on the inherent toxicity of the gases and the frequency and duration of exposure. Keeping exposure to below the permissible limits can be achieved by taking precautions. The permissible limits of concentration for the long-term exposure of humans to toxic gases are set by the threshold limit value (TLV). This is defined as the upper permissible concentration limit

of the gases believed to be safe for humans even with an exposure of 8 hours per day, 5 days per week over a period of many years (Wright & Welbourn, 2002).

Recommended TLV values are published in the hazardous substance database bank by the Occupational Safety and Health Agency (OSHA). The OSHA database is assumed to be appropriate to be used as a benchmark for toxic gas exposure limits in the South African context. With the uncertainties involved in the designation of occupational exposure standards and the variability of the occupational environment, it would be unreasonable to interpret occupational limits as rigidly as one might interpret an engineering standard or specification (Peters and Timmerhaus, 1991).

2. Materials and methods

The experimental apparatus comprised of a digital weightometer, POCA ceramic lined stove and extraction system complete with a chimney. The gas extraction manifold was linked to a 980 mm stainless steel pipe of 90 mm diameter and 2 mm thickness as shown in Figure.2. A multi-purpose gas probe was installed 50 mm above the manifold for continuous gas sampling and analysis. Emissions from the eco-fuel briquettes combustion chamber were sampled directly from the chimney tunnel through the multi-purpose probe on a real time basis and measured through the Testo 350 analyzer electrochemical cells. Eco-fuel briquettes of known mass were combusted in a POCA stove and a 4 litre stainless steel pot was filled with cold water and put on the stove. The stove and pot were transferred to a weightometer in order to monitor the fuel consumption rate and heat transfer efficiencies. Data was collected over a 210 minute period for analysis. The velocity of natural incoming air was measured using an anemometer and this together with the cross sectional area of the incoming path was used to establish the air flow rate.

The combustion behaviour of the briquettes could be predicted and modified by varying the manufacturing conditions, mainly the diameter factor and the raw material. The unburnt ash content of the fuel briquettes can be estimated using the empirical model suggested by Tabares *et al.* (2000). The model defines the ash content as a function of fixed carbon being the principal factor of the weight characteristics during combustion. The relationship function is defined by Tabares *et.al* (2000) as follows:

$$W = fc(2.46 - 0.36fc + 3.9 \times 10^{-4}d + 0.13d_i + 0.05e^{4.59\text{-}0.037t} - 0.26\text{m} - 1.2 \times 10^{-4}C_v)$$

Where,

W is the remaining weight of ash in (w/w %).

fc is fixed carbon in (w/w %)

m is the final moisture content in the briquette in (w/w %)

d_i is the briquettes diameter in (cm)

d is briquette density in (kg/m3)

t is burning time in (minutes)

Cv is the calorific value of the briquettes in (kJ/kg)

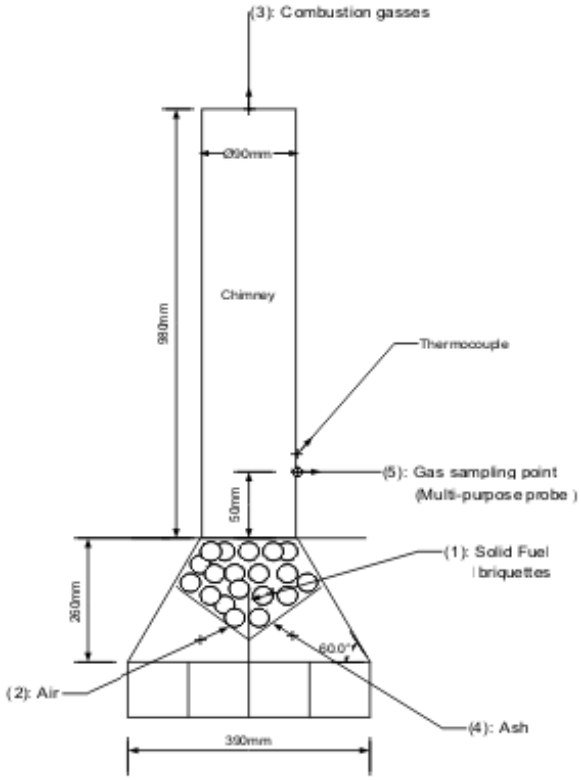

Figure 2: Schematic diagram of the combustion system used

3. Results and discussions

A survey was conducted at various informal settlements in Gauteng Province, South Africa, revealed that there is a need for alternative renewable energy source in addition to the existing ones. Table 1 summarizes the prices paid by households towards energy sources. Responses from this survey clearly indicate that, although people in the townships have access to electricity and other various energy sources, there is still a need for additional alternative energy sources such as fuel briquettes. The need for alternative sources is mainly driven by the current overall cost of energy. It has also been determined from the survey that an average home would spend around R430.00 to meet the household energy demands per month. Most people are trying to save energy so as to offset higher food prices. Paraffin and liquid petroleum gas are not widely used due to their costs and fire hazards. The briquettes could be a potential additional source of energy, not as a substitute for current sources of energy. The raw materials from which eco-fuel briquettes are produced are seasonal and may not be

Table 1: Domestic alternative fuel prices as per survey conducted in March 2009

Type	*Electricity*	*Coal*	*Wood*	*Paraffin*	*LPG*	*Eco-fuel briquettes*
Rate	R0.89/kWh	R2.6/kg	R2.80/kg	R13.50/kg	R15/kg	R2.26/kg
Energycontent	3.6MJ/kWh	25.92MJ/kg	16MJ/kg	42MJ/kg	49.3MJ/kg	18.9MJ/kg
Fuel cost	R 0.25/MJ	R 0.10/MJ	R 0.175/MJ	R0.32/MJ	R 0.304/MJ	R 0.119/MJ

consistent to meet continuous demand. Furthermore, they produce the least heat energy per kilogram compared to existing gaseous, liquid and solid fossil fuels. They are also slightly more expensive than low grade coal which is widely used as a fuel.

3.1 Properties of eco-fuel briquettes

Ultimate and proximate analyses of dry eco-fuel briquettes were conducted using the ICP-Optima model 2100DV. Eco-fuel briquettes contain 26.30% fixed carbon, 39.34% volatile matter, 10.9% moisture and 10.46% ash as per proximate analysis. The ultimate analysis show 36.65% carbon, 4.60% hydrogen, 36.3% oxygen, 0.75% nitrogen and 0.34% sulphur in the briquettes. Bomb calorimeter tests have shown the briquettes yielding a gross calorific value of 18.9MJ/kg. The dry bulk density was measured as 721 kg/m^3. It was noticed that the Tebares *et al.* (2000) correlation defined by Eq. 1 does not give an accurate ash content estimation for eco-fuel briquettes. This could be as a result of the geometry of the eco-fuel briquettes being a hollowed cylindrical shape as opposed to the solid cylindrical briquettes used to derive the Tabares *et al.* empirical correlation.

Table 2 outlines the comparisons of properties between coal and eco-fuel briquettes. This comparison indicates that coal is still a better fuel in terms of its higher calorific value (25.92MJ/kg), carbon content (61.2%) and lower ash content of 12% compared to the eco-fuel briquettes which have calorific value, carbon content and ash content of 18.9MJ/kg, 22.5% and 28.4% respectively. However, the eco-fuel briquettes are made of organic waste material with a lower sulphur content of 0.002% compared to 3.9% in coal.

3.2 Eco-fuel briquettes combustion

Variation of flame temperature with the concentration of oxygen in the combustion gases is shown in Figure 3. The oxygen concentration drops below 8.31% at the maximum combustion rate at a flame temperature of 197^{0}C. As the flue gas temperature drops, the oxygen concentration in the flue gasses increases, meaning that less oxygen is consumed when the combustion process slows down. The final oxygen concentration of 20.57% is attained when the flue gas temperature is equal to the ambient temperature, providing evidence that the combustion process stopped and oxygen was no longer consumed. The air to fuel ratio of 1.44:1 was obtained which shows that 60% of air was consumed for every 40% of fuel combusted.

Table 2: Comparison of coal and fuel briquettes properties

Combustion gas properties	*Eco-fuel briquette*	*Coal*
Gross calorific values	18.9	25.9
Specific gravity	0.71	0.86
Carbon w/w%	22.5	61.2
Hydrogen w/w%	0.71	4.3
Oxygen w/w%	43.8	7.4
Sulphur w/w%	0.0020	3.9
Nitrogen w/w%	0.0010	1.2
Ash w/w%	28.4	12.0
Water w/w%	10.9	10.0
Carbon dioxide: volume%	19.7	15.0
Oxygen: volume %	13.4	3.7
% Excess air	12.8	20.0
Nm^3/GJ:8MJ/1.14m^3	142.5	293.6

3.3 Eco-fuel briquettes emissions

Table 3 shows a comparison between the actual gas emissions from fuel briquettes and maximum human exposure limit over 8 hours. The table clearly indicates that the gas emission produced by the fuel briquettes conforms to the Occupational Safety and Health Agency (OSHA) occupational exposure standards as indicated in Table 4. High carbon dioxide concentration indicates compete combustion resulting in carbon monoxide been oxidized to less toxic carbon dioxide which is more of a greenhouse gas as opposed to other toxic emissions presents in Table 3. Proper ventilation for dilution of high carbon dioxide concentration in the emission is essen-

Table 3: Emissions for the selected toxic emissions vs. the maximum exposure limit over 8 hours

CO_2(ppm)	*CO(ppm)*	*H_2S (ppm)*	*SO_2 (ppm)*	*NO (ppm)*	*NO_2 (ppm)*	
21332	73.78	4.32	3.67	1.34	2.73	Briquettes emissions
5000	50 -200	20	5	25	5	OSHA limit

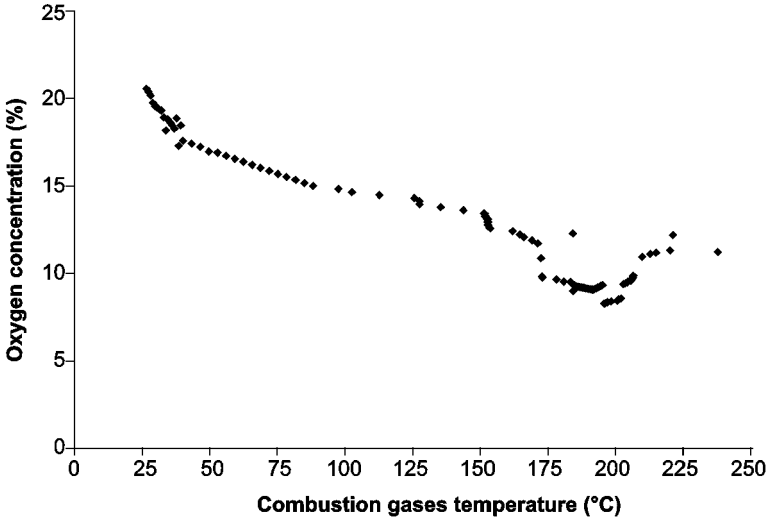

Figure 3: Flue gas temperatures with oxygen concentrations

tial, not only for prolonged exposure but also to ensure that enough oxygen in the air is provided for efficient combustion.

Although the other gases are in low concentrations as shown in Figure 4, the maximum safe exposure time to the combustion gasses produced by the fuel briquettes is 11.25 minutes due to the high carbon dioxide concentration. In principle, the fuel briquette is deemed a clean fuel compared to other fossil fuels. The carbon dioxide produced is 2 892 times the carbon monoxide, which indicates complete combustion. Furthermore, carbon dioxide is less toxic than carbon monoxide; therefore, combustion of fuel briquettes is even more suitable for well ventilated indoor applications.

Table 5 summarizes the flue gas compositions for natural gas, fuel oil and coal. From this summary, it is evident that combustion of eco-fuel briquettes emits less toxic gasses compared to other fossil fuels. A theoretical air requirement for combustion of the fuel briquettes was estimated as 2.57m^3 of air for every kg of fuel combusted. The experimental dry air consumed during combustion was measured as 752.65g at absolute pressure of 82.96 kPa. The average volumetric flow rate of the flue gas was measured as 0.4m^3/h over a period of 210 minutes and absolute pressure of 82.96 kPa, which is equivalent to 3.20m^3 of flue gas production per kilogram of eco-fuel combusted.

4. Conclusions

Combustion of fuel briquettes in a laboratory-scale POCA ceramic stove was investigated to evaluate its combustion characteristics and gas emission quality. The results show that high combustion efficiencies could be achieved by choosing appropriate operating conditions. The efficiencies were between 91-95% for carbon utilization efficiency and over 99.5% for CO combustion efficiency at an estimated air-to-fuel ratio of 1.44:1. The average burning rate of 2g/min was obtained from the test work, meaning that 1 kg of eco-fuel briquettes can burn

Table 4: Occupational Safety and Health Agency (OSHA) occupational exposure standard, obtained from the hazardous substance data bank

Gas component	Occupational exposure standard
Carbon monoxide (CO)	CASRN: 630-08-0 OSHA Standards: [29 CFR 1910.1000 (7/1/98)]. Permissible Exposure Limit: 8-hr Time Weighted Average: 50 ppm (55 mg/cu m). Vacated 1989 OSHA PEL WA 35 ppm (40 mg/cu m); Ceiling limit 200 ppm (229 mg/cu m) is still enforced in some states.
Nitrogen oxide (NOx)	CASRN: 10102-43-9 OSHA Standards: [29 CFR 1910.1000 (7/1/98)]. Permissible Exposure Limit: 8-hr Time Weighted Average: 25 ppm (30 mg/cu m).
Hydrogen sulphide (H_2S)	CASRN: 7783-06-4 OSHA Standards: [29 CFR 1910.1000 (7/1/98)] Permissible Exposure Limit: Acceptable Ceiling Concentration: 20 ppm. Permissible Exposure Limit: Acceptable maximum peak above the acceptable ceiling concentration for an 8-hour shift. Concentration: 50 ppm. Maximum Duration: 10 minutes once, only if no other meas. exp. occurs.
Sulphur oxides (SO_x)	CASRN: 7446-09-5 OSHA Standards: 1910.1000 (7/1/98)] Permissible Exposure Limit: 8-hr Time Weighted Average: 5 ppm (13 mg/cu m). [29 CFR]

Table 5: Comparison of flue gas quality of various fuels

Chemical species	*OSHA-max limit (ppm)*	*Natural gas*	*Fuel oil*	*Coal*	*Eco-Fuel Briquettes*
Nitrogen (N_2)	-	78-80%	78-80%	78-80%	60.3%
Carbon dioxide (CO_2)	5,000	10-12%	12-14%	10.6%	21.3%
Oxygen (O_2)	-	2-3%	2-6%	7%	12.8%
Carbon monoxide (CO)	50-200	70-110ppm		5,579ppm	74ppm
Nitrogen dioxide (NO_2)	5			1%	2.73ppm
Nitric oxide (NO)	25			1%	1.34ppm
Ammonia (NH_3)	50				
Sulphur dioxide (SO_2)	5			>2,000ppm	3.67ppm
Hydrocarbon (C_xH_y)	-				
Hydrogen sulphide (H_2S)	20				4.32ppm
Ash	-	0	0	12%	28.4%

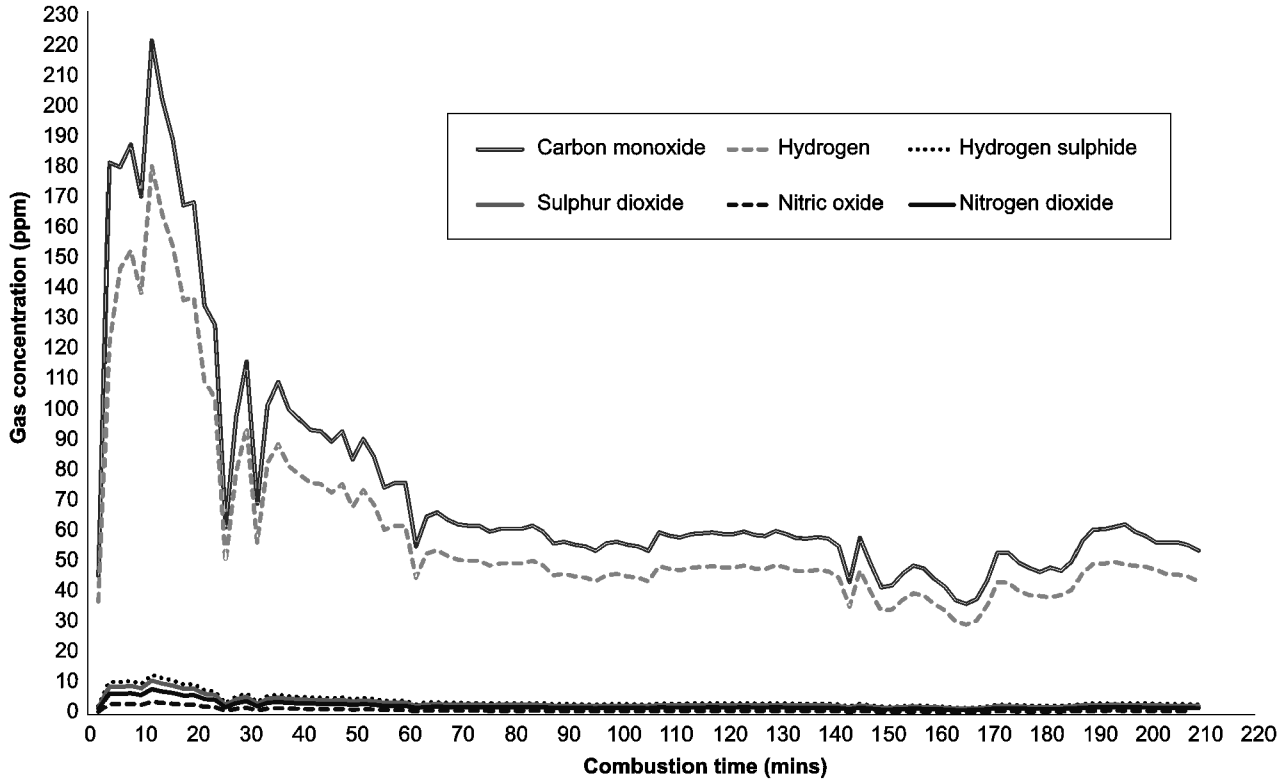

Figure 4: Variations of low concentration emissions in the flue gas

for 7 hours which makes it ideal for domestic applications. The standard enthalpy of formation of the briquettes was estimated as -1619.3kJ/mol.

The flue gas produced from this reaction consisted of 2.13 vol% CO_2, 74 ppm CO, 4.32 ppm H_2S ,1.34 ppm NO, 3.67 ppm SO_2, 5.5 vol% water vapour (H_2O), 59.8 ppm hydrogen(H_2), 60.3 vol% nitrogen (N_2) and 12.8 vol% oxygen (O_2). The gas was mostly dominated by inert atmospheric nitrogen, oxygen, carbon dioxide and water vapour. The test results have shown that combustion of Eco- fuel briquettes emits less toxic emissions compared to fossil fuels based on controlled condition combustion and atmospheric combustion.

5. Recommendations

The effects of operating parameters on fuel briquettes combustion, such as gas velocity and excess air, and preheated air temperature and velocity may need to be investigated in details in order to model the combustion efficiency of the briquettes under given conditions. The empirical correlation suggested by Tabares *et.al* (2000) for estimating the ash content of the eco-fuel briquettes may need to be studied for various briquettes geometry.

Although eco-fuel briquettes burn cleanly within the acceptable OSHA emission exposure limits, consumers need to be educated of the health hazards associated with the exposure of combustion

gasses over prolonged periods, and without sufficient ventilation, in addition, combustion of eco-fuel briquettes using uncertified stoves may cause excessive emissions due air-fuel ratio imbalances.

Acknowledgement

The authors would like to acknowledge the National Research Foundation (NRF) of South Africa and Phumani Paper for the financial support. We would like to express our sincere appreciation to Prof Kim Berman and Ms Nthabiseng Phiri for promoting this study and financing the design and fabrication of the screw press. The professional and technical support from National Brands Limited (Pty) Ltd and the University of Johannesburg is greatly appreciated.

References

Debdoubi, A, El amarti, A., Colacio, E. (2005). Production of fuel briquettes from esparto partially pyrolyzed, Energy Conversion and Management, Vol.46, pp.1877–1884.

Demirbas, A., and Sahin, A., (1998), Evaluation of biomass residue: Briquetting waste paper and wheat straw mixtures. *Fuel Processing Technology*, Vol. 55, pp.175-183.

Granada E., Lopez Gonzelez L.M., Miguez J.L., and Moran J., (2002), Fuel lignocellulosic briquettes die design and product study. *Renewable Energy*, Vol. 27, pp.561-573.

Husain, Z., Zainac, Z. and Abdullah, Z., (2002), Briquetting of palm fibre and shell from the processing of palm nuts to palm oil. *Biomass and Energy*, Vol. 22, pp. 505-509.

Mani, S., Tabil, L.G. and Sokhansanj, S., (2006). Specific energy requirement for compacting corn stover. *Bioresource Technology*, Vol. 97, pp. 1420-1426.

Peters, M.S. and Timmerhaus, K.D., (1991). Plant Design and Economics for Chemical Engineers, 4th Edition, McGraw-Hill.

Raymer, A.K.P, (2006). A comparison of avoided greenhouse gas emissions when using different kind of wood energy. *Biomass and Bioenergy*, Vol. 30, pp.605-617.

Tabares, J.L.M, Ortiz, L., Granda E., and Viar F.P., (2000). Feasibility study of Energy use for densificated lignocellulosic (briquettes). *Fuel*, Vol. 79, pp. 1229-1237.

Wright D.A. and Welbourn P., (2002). Environmental toxicology, Cambridge University Press.

Yaman, S., SahanSahan, M., Haykiri-Acma, H., Sesen, K., and Kucukbayrak, S. (2001). Fuel briquettes from biomass–lignite blends. *Fuel Processing Technology*, Vol. 72, pp. 1–8.

Received 4 June 2012; revised 25 October 2013

Experimental study on natural convection greenhouse drying of papad

Mahesh Kumar
Mechanical Engineering Department, Guru Jambheshwar University of Science and Technology, Hisar, India

Abstract
In this paper, the convective heat transfer coefficients of papad for greenhouse drying under a natural convection mode are reported. Various experiments were conducted during the month of April 2010 at Guru Jambheshwar University of Science and Technology Hisar, India (29°5'5" N 75°45'55" E). Experimental data obtained for the natural convection greenhouse drying of papad was used to evaluate the constants in the Nusselt number expression by using simple linear regression analysis. These values of the constant were used further to determine the values of the convective heat transfer coefficient. The average value of a convective heat transfer coefficient was determined as 1.23 W/m^2 °C. The experimental error in terms of percent uncertainty was also evaluated.

Keywords: papad, papad drying, convective heat transfer coefficient, natural convection greenhouse

Nomenclature

A_t Area of tray, m^2
C Experimental constant
C_v Specific heat of humid air, J/kg °C
g Acceleration due to gravity, m/s^2
Gr Grashof number = $\beta g X^3 \rho_v^2 \Delta T/\mu_v^2$
h_c Convective heat transfer coefficient, W/m^2 °C
$h_{c,av}$ Average convective heat transfer coefficient, W/m^2 °C
K_v Thermal conductivity of humid air, W/m °C
m_{ev} Mass evaporated, kg
n Experimental constant
N Number of observations in each set
N_o Number of sets
Nu Nusselt number = h_c X/ K_v
Pr Prandtl number = $m_v C_v/K_v$
$P_v(T)$ Partial vapour pressure at temperature T, N/m^2
Q_e Rate of heat utilized to evaporate moisture, J/m^2 s
T_p Temperature of papad surface, °C
T_e Temperature just above the papad surface, °C
T_g Temperature inside the greenhouse, °C
t Time, s
ΔT Effective temperature difference, °C
X Characteristic dimension, m

Greek symbols

β Coefficient of volumetric expansion (K-1)
σ Standard deviation
γ Relative humidity (%)
λ Latent heat of vaporization, J/kg
μ_v Dynamic viscosity of humid air, Ns/m^2
ρv Density of humid air, kg/m^3

1. Introduction

Papad is an important oriental snack food item particularly popular in South and South-East Asian countries. Its preparation involves gelatinization of the flour of different pulses with water contents generally varying from 27% to 30% per kg of papad weight. The kneaded dough is made into balls and then rolled with the help of a rolling pin into a circular thin disc of 130 mm to 210 mm diameter of thickness varying from 0.4 mm to 0.7 mm. It is dried by different means to a moisture level of 14% to 15% (Math *et al.,* 2004; Velu *et al.,* 2004; Kumar *et al*., 2011; Parab *et al.,* 2012; Kamat and Yenagi, 2012; Teradal and Ravindra, 2013). Papad drying involves removal of moisture in order to preserve it. Though the preservation for enhanced life is the primary reason for drying, it also brings substantial reduction in weight and volume.

Papad drying is basically a heat and mass transfer process in which heat from the surrounding air and the sun transfers to the papad surface by different heat transfer modes. A part of this heat travels to the interior of papad and removes moisture from the interior to its surface by heat transfer taking the latent heat of vaporization. The remaining part of heat is utilized to increase the papad surface temperature which causes evaporation of the moisture to the surrounding air in the form of sensible heat.

Open sun drying is the most primitive (traditional) method of papad drying which is weather dependant and also prone to microbial and other contamination. In spite of many disadvantages, open sun drying is still practiced in places throughout the world. Although the hot air industrial driers are available to get the good quality of the product, they consume large amount of energy. The scarcity of fossil fuels, steep rise in the energy cost, and environmental pollution are the driving factors in the use of energy efficient and renewable drying processes. Solar energy is an important alternative source of energy and preferred to other energy sources because it is abundant, non-pollutant, and inexhaustible. Also, it is environmentally benign, cheap, and renewable which can be effectively used for drying purposes, if harvested properly. An advanced and alternative technique to the traditional method is greenhouse drying, in which the product is placed in trays and receives solar radiation through the plastic cover, while moisture is removed by natural convection or forced air flow. The uses of appropriate greenhouse dryers lead to reduction of drying time interval as well as improve the quality of the product in terms of texture, colour and taste. Furthermore, the contamination by insects, microorganisms, and bacteria can be prevented (Esper and Muhlbauer, 1998; Condori *et al.,* 2001; Tiwari, 2003; Kadam *et al*., 2011; Kumar, 2013).

The convective heat transfer coefficient is an important parameter in drying rate simulation, since the temperature difference between the air and the product varies with this coefficient (Anwar & Tiwari, 2001).The convective heat transfer coefficient depends on the physical properties of the humid air surrounding the papad and the temperature difference between the papad surface and the air. Papad research has been carried out by various workers relating to its diametrical expansion, water and oil absorption, chemical composition, texture, flavour, quality etc. (Bhattacharya & Narasimha, 1999; Math *et al*., 2004; Velu *et al.,* 2004; Nazni & Pradheepa, 2010; Parab *et al*., 2012; Veena *et al.,* 2012). Kumar *et al*., (2011) evaluated the convective heat transfer coefficients of papad drying under open sun and indoor forced convection conditions. The average values of convective heat transfer coefficients under open sun and forced convection drying modes were reported to be 3.54 W/m^2 ^{o}C and 1.56 W/m^2 ^{o}C respectively. Recently, Kumar (2013) evaluated the convective and evaporative heat transfer coefficients of papad under forced convection greenhouse mode. The average values of convective and evaporative heat transfer coefficients were determined as 0.759 W/m^2 ^{o}C and 23.48 W/m^2 ^{o}C respectively.

The usage of greenhouse for papad drying under natural convection mode is a new approach in papad preservation. The present study has been undertaken to evaluate the convective heat transfer coefficient of papad for greenhouse drying under natural convection. This research work would be helpful in designing a dryer for drying papad to its optimum storage moisture level of about 14% to 15%.

2. Materials and methods

2.1 Experimental set-up and instrumentation

A roof type even span greenhouse of 1.2×0.8 m^2 effective floor area was fabricated of PVC pipe and an ultraviolet film covering of thickness 200 microns. The central height and the walls were

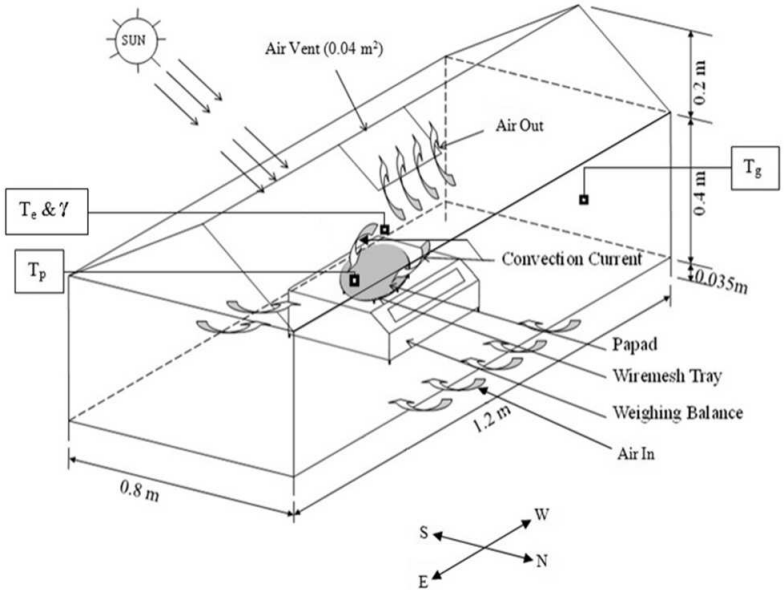

Figure 1: Schematic view of the experimental unit

maintained as 0.6 m and 0.4 m respectively. An air vent with an effective opening of 0.04 m^2 was provided at the roof for natural convection. The schematic view of the experimental unit for greenhouse drying in the natural convection mode is shown in Figure 1 and its photograph is shown in Figure 2.

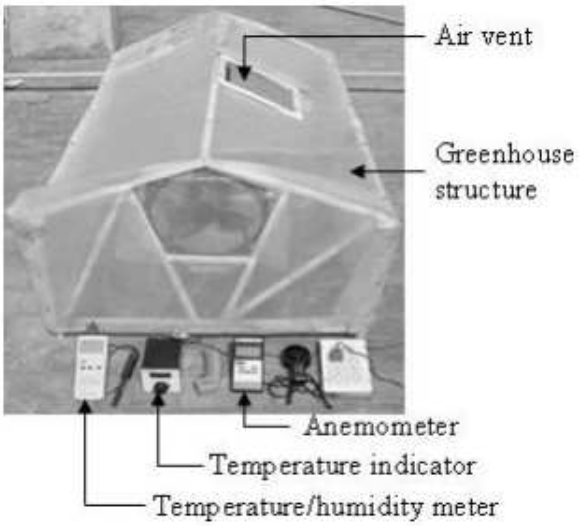

Figure 2: A photograph of an experimental unit for papad drying

A circular shaped wire mesh tray of diameter 0.180 m was used to accommodate the papad for single layer drying. It was kept directly over the digital weighing balance of 6 kg capacity (model TJ-6000, Scaletech, made in India) having a least count of 0.1 g. The papad surface temperature (T_p) and air temperature at different locations were measured by calibrated copper-constantan thermocouples connected to a ten channel digital temperature indicator with a least count of 0.1 °C (an accuracy of ±0.1%). The relative humidity () and the temperature just above the papad surface (T_e) was measured by a digital humidity/temperature meter (model Lutron-HT 3006, made in Taiwan). It had a least count of 0.1% relative humidity (an accuracy of ±3% on the full scale range of 10% to 95% of relative humidity) and 0.1 °C temperature (an accuracy of ± 0.8 °C on the full scale range of 50 °C).

2.2 Sample preparation and experimental observations

Papad was prepared by taking the flour of moong bean (Indian trade name – moong) and phaseolus mungo (Indian trade name – urad dal) mixed with 27.5% water content per kg of papad weight. The flour was purchased locally, and that fraction of flour which passed through an eighty five mesh (180 microns) British Standard sieve was used for making papad. The dough was kneaded and rolled in a circular shape of 0.7 mm thickness and 180 mm diameter with the help of pastry-board and pastry-roller. The freshly prepared papad of 23.5 g was used for each run of the greenhouse papad drying under natural convection.

Experiments were performed during the month of April 2010 at Guru Jambheshwar University of Science and Technology Hisar (29°5'5" N 75°45'55" E). The orientation of the greenhouse during the experimentation was kept east-west. Experimental setup was located on the open floor of a three-floor building to have a good exposure to the solar radiation. Each observation was taken for papad drying after half an hour time interval. The papad sample was kept in the wire mesh tray over the digital weighing balance. The moisture evaporated was calculated by taking the difference of mass of papad between two consecutive readings. The papad sample was dried till no variation in its mass was observed. In order to obtain accurate results, the experimentation procedure was repeated four times for each freshly prepared new papad sample of the same size (i.e., 180 mm diameter and 0.7 mm thickness) on consecutive days at the same timing. The initial mass of papad sample for each run of drying was kept constant (i.e., 23.5 g).

3. Theory

3.1 Thermal modelling

The convective heat transfer coefficient for evaporation under natural convection can be determined by using the following relations (Tiwari and Suneja, 1997; Kumar *et al.,* 2011):

$$h_c = \frac{K_v}{X} C(Gr\,\mathrm{Pr})^n \quad (1)$$

The rate of heat utilized to evaporate moisture is given as (Malik *et al.,* 1982):

$$\dot{Q}_e = 0.016\, h_c \left[P(T_p) - \gamma\, P(T_e)\right] \quad (2)$$

On substituting h_c from Eq. (1), Eq. (2) becomes

$$\dot{Q}_e = 0.016 \frac{K_v}{X} C(Gr\,\mathrm{Pr})^n \left[P(T_p) - \gamma\, P(T_e)\right] \quad (3)$$

The moisture evaporated is determined by dividing Eq. (3) by the latent heat of vaporization (λ) and multiplying the area of papad drying tray (At) and time interval (t).

$$m_{ev} = \frac{\dot{Q}_e}{\lambda} A_t\, t = 0.016 \frac{K_v}{X\lambda} C(Gr\,\mathrm{Pr})^n \left[P(T_p) - \gamma\, P(T_e)\right] A_t\, t \quad (4)$$

Let $0.016 \frac{K_v}{X\lambda} \left[P(T_p) - \gamma\, P(T_e)\right] A_t\, t = Z$

$$\frac{m_{ev}}{Z} = C(Gr\,\mathrm{Pr})^n \quad (5)$$

Taking the logarithm of both sides of Eq. (5),

$$\ln\left[\frac{m_{ev}}{Z}\right] = \ln C + n\ln(Gr\,\mathrm{Pr}) \quad (6)$$

This is the form of a linear equation,

$$Y = mX_0 + C_0 \quad (7)$$

Where

$Y = \ln\left[\frac{m_{ev}}{Z}\right]$,

$m = n$,

$X_0 = \ln(Gr\,\mathrm{Pr})$, and

$C_0 = \ln C$

Thus, $C = e^{C_o}$

Values of m and C_0 in Eq. (7) are obtained by using the simple linear regression method by using the following formulae:

$$m = \frac{N\sum X_0 Y - \sum X_0 \sum Y}{N\sum {X_0}^2 - \left(\sum X_0\right)^2} \quad (8)$$

and

$$C_0 = \frac{\sum {X_0}^2 \sum Y - \sum X_0 \sum X_0 Y}{N\sum {X_0}^2 - \left(\sum X_0\right)^2} \quad (9)$$

3.2 Experimental error

The experimental error was evaluated in terms of percent uncertainty (internal + external) for the moisture evaporated. The following two equations were used for internal uncertainty (Nakra and Choudhary, 1991):

$$U_I = \frac{\sqrt{{\sigma_1}^2 + {\sigma_2}^2 + \ldots {\sigma_N}^2}}{N_o} \quad (10)$$

and

$$\sigma = \sqrt{\frac{\sum\left(X - \bar{X}\right)^2}{N}} \quad (11)$$

Therefore, the percent internal uncertainty was determined using the following expression:

% internal uncertainty = (U_I/mean of the total observations) ×100 (12)

For external uncertainty, the least counts of all the instruments used in measuring the observation data were considered.

3.3 Computation technique

The average of papad surface temperature (T_p) and temperature just above the papad surface (T_e) inside greenhouse were calculated at half an hour time intervals for corresponding moisture evaporated. The physical properties of humid air were evaluated for the mean temperature (T_i) of T_p and T_e by using the following equations (Kumar *et al.*, 2011):

$$C_v = 999.2 + 0.1434T_i + 1.101\times 10^{-4}T_i^2 - 6.7581\times 10^{-8}T_i^3 \quad (13)$$

$$K_v = 0.0244 + 0.7673\times 10^{-4}T_i \quad (14)$$

$$\rho_v = \frac{353.44}{(T_i + 273.15)} \quad (15)$$

$$\mu_v = 1.718\times 10^{-5} + 4.620\times 10^{-8}T_i \quad (16)$$

$$P(T) = \exp\left[25.317 - \frac{5144}{(T_i + 273.15)}\right] \quad (17)$$

These physical properties of humid air were used for determining the values of the Grashof number (*Gr*) and Prandtl number (*Pr*). The values of constant *C* and exponent in the Nusselt number expression were determined by simple linear regression analysis and were used further to determine the values of convective heat transfer coefficient (h_c) from Equation (1) at the increment of every half an hour of observation.

4. Results and discussion

The experimental data obtained for papad drying under natural convection greenhouse mode are given in Tables 1–4.

Table 1: Observations for natural convection greenhouse drying of first papad sample (April 3, 2010)

Time	T_p (°C)	T_e (°C)	$m_{ev} \times 10^{-3}$ (kg)	γ (%)
9.30 am	36.6	42.4	3.1	35.6
10.00 am	40.0	45.0	2.6	38.2
10.30 am	41.4	45.2	1.8	36.0
11.00 am	44.4	46.8	1.3	35.3
11.30 am	50.2	51.5	1.1	36.4

Table 2: Observations for natural convection greenhouse drying of second papad sample (April 4, 2010)

Time	T_p (°C)	T_e (°C)	$m_{ev} \times 10^{-3}$ (kg)	γ (%)
9.30 am	37.8	42.8	2.8	36.8
10.00 am	41.2	43.8	2.5	39.4
10.30 am	42.6	44.0	2.0	37.2
11.00 am	45.6	45.6	1.5	36.5
11.30 am	51.4	50.3	1.0	37.6

Table 3: Observations for natural convection greenhouse drying of third papad sample (April 5, 2010)

Time	T_p (°C)	T_e (°C)	$m_{ev} \times 10^{-3}$ (kg)	γ (%)
9.30 am	38.0	42.0	2.9	37.0
10.00 am	41.4	44.0	2.6	39.6
10.30 am	42.6	44.2	2.2	37.4
11.00 am	45.8	45.8	1.2	37.5
11.30 am	51.8	50.2	1.0	37.8

Table 4: Observations for natural convection greenhouse drying of fourth papad sample (April 6, 2010)

Time	T_p (°C)	T_e (°C)	$m_{ev} \times 10^{-3}$ (kg)	γ (%)
9.30 am	37.2	42.6	3.0	36.2
10.00 am	40.6	44.4	2.7	38.8
10.30 am	42.0	44.6	1.9	36.6
11.00 am	45.0	46.2	1.4	35.9
11.30 am	50.8	50.9	1.1	35.1

The data given in Tables 1–4 were used to determine the values of constant and exponent *n* in the Nusselt number expression by simple linear regression analysis. Then the values of constant *C* and exponent *n* were considered further for determining the values of the convective heat transfer coefficient by Eq. (1). The values of constants (*C* & *n*) and the convective heat transfer coefficients for papad drying during natural convection greenhouse drying mode are presented in Table 5. The ranges of Grashof number were also given. The product of Grashof and Prandtl number indicates that the entire drying of papad for natural greenhouse mode falls within a laminar flow, because *Gr* Pr $\leq 10^7$(Holman, 2004).

The values of constant and exponent were found to vary from 0.906 to 0.925 and 0.144 to 0.155 respectively. The convective heat transfer coefficients were observed to vary from 1.08 W/m^2 °C to 1.40 W/m^2 °C (Table 5). It was observed that different values of the convective heat transfer coefficient were obtained for similar papad sample dried on consecutive days. This variation could be due to change in operating conditions on each day.

It is observed from Tables 1–4 that the rate of moisture removal increases initially and then decreases for a given day. This can be explained in terms of the convective heat transfer coefficient. The variation of convective heat transfer coefficients with respect to drying time is illustrated in Figure 3. It can be seen from Figure 3 that the values of convective heat transfer coefficient decreases as the drying period progresses for the entire papad sample on each day. The average values of constants (&) and the convective heat transfer coefficient were also calculated which are presented in Table 6.

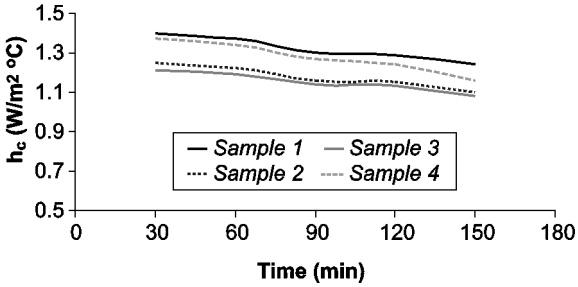

Figure 3: Variation of h_c versus drying time

Table 6: Average values of constants and the convective heat transfer coefficient

C	*n*	$h_{c,av}$ (W/m^2 °C)
0.920	0.149	1.23

Table 5: Values of experimentally evaluated parameters and the convective heat transfer coefficients

c	*n*	*Gr*	Pr	h_c (W/m^2 °C)
First Papad Sample (April 3, 2010)				
0.924	0.154	1.598×10^6 – 4.403×10^6	0.695 – 0.696	1.24 – 1.40
Second Papad Sample (April 4, 2010)				
0.925	0.146	1.543×10^6 – 4.288×10^6	0.695 – 0.696	1.10 – 1.24
Third Papad Sample (April 5, 2010)				
0.925	0.144	1.594×10^6 – 4.242×10^6	0.695 – 0.696	1.08 – 1.21
Fourth Papad Sample (April 6, 2010)				
0.906	0.155	1.102×10^6 – 3.862×10^6	0.695 – 0.696	1.16 – 1.37

The percent uncertainty (internal + external) was evaluated in the range of 33.71% to 38.92% for the natural convection greenhouse papad drying and the different values of the convective heat transfer coefficients were found to be within this range. The experimental percent uncertainties for papad drying under natural convection greenhouse mode are presented in Table 7. To show the variability of the convective heat transfer coefficients values from its true value (or error free value) SPSS software (Statistical Package for the Social Sciences, version 16.0) has been used which provided error bars with 95% confidence interval. The error bars for the convective heat transfer coefficients are illustrated in Figure 4.

Table 7: Experimental percent uncertainties

Sample number	*Internal uncertainty (%)*	*External uncertainty (%)*	*Total uncertainty (%)*
First	38.52	0.4	38.92
Second	33.31	0.4	33.71
Third	38.12	0.4	38.52
Fourth	36.16	0.4	36.56

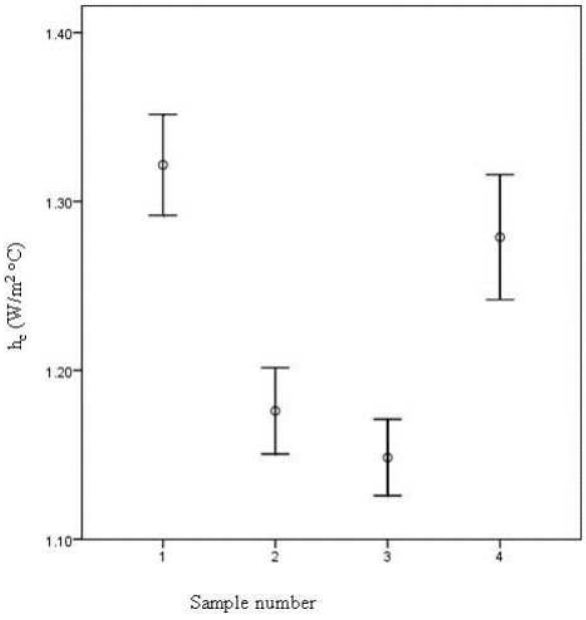

Figure 4: Error bars for the convective heat transfer coefficients

5. Conclusions

The research reported herein was set forth in order to evaluate the convective heat transfer coefficients for natural convection greenhouse drying of papad. The experimental data was analysed by using Nusselt number expression with the help of simple linear regression analysis. The average values of constant and exponent in the Nusselt number expression were found to be 0.920 and 0.149 respectively. The values of convective heat transfer coefficient were observed to vary from 1.08 W/m^2 °C to 1.40 W/m^2 °C. The average value of convective heat transfer coefficient for papad drying under natural convection greenhouse mode was found to be 1.23 W/m^2 °C. The experimental errors were evaluated within range of 33.71% to 38.94%. This research work would be helpful in designing a dryer for drying papad to optimum moisture level for retaining its quality during storage period.

References

Anwar, S.I. and Tiwari, G.N. (2001). Evaluation of convective heat transfer coefficient in crop drying under open sun drying conditions. *Energy Conversion Management*, 42(5): 627-637.

Bhattacharya, S. and Narasimha, H.V. (1999). Characterization of papad from different blends of cereals with blackgram. *Journal of Food Quality*, 22(2): 157-166.

Condori, M., Echazu, R. and Saravia, L. (2001). Solar drying of sweet pepper and garlic using the tunnel greenhouse drier. *Renewable Energy*, 22(4): 447-460.

Esper, A. and Muhlbauer, W. (1998). Solar drying-an effective means of food preservation. *Renewable Energy*, 15: 95-100.

Holman, J.P. (2004). Heat transfer, Tata McGraw Hill, New Delhi.

Kadam, D.M., Nangare, D.D., Singh, R. and Kumar, S. (2011). Low-cost greenhouse technology for drying onion (Allium Cepa L.) slices. *Journal of Food Process Engineering*, 34: 67-82.

Kamat, S. and Yenagi, N. (2012). Evaluation of indigenous technology of preparation of papad with special reference to cereals and millets. *Indian Journal of Traditional Knowledge*, 11(1): 123-133.

Kumar, M. (2013). Forced convection greenhouse papad drying: an experimental study. *Journal of Engineering, Science and Technology,* 8(2): 177-189.

Kumar, M., Khatak, P., Sahdev, R.K., and Prakash, O. (2011). The effect of open sun and indoor forced convection on heat transfer coefficients for the drying of papad, *Journal of Energy in Southern Africa*, 22(2): 40-46.

Malik, M.A.S., Tiwari, G.N., Kumar, A., and Sodha, M.S. (1982). Solar Distillation. Pergamon Press, Oxford.

Math, R.G., Velu, V., Nagender, A., and Rao, D.G. (2004). Effect of frying conditions on moisture, fat, and density of papad. *Journal of Food Engineering*, 64(2): 429-434.

Nakra, B.C. and Choudhary, K.K. (1991). Instrumentation, measurement and analysis, Tata McGraw- Hill Publishing Co, New Delhi.

Nazni, P. and Pradheepa, S. (2010). Physico-chemical analysis and organoleptic evaluation of papads prepared from jowar millet flour. *International Journal of Current Research*, 3: 33-37.

Parab, D.N., Dhalagade, J.R., Sahoo, A.K., and

Ranveer, R.C. (2012). Effect of incorporation of mushroom (Pleurotus sajor-kaju) powder on quality characteristics of papad (Indian snack food). *International Journal Food Science Nutrition,* 63(7): 866-870.

Teradal, D. and Ravindra, U. (2013). Utilization of elite cowpea (Vigna unguiculata (L.) walp) genotypes in the preparation of papad and storage studies. *Asian Journal of Bio Science*, 8(1): 72-75.

Tiwari, G.N. (2003). Greenhouse technology for controlled environment, New Delhi, Narosa Publishing House, India.

Tiwari, G.N. and Suneja S. (1997). Solar thermal engineering systems, New Delhi, Narosa Publishing House.

Veena, B., Reddy, B.S., and Sharan, S. (2012). Effect of incorporation of soya flour on the quality of papad. *Journal of Biology, Agriculture and Healthcare,* 2(5): 119-126.

Velu, V., Balaswamy, K., Nagender, A., and Rao, D.G. (2004). Effect of various ingredients and additives on papad. *Food Research International*, 15(2): 78-88.

Received 20 February 2012; revised 10 October 2013

Dirt analysis on the performance of an engine cooling system

Yashvir Singh
Mechanical Engineering Department, University of Petroleum and Energy Studies, Uttarakhand, India

Nishant Kr. Singh
Mechanical Engineering Department, Hindustan College of Science and Technology, Uttar Pradesh, India

Abstract
This present work looked at the effect of sand blocking the heat transfer area of the radiator and its effect on the engine coolant through the conduct of experiments and a mathematical model developed. The results indicated that the percentage area covered resulted in a proportional increase of the inlet and outlet temperatures of the coolant in the radiator. The mathematically model developed also predicted the experimental data very well. Regression analysis pointed out that every 10% increase area of the radiator covered with silt soil resulted in an increase of about 1.7°C of the outlet temperature of the radiator coolant. Similarly, using mud as a cover material, 10% of the area covered of the radiator resulted in an increase of about 2°C of the outlet temperature of the radiator coolant. Statistical analysis pointed to the fact that the result obtained for mud, silt and the mathematical model were not significantly different. Thus, irrespective of the type of material that blocks the radiator surface area, the coolant rises proportional of the radiator covered.

Keywords: radiator, silt, mud, coolant.

1. Introduction

When new engines are developed, they will be expected to operate under severe conditions and demanding load profiles as studied by Kem and Abros (1997), thus, increasing the demand of effective engine cooling systems. The automotive industry is continuously involved in a strong competitive market to obtain the best automobile design in multiple aspects. Some of the aspect includes performance, low fuel consumption, aesthetics, safety, cheaper and low maintenance.

According to Oliet *et al*., (2007), the air-cooled heat exchangers found in a vehicle radiator, Air-Conditioning (AC) condenser, evaporator and charge air cooler, has an important role in its weight and also in the design of its front-end module. In addition, it has a strong impact on the car aerodynamic behaviour. Looking at these challenges, the design process is optimized to obtain the optimum design.

The high working temperatures of the internal combustion engine which are the cause of its high efficiency are at the same time a source of great practical challenge in construction and operation. Moreover, there are challenges in obtaining materials capable of continuously enduring the high temperatures to which the cylinder, piston and valves are subjected to, while at the same time retaining sufficient strength to withstand the high working loads (Pulkrabek, 1997). The maximum temperature attained during combustion is approximately equal to the melting point of platinum, and the temperature even of the exhaust gas is above that of melting point of aluminium. Thus, it is essential that heat be abstracted from the combustion chamber at a sufficient rate to prevent a dangerous temperature being reached. Unfortunately, it is quite impossible to prevent the hot gas from flowing over the metal surfaces. Excessive cooling also prevents proper vaporization of the fuel, leading to further waste. In addition, it may lead to dilution of the crankcase oil by un-vaporized fuel, which gets down past the piston. On the other hand, a high operating temperature changes weight and reduces volumetric efficiency (VE) on account of the excessive heating of the incoming charge. Consequently, there is reduction of output power.

Over the years there have been increasing demands on the engine cooling system of a car. This has been caused by a steady increase in engine

output; combined with a reduction in the size of the cooling inlets and an increase in auxiliary components (Mudd, 1972). A water-cooling system is employed in almost every new car. The water coolant passes through the engine extract heat around the combustion chamber and dissipates the heat in the radiator. The radiator transfer heat from the coolant to the air flowing through the fins of the radiator. The air flowing is driven by a combination of the forward motion of the car and from a fan enclosed in a shroud attached to the radiator.

The basic requirement of a radiator is to provide a sufficiently large cooling area for transmission of heat from the coolant to the air. The construction of the centre of the radiator or core varies, but in general the water passages terminate at a header tank at the top of the radiator, and a smaller collecting or lower tank at the bottom. In addition to an opening which enables the cooling system to be topped up, the header tank allows for expansion and contraction of the coolant within the system (Kiatsiriroat, 2004). The trend towards low bonnet lines has led to the adoption by some vehicle manufacturers of a cross-flow radiator, the water tubes being placed cross-wise with a small collection tank at each side, and a separate header tank. The alternative to a cross –flow would be to have a large number of short vertical tubes, but this would increase the amount of soldering and hence the chance of leakage (Nuntapha and Kiatsiriroat, 2004).

The main objective of this research is to look at the critical quantification of dirt on the radiator and its effect on the engine performance. The focus will be to look at the effect of mud or silt on the radiator fins and its impact on temperature variation in the inlet and outlet of the radiator hoses. The study will look at the way forward to minimize overheating.

2. Materials

2.1 Engine

The engine used for the experiments was the four-cylinder four stroke engine shown in Figure 1. The engine is a water cooled engine with a tank capacity of 5.5 litres. It is a petrol engine which has a compression ratio of 9.8 to 1 and operates on the Otto-cycle.

2.2 Radiator

The radiator of the engine was a General Motors' serpentin-fin cross-flow type of size 65 mm × 35 mm in length and breadth respectively. The numbers of tubes were one row of 66 tubes with a thickness of 2 mm. The fins were copper made with a thickness of 0.5 mm, a height of 16 mm and spaced 3 mm apart.

2.3 Thermometer

Two different types of thermometers were used for the experiment. Two thermocouple probes were used to read the input and the output temperatures coolant in the radiator. The thermocouple was manufactured by Cola-Parma Instrument Company with model number 8110-10 and an accuracy of 0.10 °C. A mercury-in bulb thermometer was used to measure the ambient temperature.

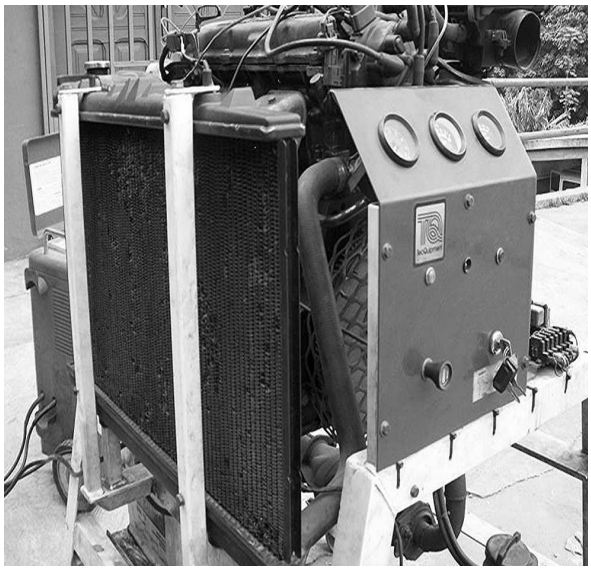

Figure 1: Engine for experimental setup

2.4 Covering material

Two different soil types were used. Silt and clay soil were chosen for the experiment because of their ability to stick to the radiator surface area.

3. Experimental setup

The specifications for the engine used are shown in Table 1.The engine was fitted with two thermocouple probes to read the inlet and outlet temperature of the water in and out of the radiator. The radiator was first cleaned to get rid of all particles trapped in the fins and on the engine. The rotational speeds of the engine and the fan speed were held constant throughout the experiment. The effective heat transfer area of the radiator was divided into ten (10) equal parts representing 10% of the effective heat transfer area. The effective heat transfer area was then partially covered with either mud or silt soil to the required percentage before running the engine. The engine was run for about fifteen (15)

Table 1: Specifications of the engine

Year	2003
Manufacturer	Nissan
Engine capacity	1597 cc
Engine type	GA 16
No. of cylinders	4/DOHC
Compression ratio	9.8:1
Cooling system capacity	5.5 litres of capacity

minutes to attain stable conditions before readings were taken.

For each set-up, three readings were taken at intervals of two minutes. After each experiment, the radiator was removed and washed to get rid of all the sand particles and then dried in open air. Each experiment was repeated three times according to the random sample technique adopted.

3.1Radiator heat transfer model

There are two common models available in the literature for analysing the heat transfer process in a radiator. The two methods are:

- Log mean temperature difference; and
- Effectiveness-Number of heat transfer units method.

In modelling, the radiator and the □-NTU was used because the focus of the work is on the outlet and inlet temperature of the water after the effective heat transfer area is then partially covered with either clay or silt soil to the required percentage before running the engine. The model was developed to predict the outlet temperature of the coolant from the radiator given the dimensions of the radiator, the flow rates of the fluids and the cooling load. In order to solve the analytical model, the following assumptions were made:

(i) Constant coolant flow rate and fluid temperatures at both the inlet and outlet temperatures, the system operated at a steady state
(ii) There were no phase changes in the coolant
(iii) Heat conduction through the walls of the coolant tube was negligible
(iv) Heat loss by coolant was only transferred to the cooling air, thus no other heat transfer mode such as radiation was considered
(v) Coolant fluid flow was in a fully developed condition in each tube
(vi) All dimensions were uniform throughout the radiator and the heat transfer of surface area was consistent and distributed uniformly
(vii) The thermal conductivity of the radiator material was considered to be constant
(viii) There was no fluid stratification, losses and flow misdistribution.

The relevant equations are given from equation 1 to 7.

$$F_l = \pi R_f + \frac{F_h - 2R_f}{cos\alpha} \quad (1)$$

The radiator core frontal area, A_{fr} is given by:

$$A_{fr} = B_H B_W \quad (2)$$

Coolant tube frontal area, $A_{fr,t}$ is given by:

$$A_{fr,t} = Y_{CW} Y_l N_{Ct} \quad (3)$$

$$A_{fr,t} = Y_{CW} Y_l N_{Ct} \quad (3)$$

Fin heat transfer area, A_f, is given by:

$$A_f = 2.B_T F_T N_f Y_l N_P \quad (4)$$

The total heat transfer area on air side, A_a is given by:

$$A_a = A_f + 2N_{ct} Y_l N_f [(Y_{cl} - 2R_t) + (2\pi R_t)] \quad (5)$$

The total heat transfer area on coolant side, A_c is given by:

$$A_c = [2\pi(R_t - Y_t) + 2(Y_{cl} - 2R_t)] Y_l N_{ct} N_r \quad (6)$$

The total coolant pass area, $A_{p,c}$ is given by:

$$A_{p,c} = [\pi(R_t - Y_t)^2 + (Y_{cw} - 2Y_t)(Y_{cl} - 2R_t)] N_{ct} N_f \quad (7)$$

The heat transfer rate in the radiator is given by:

$$Q = \epsilon C_{min}(T_{ci} - T_{ai}) \quad (8)$$

Where C_{min} = minimum heat capacity rate.

The radiator thermal efficiency ε is defined as the ratio of the actual transfer rate from the hot fluid (coolant) to the cold fluid (air) in a given radiator to the maximum possible heat transfer rate. It is expressed as:

$$\varepsilon = Q/Q_{min} \quad (9)$$

The actual heat transfer balance equation at a steady state, which is defined in terms of energy loss on coolant side and energy gained on the air side is given by:

$$Q = C_c(T_{ci} - T_{co}) = C_a(T_{ao} - T_{ai}) \quad (10)$$

The heat capacity ratio is defined as the product of the mass flow rate and the specific heat of the fluid:

$$For\ air, C_a = m_a x C_{p,a} = A_a \rho_a V_a C_{p,a} \quad (11)$$

$$For\ water, C_c = m_c x C_{p,c} = A_c \rho_c V_c C_{p,c} \quad (12)$$

The heat capacity ratio is defined as the ratio of the smaller to the larger capacity rate for the two fluid streams and is expressed as:

$$C_r = \frac{C_{min}}{C_{max}} \quad (13)$$

Where C_{min} is the smaller of C_a and C_c.

$$For\ water, C_c = m_c x C_{p,c} = A_c \rho_c V_c C_{p,c} \quad (12)$$

The heat capacity ratio is defined as the ratio of the smaller to the larger capacity rate for the two fluid streams and is expressed as:

$$C_r = \frac{C_{min}}{C_{max}} \quad (13)$$

Where C_{min} is the smaller of C_a and C_c.

Hence, $C_{min}=C_a$ and $C_{max}=C_c$ (14)

It follows therefore that the heat transfer rate is given by:

$$Q = \epsilon C_a (T_{ci} - T_{ai}) \quad (15)$$

The number of heat transfer units (NTU) is the ratio of overall conductance UA to the smaller capacity rate C_{min}:

$$NTU = \frac{UA_{fr,r}}{C_{min}} = \frac{1}{C_{min}} \int U.dA_{fr,r_A} \quad (16)$$

The radiator effectiveness is defined as a function of both the NTU and the C_r by

$$\epsilon = 1 - \exp\{\frac{NTU^{0.22}}{C_r}[\exp(-C_r NTU^{0.78}) - 1]\} \quad (17)$$

Based on the equations outlined, the model was developed using MATLAB.

4. Results and discussions

Results obtained from the running of the experiments and comparing them with results of the model developed follow.

4.1 Mud as the cover material

As shown in Figure 2, the temperature of the coolant from the radiator increased with an increase in the area of the radiator covered. As the area covered increased, there was also a corresponding increase in the temperature of the coolant coming from the engine.

The highest temperature obtained for the coolant into the radiator was achieved when 100% of the radiator was covered. During the experiment it was noticed that the engine stopped running after a short time when the radiator was completely covered. This was due to the inability of the coolant from taking away enough heat from the walls of the engine thereby causing overheating and subsequently forcing the engine to stop running in order to prevent substantial damage to the engine.

At 80% coverage of the radiator, it was observed that the engine idling was not stable. The engine vibrated excessively. The water within the expansion tank began to overflow and the coolant tube was also observed to be very hot.

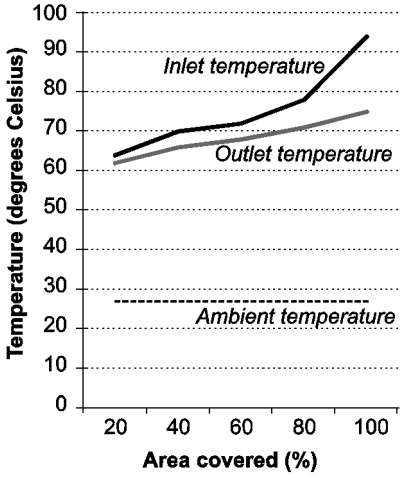

Figure 2: Variation of temperature with the area of radiator covered with the mud

4.2 Silt as the cover material

As shown in Figure 3, the results obtained using silt as the covering material were identical to that of clay as covering material. It can be observed that as the percentage area covered increased, there was a corresponding increase in the outlet and inlet temperatures of the coolant fluid. When 80% of the radiator surface was covered, it was observed that the engine idling was not stable and the engine vibrated excessively. Also, the water within the expansion tank began to overflow just as it was observed when clay was used as the covering material. At 100% covering, the engine could not stay on and after a short time of running the engine stopped running. The highest inlet temperature of the coolant recorded was 74 °C and this was when100 % of the radiator surface was covered.

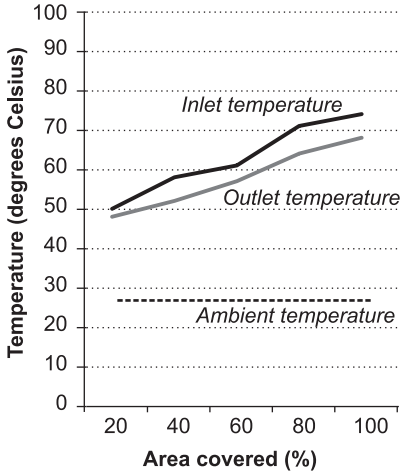

Figure 3: Variation of the temperature with the area of radiator covered with the silt

4.3 Discussions

When results obtained using mud were compared to that obtained using silt as shown in Figures 4 and 5, it was observed that the coolant temperature in the radiator was higher when mud was used as the cover material than when silt was used. This could be explained by the fact that mud stuck better on the radiator surface than silt. Because silt is loose, pocket of air space was observed on the covered radiator surface. This resulted in some amount of air passing through the air spaces to aid in the cooling of the coolant to a lower temperature than when mud was used. Since less heat was removed from the coolant, the resultant temperature of the coolant obtained from the radiator was also found to be higher for mud than silt as shown in Figure 5 below.

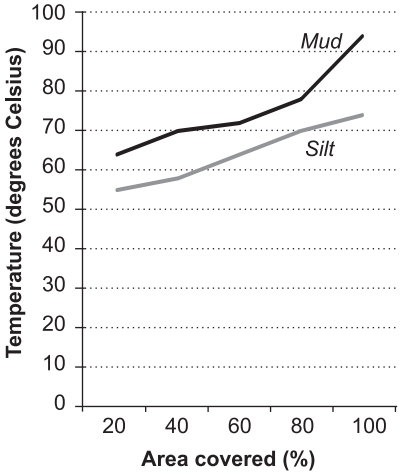

Figure 4: Variation of the temperature water inlet to the radiator with the area of radiator covered

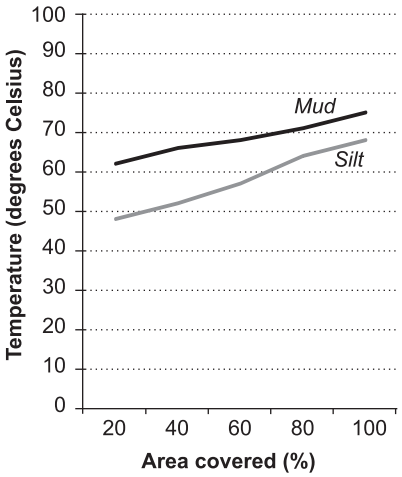

Figure 5: Variation of the temperature of the outlet water to the radiator with the area of radiator covered

Also, when the result of the model was compared to the results obtained for the experiment as shown in Figure 6), it was observed that the model predicted the heat transfer phenomenon quite well. In spite of the many assumptions, it was observed that the temperature of the coolant from the radiator was comparable to results obtained for the experiments. The model predicted closely, the results obtained when clay was the covering material better than silt. This is perhaps due to the fact that clay was a better coverage material than silt as already mentioned. It was generally observed that as the area of the radiator covered was increased, the temperature of the coolant from the radiator also increased considerably. This can be explained by the fact that the effective heat transfer area was reduced, thereby limiting the quantity of air admitted through the radiator for purposes of cooling the coolant. In all cases this trend of increasing outlet temperature of the coolant from the radiator was observed. As shown in the Figure 6, the temperature of the ambient air was found to be relatively constant. This therefore did not significantly affect the rate of heat transfer because the air mass was almost constant just as the thermal properties of the air.

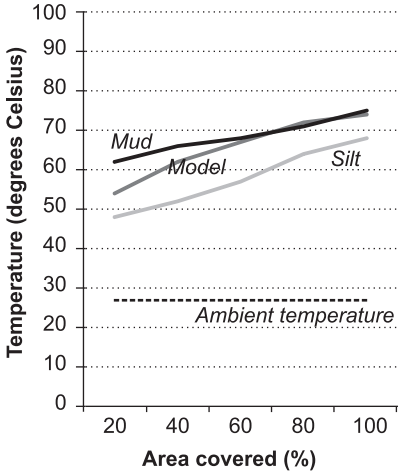

Figure 6: Comparison of model results of temperature of water out of the radiator with results obtained with silt and mud

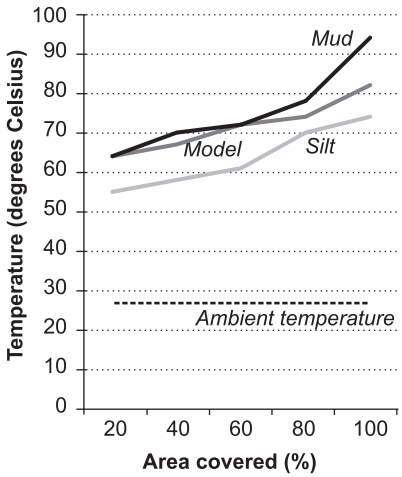

Figure 7: Comparison of results of inlet temperature of water into the radiator for the model with that of silt and mud

Comparing the temperature of the coolant into the radiator for three scenarios – the model, mud covering and silt covering, it can be observed in Figure 8 that the results obtained were similar. The model was able to predict the heat transfer process quite well. In all the three cases, the temperature of the coolant into the radiator increased as the area of the radiator covered also increased. This is due to the fact that when the surface area of the radiator is reduced by covering, less heat is taken out of the coolant, thus increasing the outlet temperature of the coolant from the radiator as observed. Since the coolant is not well cooled, it picks up heat from the engine which increases its temperature higher than expected before entering the radiator.

4.4 Regression and Anova analysis

Presented in Figures 8, 9 and 10 are the graphical regression relationships between the radiator coolant outlet temperatures and the proportion of the radiator surface area covered with mud, silt and Matlab simulation respectively. As expected, it can be seen that as the percentage of the radiator surface covered increases the outlet temperature of the radiator coolant increases.

Table 2 shows the regression models used to predict the outlet temperatures of radiator coolant from the percentage of area covered of the radiator. The three models were developed using silt and mud to cover the radiator. The Matlab model was a simulated model to evaluate the validity of the silt and mud models. All the three models predicted well and were statistically significant at a 1% probability level. The coefficient of determination (R^2) of the three models ranged from 0.98 to 0.99. At least 99% of the variation in the outlet coolant temperatures was explained by the percentage of the area covered of the radiator. For the silt model, for every 10% increase or decrease of the area covered of the radiator resulted in an average increase or decrease

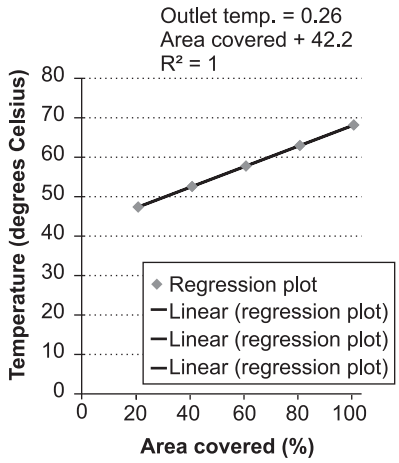

Figure 8: Regression relationship between radiator outlet temperature and the percentage of radiator surface area covered with mud

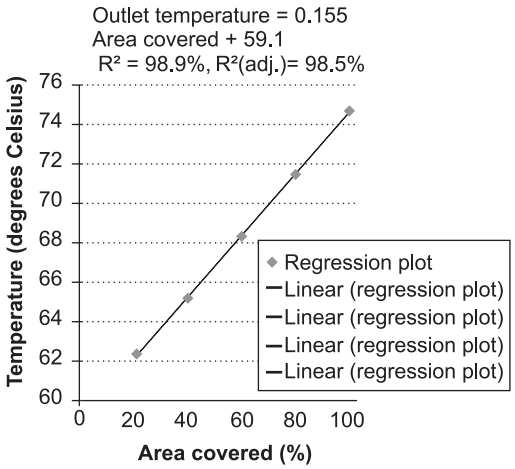

Figure 9: Regression relationship between radiator outlet temperature and the percentage of radiator surface area covered with silt

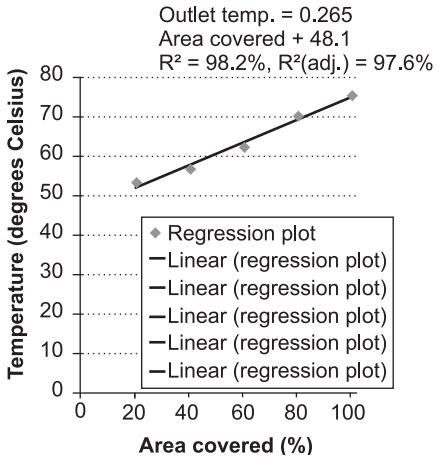

Figure 10: Regression relationship between radiator outlet temperature and the percentage of radiator surface area covered using Matlab simulation

Table 2: Models to predict outlet temperature (°C) of coolant from the Area covered of the radiator (%)

Model	Regression Equation	R^2	T-Test	P-Value
Mud	Outlet temp.(°C) = 59.1 + 0.155 area covered (%)	0.989	76.87	<0.001
Silt	Outlet temp.(°C) = 42.2 + 0.260 area covered (%)	0.991	26.61	<0.001
Matlab	Outlet temp.(°C) = 48.1 + 0.265 area covered (%)	0.982	22.32	<0.001

of about 1.7 degree Celsius of the outlet temperature of the radiator coolant. In the case of the mud model, a 10% increase or decrease of the area covered of the radiator resulted in about 2.1 degrees Celsius of the outlet temperature of the radiator coolant (Table 2). In the Matlab model, a change in 10% of the area covered of the radiator resulted in a change of about 2 degrees Celsius of the outlet temperature of the radiator coolant.

Analysis of variance (Anova) was conducted to find out if there were statistically significant differences among the three models (Table 3). As shown in Table 3, there were no statistically significant differences among the three models. This indicates that the Matlab model was consistent with the mud and silt models. It can also be said when the same amount of mud or silt covers the same area of a radiator the same temperature rise of the radiator coolant will result.

5. Conclusions

Experiments were successfully conducted on the radiator of a four cylinder diesel at base load. Two different soil types, namely silt and mud, were used as covering material to cover the heat transfer area of the radiator to determine the heat transfer process during the running of the engine. It was observed that the inlet temperature of the coolant in the radiator increased as the percentage area of the radiator covered increased. It was also observed that the outlet temperature of the coolant from the radiator increased monotonically with increases in the percentage area of the radiator covered. In both cases, at 80% coverage of the heat transfer area of the radiator the engine vibrated excessively and the idling was not stable. The engine stopped running after a short while. At 100% coverage the engine stopped running immediately after starting. This phenomenon was expected because as the effective transfer area of the radiator is reduced, less heat is taken out and thereby affecting the temperature of the coolant and hence the performance of the engine.

A mathematical model was developed to predict the heat transfer phenomenon. The model developed predicted the heat transfer so well. It was observed that the inlet temperature of the coolant in the radiator increased as the percentage area of the radiator covered increased. The outlet temperature of the coolant from the radiator also increased as the percentage of the area of the radiator increased. It was also observed that the heat transfer model developed agreed with the experimental results.

The analysis of variance results pointed to the fact that the results obtained for silt, mud and the mathematical model were not significantly different at 95% confidence interval. This point to the fact that, irrespective of the covering material, the effect of temperature rises will effectively be the same.

References

Kem, J. and Ambros. P. (1997). Concepts for a controlled Optimized Vehicle Engine Cooling System. Society of Automotive Engineers Publication, 971816, 357-362.

Oliet, C., Oliva, A., Castro, J., Perez-Segarra, C.D. (2007). Parametric studies on automotive radiators, *Applied Thermal Engineering,* 2033-2043.

Pulkrabek, W.W. (1997). Engineering Fundamentals of the Internal Combustion Engine, pages 270-280.

Mudd, S.C. (1972). Technology for Motor Vehicle Mechanics, Euston Road London, Oxford Press.

Kiatsiriroat, T. (2004). The application of automobile radiator in waste heat recovery process, Final Report, Energy Planning and Policy Office, Thailand.

Nuntaphan, A. and Kiatsiriroat,T. (2004). Performance of thermosyphon heat exchanger modified from automobile radiator, in: The 18th Conference of Mechanical Engineering Network of Thailand, Kon Kaen, Thailand.

Received 4 May 2012; revised 30 October 2013

Table 3: Analysis of variance (Anova) for comparison outlet temperatures based on the silt, mud and Matlab models

	Sum of squares	D_f	*Mean square*	*F-value*	*p-value*
Between groups	106246	2	53123	1425	0.225
Within groups	1230285	33	37283		
Total	1336531	35			

System and component modelling of a low temperature solar thermal energy conversion cycle

Shadreck M Situmbeko

Freddie L Inambao

University of KwaZulu-Natal, Howard College, Mechanical Engineering, Durban, South Africa

Abstract

Solar thermal energy (STE) technology refers to the conversion of solar energy to readily usable energy forms. The most important component of a STE technology is the collectors; these absorb the shorter wavelength solar energy (400-700nm) and convert it into usable, longer wavelength (about 10 times as long) heat energy. Depending on the quality (temperature and intensity) of the resulting thermal energy, further conversions to other energy forms such as electrical power may follow. Currently some high temperature STE technologies for electricity production have attained technical maturity; technologies such as parabolic dish (commercially available), parabolic trough and power tower are only hindered by unfavourable market factors including high maintenance and operating costs. Low temperature STEs have so far been restricted to water and space heating; however, owing to their lower running costs and almost maintenance free operation, although operating at lower efficiencies, may hold a key to future wider usage of solar energy. Low temperature STE conversion technology typically uses flat plate and low concentrating collectors such as parabolic troughs to harness solar energy for conversion to mechanical and/or electrical energy. These collector systems are relatively cheaper, simpler in construction and easier to operate due to the absence of complex solar tracking equipment. Low temperature STEs operate within temperatures ranges below 300oC. This research work is geared towards developing feasible low temperature STE conversion technology for electrical power generation. Preliminary small-scale concept plants have been designed at 500Wp and 10KWp. Mathematical models of the plant systems have been developed and simulated on the EES (Engineering Equation Solver) platform. Fourteen candidate working fluids and three cycle configurations have been analysed with the models. The analyses included a logic model selector through which an optimal conversion cycle configuration and working fluid mix was established. This was followed by detailed plant component modelling; the detailed component model for the solar field was completed and was based on 2-dimensional segmented thermal network, heat transfer and thermo fluid dynamics analyses. Input data such as solar insolation, ambient temperature and wind speed were obtained from the national meteorology databases. Detailed models of the other cycle components are to follow in next stage of the research. This paper presents findings of the system and solar field component.

Keywords: low temperature solar thermal energy, mathematical model, EEES computer simulations, working fluids, cycle configuration, component and system models

1. Introduction

Most naturally occurring energies such as light energy from the sun, chemical energy in fossil and biomass fuels, mechanical energy in hydro-streams of rivers and oceans, in tidal waves, and in wind etc., thermal energy in geothermal resources, and nuclear energy in nuclear fuels are present not in a readily usable form and sometimes presents a technical burden if an attempt is made to transport it in its natural form. Energy conversion systems allow us to transform the natural energy to conveniently usable, storable and transportable forms. This paper looks at the conversion of low temperature solar thermal energy to electrical energy.

STE technology refers to the conversion of shorter wavelength solar energy (400-700nm) to longer wavelength (about 10 times as long) heat energy. The most important component of a STE technology is the collectors which absorb and convert solar energy into electrical power, for example.

Currently some high temperature solar thermal energy (HTSTE) technologies for electricity production have attained technical maturity and are only hindered by unfavourable market factors including high maintenance and operating costs. Examples of HTSTE technologies include parabolic dish, parabolic trough, and power tower systems (Groenendaal, 2002).

Low temperature solar thermal energy (LTSTE) technologies have so far been restricted to water and space heating with little or no emphasis on power generation. Examples of applications include:

- Evaporation ponds for extraction of sea water salt;
- Concentrating brine solutions in leach mining and removing dissolved solids from waste streams;
- Domestic and process water heating;
- Preheating of ventilation air; and
- Crop drying as in drying of coffee beans and marigolds.

However, owing to their lower running costs and almost maintenance free operation, LTSTE technologies, although operating at lower efficiencies, may hold a key to future wider usage of solar energy.

Current research on LTSTE for power generation include solar thermal organic Rankine cycle, solar thermal Kalina cycle, Solar Chimney and SNAP (Groenendaal, 2002). Figure 1 shows schematic illustrations of the Solar Chimney, SNAP Plants, Organic Rankine and Kalina Cycles.

2. Feasibility study for development of low temperature solar thermal energy

LTSTE conversion technology typically uses flat plate and low concentrating collectors such as parabolic troughs to harness solar energy for conversion to mechanical and/or electrical energy. These collector systems are relatively cheaper, simpler in construction and easier to operate due to the absence of complex solar tracking equipment found in HTSTE systems. LTSTE operate within temperatures ranges below 300°C.

Figures 2 and 3 show two possible experimental setups. The general layout consists of the solar collector, heat exchangers, turbine-generator, pumps and piping. The first concept sketch shows the first experimental setup whereby the heat transfer fluid is pumped through the solar collector where it is heated and is then passed through the evaporator where heat is transferred to the working fluid. In the second experimental setup, as shown in the second concept sketch, the working fluid is directly heated and evaporated by a solar collector. Whereas the first setup has the advantage of eliminating one heat exchanger, the evaporator, and reducing the required piping, it presents other design challenges; for instance the solar collector must have the required corrosion resistance and be able to withstand higher pressures associated with the working fluid.

Preliminary small-scale concept plants have been designed at 500Wp and 10KWp, where the smaller model is intended as a laboratory experiment and the larger as a field experiment. The aim of this laboratory test is to get an insight in the experimental test setup and results recording and analyses as well as to implement any needed improvements. The field experimental setup will involve the 10kWp Low Temperature Solar Energy Conversion Model.

Designing the cycle involves optimally sizing its main components so as to attain the intended output. The main cycle components are the evaporator and condenser heat exchangers, and the turbine and pumps work devices, the solar collectors array and the generator. The other design aspect involves sizing the duct network so as to minimise both pressure and heat losses and determining the quantities

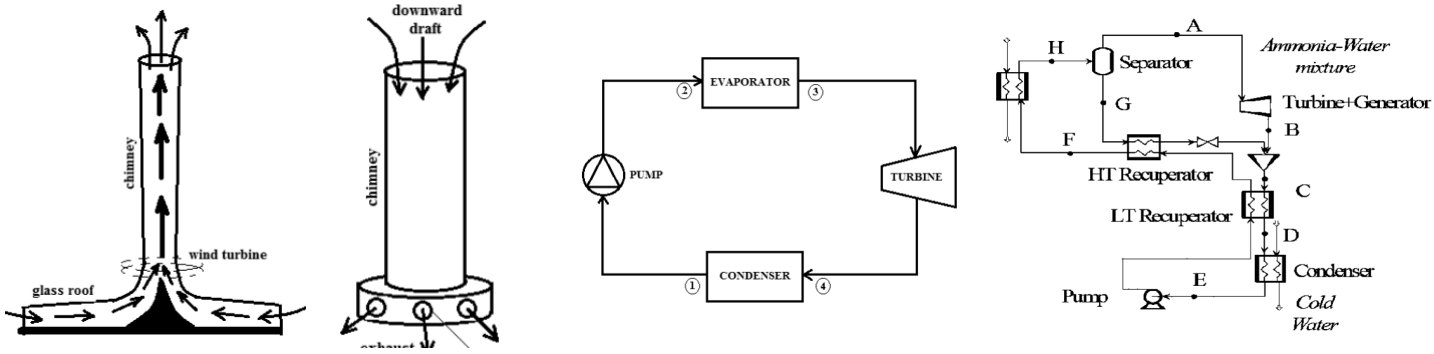

Solar chimney (Schlaich, 1995) *SNAP plant* *Organic Rankine Cycle (montaraventures.com)* *Kalina Cycle (www.eng.usf.edu)*

Figure 1: Examples of low temperature solar thermal energy technologies

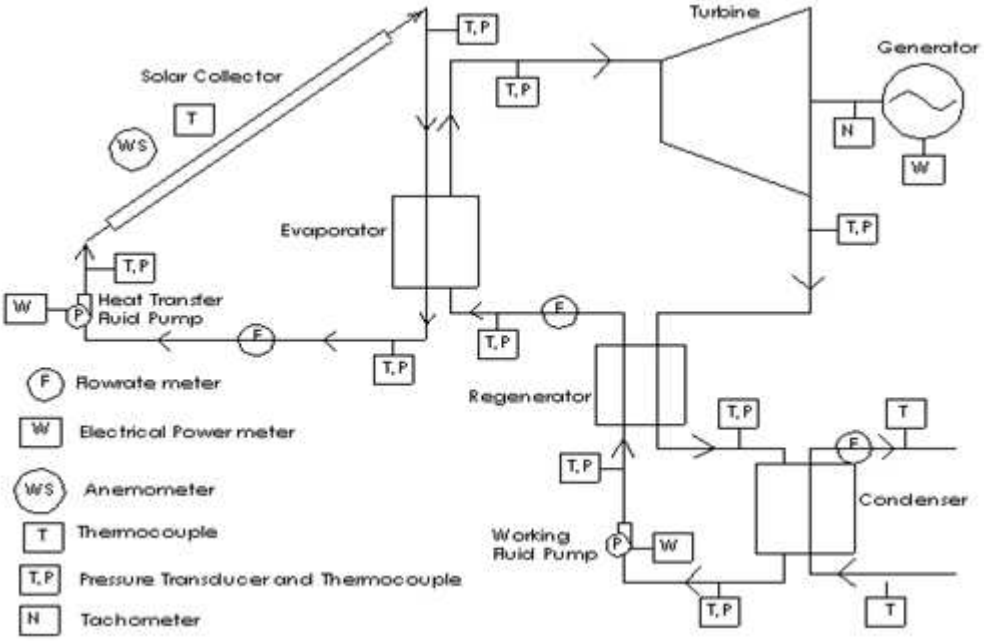

Figure 2: Experimental setup concept 1

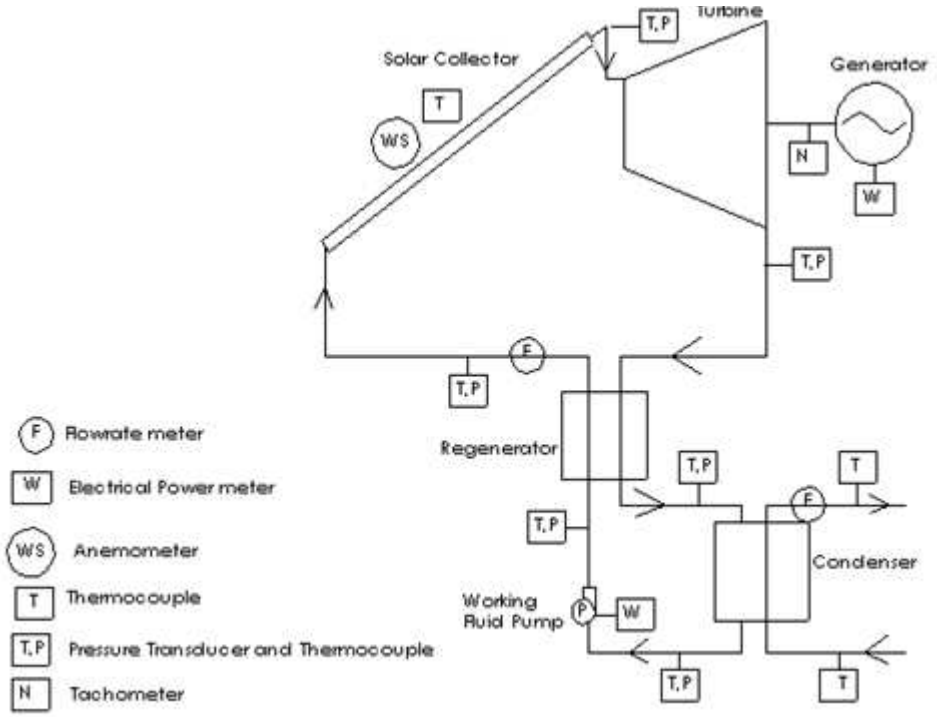

Figure 3: Experimental setup concept 2

of both the working and heat transfer fluids as well as specifying the type of insulation.

The solar field is an important aspect of this design as it involves not only determining the size of the field but also the layout of the solar collectors array.

The preliminary array design is based on the Solardome SA Solar Collector size 1840 x 1650 mm, giving area of 3.04 m^2 (www.solardome.co.za). The efficiencies of flat plate collector from Thermomax Industries (www.thermotechs.com) range from 35 to 50 % for domestic hot water with mean temperature $T_m \approx 55^oC$. Where T_m is the average temperature of fluid in the collector and is given by:

$$Tm = \frac{T_{in} + T_{out}}{2} \quad (1)$$

where T_{in} and T_{out} are respectively the solar collector inlet and outlet temperatures. The range of efficiencies for Rankine cycle operating at low to medium temperatures ranges from 9.9 to 14.1%

(Nishith, 2009). Taking averages the overall system efficiency could be taken as 5.1%. Thus the solar thermal energy available should be about 9.8kW$_{Th}$ for the laboratory model and 196kW$_{Th}$ for the field model. Durban Insolation data averages 4.328 kWh/m^2/day (www.gaisma.com). First approximations of the corresponding solar fields are shown in Table 1 and preliminary solar array layouts are shown in Figures 4 .

Table 1: First pass size estimates of the solar arrays

Parameter	*Lab. model (solar collector)*	*Field model (solar collector)*	*Units*
Output power	0.5	10	kW
ORC mean efficiency	12	12	%
Solar mean efficiency	42.5	42.5	%
Input power	9.80	196.08	kW
Durban insolation kWh/m^2/day	4.328	4.328	
Incident area	27	545	m^2
Solar collector area	3.04	3.04	m^2
No. of solar collectors	9	179	

3. Mathematical modelling

Mathematical models of the plant systems have been developed and simulated on the EES (Engineering Equation Solver) platform. Fourteen candidate working fluids and three cycle configurations have been analysed with the models. The analyses include a logic model selector through which an optimal conversion cycle configuration and working fluid mix is established.

3.1 First pass mathematical modelling (Situmbeko, 2011)

The first pass model gives an initial insight into the performance of the proposed energy conversion system design. This first pass model output together with the more detailed specifications of components for the proposed system design will yield a more detailed model with more realistic performance parameters that can now be incorporated in the design, development and validation of the physical model. In this work a more generalized model is first proposed as in Figure 6. This is then further customized to the thermo-physical properties of the different proposed working fluids. In particular a mathematical logic model is incorporated to assign an appropriate cycle configuration to each proposed working fluid.

The first pass model makes a number of assumptions such as:

- pumping and expansion efficiencies are assumed as hpump = 0.65, hturbine = 0.85
- modelling of heat exchangers at this stage is only performed as a thermal process to determine required input thermal energy and required exhaust thermal energy (detailed heat exchanger modelling will be done at a later stage)
- thermal losses in the cycle components and ducting are negligible;
- pressure head losses in the heat exchangers are negligible; and
- no work and no heat transfer occur in the valves, etc.

Three types of models can be identified with low temperature thermal cycles depending on the nature of the working fluid. Based on the fluids' T-s (temperature versus entropy) saturation curves these three types of energy conversion systems are: the conventional Rankine cycle, Rankine cycle with a recuperator and Rankine cycle with a superheater as shown in Figure 7. A summary of results of computer simulations of the first pass model is shown in Table 2.

3.2 Detailed component models: Solar field collector modelling

Detail modelling of a solar collector requires knowledge of the geometrical measurements and thermal

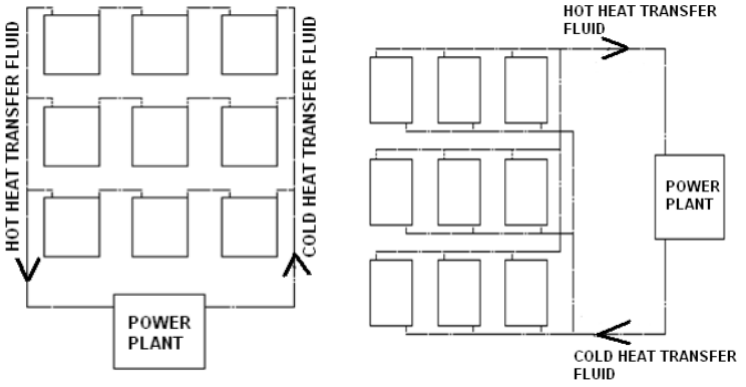

Figure 4: Two layouts options for 500 Wp solar field (requires 9 solar collectors with two layout options)

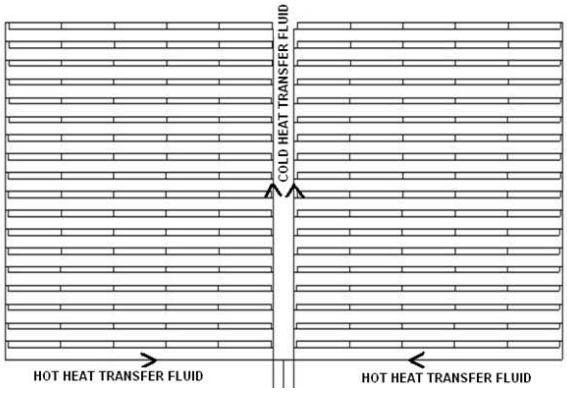

Figure 5: Possible layout for 10kWp solar field (requires 180 solar collectors)

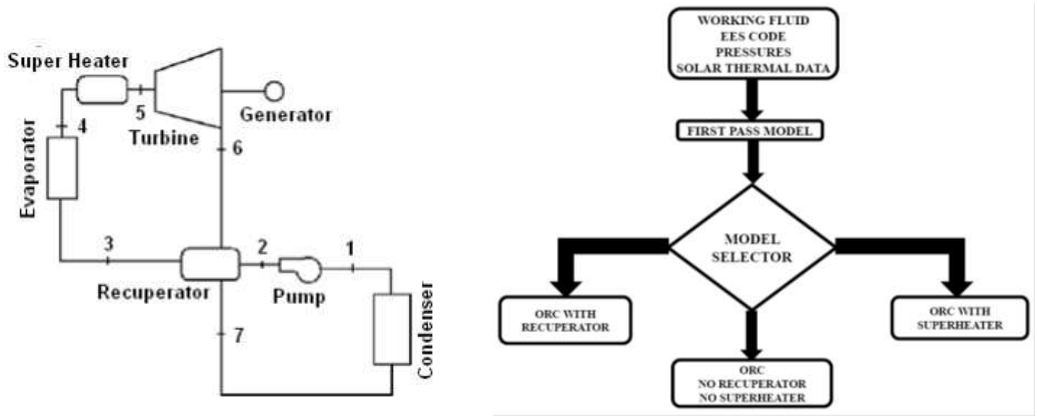

Figure 6: General configuration of a LTSTE technology and a Model Logic Selector

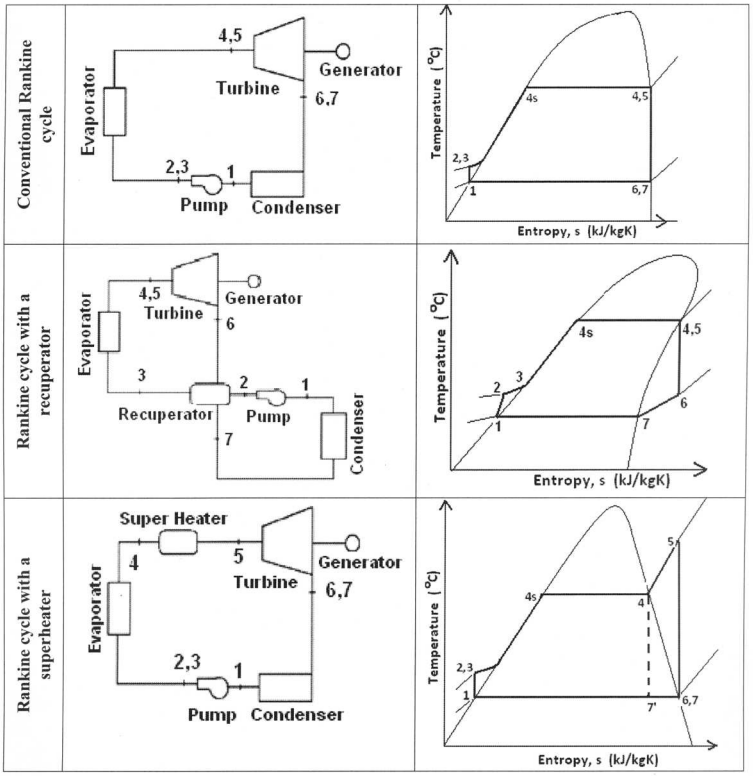

Figure 7: Three configuration options

properties of materials used in the construction. The process is based on carrying out an energy balance which can be either steady state or transient. A transient model is more useful when the solar data can be measured and fed synchronously to the simulation model.

Figure 8 shows the cross-section of a One-Riser-Pipe Solar Thermal Collector that was used to develop the energy balance represented in equations 2 to 6 below.

For the glass cover:

$$Q_{store,C} = Qin,C - Q_{conu,C\to a} - Q_{rad,C\to a} + Q_{conu,A\to C} + Q_{rad,A\to C} \quad (2)$$

For the absorber plate:

$$Q_{store,A} = Qin,A - Q_{conu,A\to C} - Q_{rad,A\to C} - Q_{cond,A\to F} - Q_{cond,A\to a} \quad (3)$$

For the heat transfer fluid:

$$Q_{cond,A\to F} = Q_{cond,F\to a} + Cth \quad (4)$$

For the storage tank:

$$Q_{store,T} = Qth - Q_{cond,T\to a} \quad (5)$$

Thermal efficiency:

$$\eta_{th} = \frac{\int Q_{th}dt}{A_c \int Gdt} \quad (6)$$

Table 2. Thermal efficiencies of different Organic Rankine Cycle configurations and different working fluids

Model type	*Working fluid*	*Q_dot_ r evaporato*	*Q_dot_ recuperator*	*Q_dot_ superheater*	*Power*	*eta_ therm*
		(kW)	(kW)	(kW)	(kW)	(%)
Rankine with recuperator no superheater	n-pentane	4.07	0.40	0	0.50	12.04
Conventional Rankine no recuperator no superheater	Benzene	4.68	0	0	0.53	11.11
Conventional rankine no recuperator no superheater	n-butane	4.56	0	0	0.54	11.60
Rankine with recuperator no superheater	n-hexane	3.75	0.61	0	0.46	12.10
Conventional Rankine no recuperator no superheater	Isobutene	4.31	0	0	0.52	11.72
Conventional Rankine no recuperator no superheater	R141b	2.60	0	0	0.30	11.30
Rankine with recuperator no superheater	Is pentane	3.90	0.38	0	0.49	12.20
Conventional Rankine no recuperator no superheater	R245fa	2.30	0	0	0.24	10.38
Rankine with recuperator no superheater	R113	1.64	0.16	0	0.20	11.89
Conventional Rankine no recuperator no superheater	R123	2.02	0	0	0.23	11.02
Rankine with superheater no recuperator	R22	2.50	0	0.21	0.33	12.01
Rankine with recuperator no superheater	Toluene	4.09	0.45	0	0.49	11.75
Rankine with superheater no recuperator	R134a	2.41	0	0.08	0.28	10.99
Rankine with superheater no recuperator	Water	23.29	0	2.57	2.80	10.81

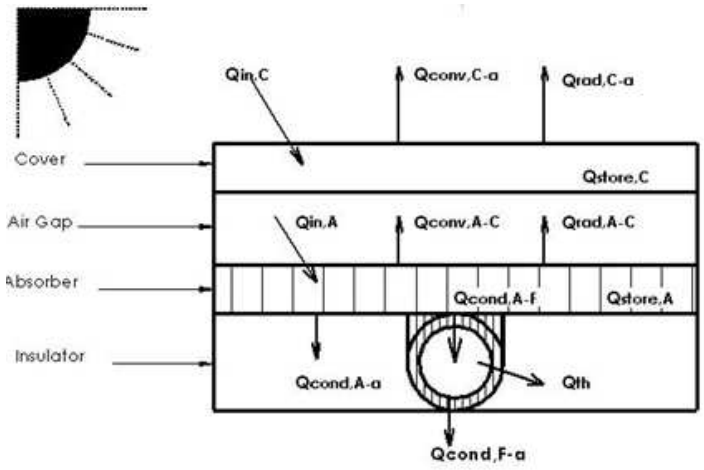

Figure 8: One pipe solar collector model

For the air gap the correlation used to determine the convective heat transfer coefficient is that given by Hollands et al (Duffie, 1991); for inclined parallel plates with a tilt angle of 0–75° which is given as:

$$Nu = 1 + 1.44\left[1 - \frac{1708(sin\ 1.8\beta)^{1.6}}{Racos\beta}\right]\left[1 - \frac{1708}{Ra\cos\beta}\right]^{+} + \left[\left(\frac{Ra\cos\beta}{5830}\right)^{1/3} - 1\right]^{+} \quad (7)$$

where the meaning of the + exponent is that only positive values of the terms in the square brackets are to be used (i.e., use zero if the term is negative); and the Nusselt number Nu and the Rayleigh number Ra are given by:

$$Nu = \frac{hL}{k} \text{ and } Ra = \frac{g\beta'\Delta TL^3}{\nu\alpha} \quad (8)$$

where:
h = heat transfer coefficient,
L = plate spacing
k = thermal conductivity

g = gravitational constant
β = volumetric coefficient of expansion (for an ideal gas, β=1/T)
ΔT = temperature difference between plates
ν = kinematic viscosity
α = thermal diffusivity

For laminar flow in circular pipes the correlation used is that given by Incropera (2007):

$$Nu_D \equiv \frac{hD}{k} = 4.36 \quad (9)$$
$$for\ uniform\ surface\ heat\ flux$$

$$Nu_D \equiv \frac{hD}{k} = 3.66 \quad (10)$$
$$forconstant\ surface\ temperature$$

For this case the transfer to the heat transfer fluid lies in between the two conditions and therefore the Nusselt number used is the average of the two.

For the Wind Convection Coefficients, Duffie (1991) recommend using:

$$h_W = \max[5, \frac{8.6V^{0.6}}{L^{0.4}}] \quad (11)$$

where V (m/s) is wind speed and L (m) is the cube root of the house volume.

The average hourly radiation can be estimated from the total daily radiation by using the following equation (Silva, 2011):

$$I = Hr_t \quad (12)$$

The coefficient to convert total daily radiation, H (Wh/m^2-day) to average hourly radiation I (W/m^2) is given by:

$$r_t = \frac{\pi}{24}(a + bcosw)\frac{cosw - cosw_s}{sinw_s - \frac{\pi w_s}{180}cosw_s} \quad (13)$$

where w is the hour angle and W_s is the sunset hour angle in degrees. The coefficients a and b are given by:

$$a = 0.409 + 0.5016\sin(w_s - 60)$$
$$b = 0.6609 - 0.4767sin(w_s - 60) \quad (14)$$

The model also requires inputs of ambient temperatures; these are included in Table 3.

Transient conditions
Considering the steady-state model above, corresponding transient models can be developed. These are however not used in the current model as the transiency is modelled into the time step segmented model.

Table 3: Hourly ambient temperatures for the modelled day (www.weather.com)

Time	*Temp. (°C)*	*Time*	*Temp. (°C)*	*Time*	*Temp. (°C)*
5am	20	1pm	26	9pm	23
6am	20	2pm	27	10pm	22
7am	20	3pm	26	11pm	21
8am	20	4pm	26	12am	21
9am	22	5pm	26	1am	21
10am	23	6pm	24	2am	20
11am	25	7pm	24	3am	20
12pm	25	8pm	23	4am	20

Storage model
The thermal storage model consists of an energy balance consisting of charging, discharging and thermal losses. In this model, however, only charging has been considered. The discharging and thermal losses will be considered at the time of coupling the solar cycle sub-model to the thermal conversion cycle sub-model. The charging model is given by the equations:

$$\dot{Q}_{tank} = \dot{m}_{wg} * Cp_{wg} * \left(T_{wg,out,30} - T_{tank}\right)$$

$$\dot{Q}_{tank} = m_{wg,tank} * Cp_{wg} * \left[\frac{T_{tank} - T_{wg,in,1}}{t_{cycle}}\right] \quad (15)$$

where:
$\dot{Q}_{tank}$ (J/s) is the heat transfer rate to the thermal storage;
$\dot{m}_{wg}$ (kg/s) is the mass flow rate of the water ethylene glycol working fluid;
$m_{wg,tank}$ (kg) is the mass of the water ethylene glycol in the storage tank;
Cp_{wg} (J/kg-K) is the specific heat capacity of the water ethylene glycol;
t_{cycle} (s) is the cycle time for the current cycle;
$T_{wg,out,30}$ (°C) is the temperature of the working fluid exiting the collector model and entering the storage tank for the current cycle;
$T_{wg,in,1}$ (°C) is the temperature of the working fluid entering the collector model at the previous cycle (it is also the temperature of the storage tank at previous cycle); and
T_{tank} (°C) is the new storage tank temperature for the current cycle.

4 Computer simulations

4.1 Description of the computer model

The model consists of a code written in EES. EES has the advantage that apart from its flexible solver capabilities it also already contains thermodynamic properties of most working fluids and materials including the ethylene glycol water mixture used in this model and the air contained in the air gap. The thermodynamic properties include density, specific

heat, thermal conductivity, viscosity, etc.

The code is arranged in the following format:

- Main Program: Calls the two procedures NusseltNumber and HourCycle; and outputs thermal storage data.
- SubProgram SegmentedModel: calculates the energy balance for each cycle; calls the I_sol
- Function I_sol: calculates the hour solar radiation
- Procedure NusseltNumber: calculates the Nusselt number for each segment of the air gap.
- Procedure HourCycle: compiles energy data for all cycles in each hour

4.2 Model validation

The model was run for the selected hourly ambient temperatures of the typical March-April day as in Table 3. The model calculated the hourly total radiation as in equations 12 to 14. Two tests were done for the 9-solar-collectors field and the 180-solar-collectors field. The model used was a one pipe model; thus it was assumed for the 9 solar collectors that three one-pipe solar collectors were connected in series and for the 180 solar collectors that eighteen one-pipe solar collectors were connected in series. The geometrical sizes and thermal properties of the single riser pipe solar collectors model are given in Table 4.

5. Results of computer models and simulations

The results of the solar model computer simulations are presented in the following charts:

5.1 Computer solar radiation model

Figure 9 shows the computed hour radiation values. The computed solar radiation is highest at noon and is almost symmetrically reducing to zero on sides, the forenoon and the afternoon. The peak at noon is 613.2 W/m^2. The simplified model seems adequate for design purposes. In actual situations the model would have to take into account other weather parameters such as cloud cover, wind and precipitation. The solar radiation curve closely follows the fourth order polynomial:

$$y = 0.296x^4 - 8.306x^3 + 59.70x^2 - 21.82x - 27.03$$

5.2 Temperature modelling results

Figure 10 shows the temperature profiles along the segments of the collectors. T_p is the temperature profile for the absorber plate and T_wg is the temperature profile for the water ethylene glycol working fluid. The numbers enclosed in the parentheses represent the number of the one-pipe-model collectors as they are connected in series. These results are for a one cycle pass with no storage model connected.

Figure 11 shows the energy profiles along the segments of the collectors. Q_dot_wg is the heat transfer profile to the working fluid and Q_dot_loss represents the thermal losses from the collector at each segment. Similarly these results are for a one cycle pass with no storage model connected.

The rate of heat gain by the working fluid decreases along linear segments of the collector whilst the rate of heat losses from the collector increases along the linear segments of the collector.

Figure 12 shows results for the 180-solar collector single pipe field model. The computer model consists of 18 one-pipe models connected in series to represent the 180-solar collector field.

There is a steady build-up of temperature for all components along the model segments and banks.

Table 4: Description of the simulated model

Length of absorber plate	2.0 m for entire collector; 200mm for each segment model
Width of absorber plate	1.0m for entire collector; 125mm for the one-pipe model
Diameter of riser pipe	6mm internal diameter
Material of absorber plate	1mm Aluminium plate
Material of riser pipe	I.D 6mmX1mm Copper Pipe
Material of insulation	40mm Polyurethane Form
Material of transparent cover	4mm Solar Grade Glass
Transmissivity of cover	0.9
Absorptance of absorber	0.9
Emissivity of absorber	0.1
Emissivity of glass	0.85
Heat transfer fluid	Ethylene glycol water; 50% concentration
Number of thermal model segments	10 for each collector; the model collector consists of a one-pipe absorber plate 2.0m length X 125mm width
Size of storage tank	300 litres for the 9 solar collectors (i.e. for the entire solar field); or 12.5 litres for one-pipe model

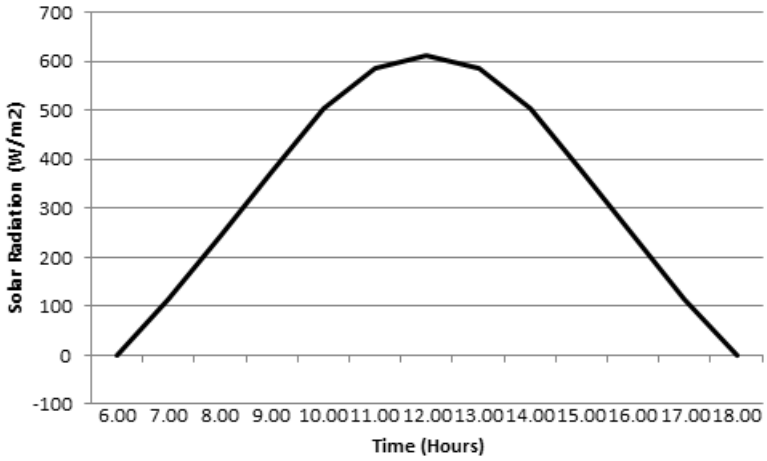

Figure 9: Simulated hourly solar radiation values

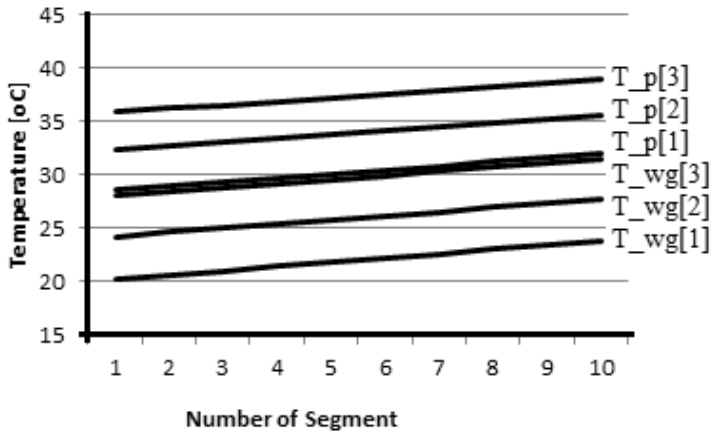

Figure 10: Plot of temperature profiles versus segment numbers

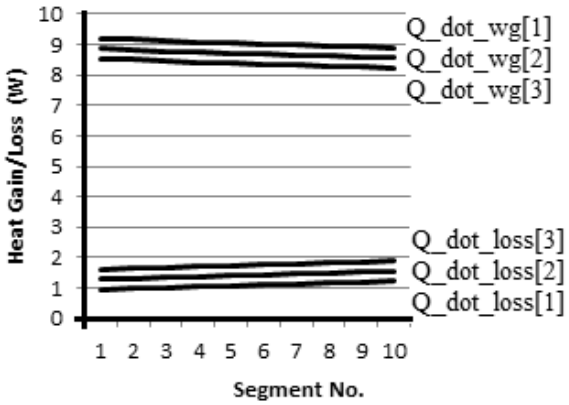

Figure 11: Energy gains and losses profiles versus segments

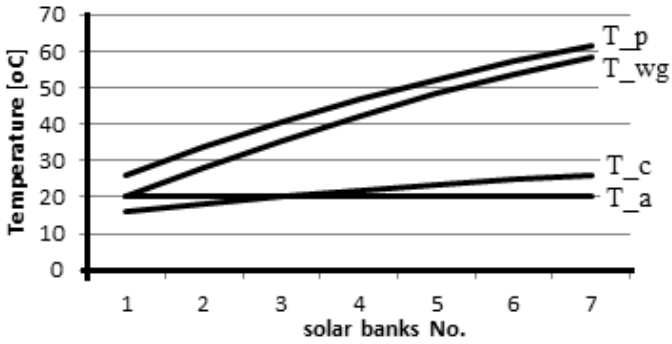

Figure 12: Temperature profile along solar banks; 180-collector model

The temperature is highest in the absorber plate and lowest in the transparent cover; also the rate of temperature increase is lowest in the transparent cover. The rate of temperature increase closely follows the same profile in both the absorber and in the working fluid.

Curve fit results yielded the following second order polynomials:

$$T\_p: y = -0.320x^2 + 8.483x + 17.93$$

$$T\_wg: y = -0.334x^2 + 9.080x + 11.32$$

$$T\_c: y = -0.087x^2 + 2.367x + 13.87$$

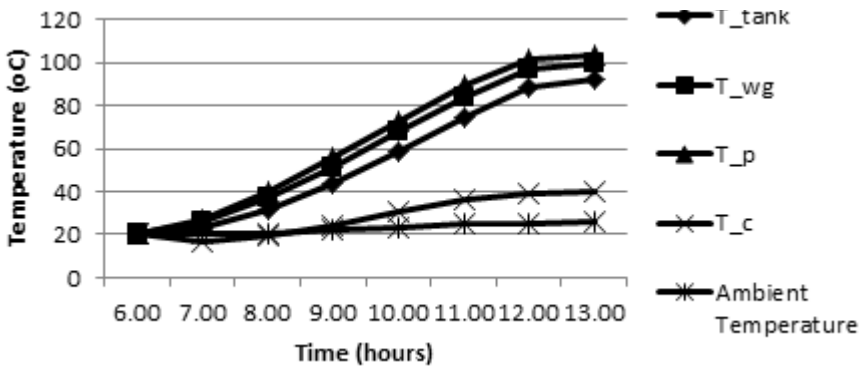

Figure 13: Hourly temperature profiles

Figure 13 shows the hourly temperature profiles. These simulations consists of several cycles (114 cycles calculated) to make an hour. The temperature measurement is taken at the end of the hour. These simulations include a thermal storage represented by the tank temperature T_tank.

The absorber plate attains the highest temperature followed by the working fluid (water ethylene glycol) at the exit of the solar field and in the tank storage. The three temperature profiles follow each other closely and build-up slowly from morning to a high about noon. The absorber increases temperature from ambient temperature of 20°C to slightly over 100°C about noon; the water ethylene glycol attains a maximum of slightly below 100°C and about 90°C at the exit of the solar collector and in the storage tank respectively. This is desirable for heat transfer to continue flowing from the absorber to the working fluid.

The transparent cover has a much lower temperature ranging from ambient temperature to about 40°C. This ensures lower thermal losses.

Curve fitting gave the following results:

T_p: $y = -0.460x^3 + 6.007x^2 - 8.466x + 23.20$

T_wg: $y = -0.439x^3 + 5.955x^2 - 10.06x + 24.93$

T_tank: $y = -0.403x^3 + 5.831x^2 - 12.62x + 27.75$

T_c: $y = -0.258x^3 + 3.694x^2 - 11.48x + 27.65$

T_ambient: $y = 0.988x + 18.17$

5.3 Energy modelling results

Figures 14 and 15 show useful heat gains and thermal losses.

The levels of heat transfer to the working fluid in the storage tank increases with time from the lowest values in the morning (7am) to the highest values in mid-morning (11am) and then decreases with time attaining lower values at noon and 1pm respectively.

The levels of heat transfer also decrease within each hour, being higher at the beginning of the hour than at the end; this, however, could be due to the hourly radiation level being assumed constant.

The level of thermal losses increases with time from the lowest at the start of the modelling time (7am) to the highest and the end of the modelling time (1pm). Sky losses are the highest ranging from about 50% to 100%.

Figure 16 shows average hourly thermal efficiency. The thermal efficiencies are highest near the commencement of the modelling period (7am, 8am and 9am are highest; the lowest efficiencies are at 1pm followed by 12pm).

The average efficiency has a high of 56% at 8pm and a low of 35% at 1pm; the regression analysis yielded the following curve fit:

$$y = 0.055x^3 - 1.321x^2 + 4.265x + 51.42.$$

6. Discussions and conclusions

Preliminary small-scale concept plants, 500Wp and 10kWp, have been presented, modelled and computer-simulated. The first pass modelling used 14 candidate organic fluids and three optional plant configurations which gave thermal efficiencies ranging from 10.38% to 12.20%; the highest being Isopentane and organic Rankine with recuperator and the lowest being R245fa with conventional organic Rankine cycle.

The solar field modelling has been done with Ethylene Glycol Water (50% concentration) as the heat transfer fluid. The model included simulations of hourly solar insolation values, and solar collector and storage tank energy balances.

The general trend exhibited by the temperature profiles for the absorber, ethylene glycol water and transparent cover along the flow direction of the heat transfer fluid is that of a second order polynomial continuously increasing but with a diminishing gradient.

The hourly temperature profiles for the absorber, transparent cover, heat transfer fluid at

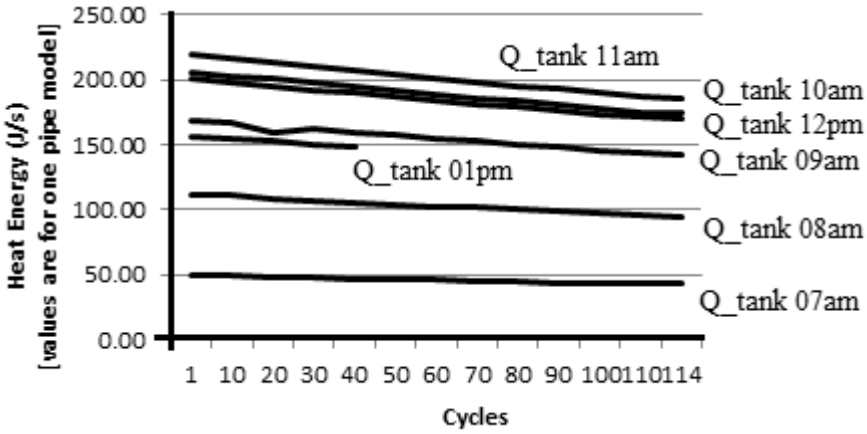

Figure 14: Heat energy rates for storage

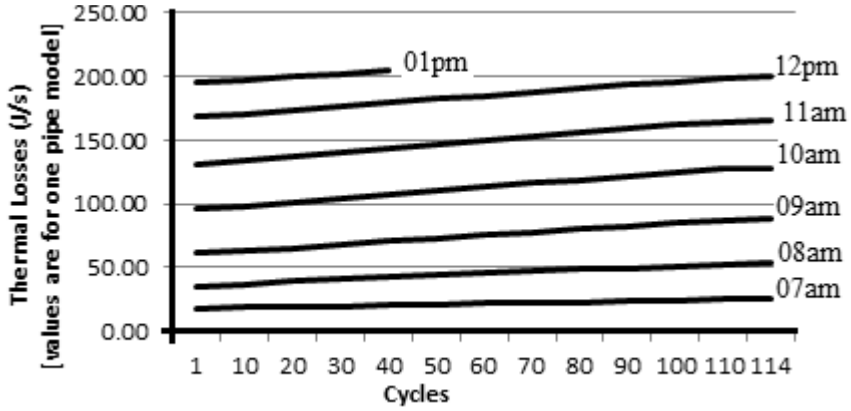

Figure 15: Thermal losses

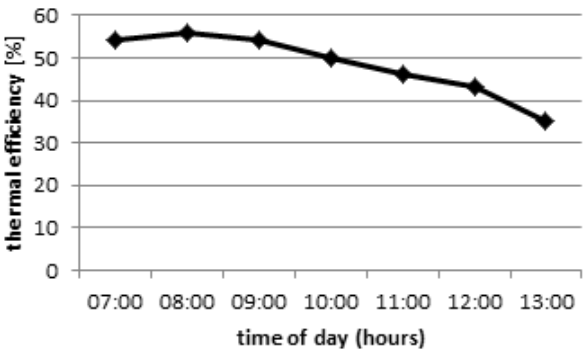

Figure 16: Average hourly thermal efficiency

collector exit, and heat transfer fluid in the storage tank, on the other hand exhibited a third order polynomial character starting with a lower gradient, developing into a steep gradient and then slowing down to a lower gradient.

The hourly efficiency curve also exhibited a third order polynomial profile starting with higher values and tailing down to lower values.

By regression one is able to mathematically determine the totals and averages for futures analyses.

A simple analysis of the 9-collector model shows the thermal energy output being less than the approximated requirements. These will be adjusted in the full simulations once the models of the other components have been finalised.

The main limitation in the simulations was the lower number of permissible variables of the academic commercial version of the software and the low computing speed to the extent that some simulation cycles had to be broken down to allow for manual entering of data midway through the simulations.

The valuable insights gained from these simulations will provide a solid basis for the final concepts designs and physical validations.

References

Duffie J.A., and Beckman W.A., (1991). Solar Engineering of Thermal Processes, 2nd Ed., John Wiley & Son, USA, p281.

Engineering Equation Solver (EES).

Groenendaal B.J., (2002). ECN project number 7.7372: Solar Thermal Power Technologies.

Incropera F.P. et al, (2007) Fundamentals of Heat and Mass Transfer; John Wiley & Sons, USA.

Nishith B. D. and Santanu B., (2009). Process integration of organic Rankine cycle, Energy Journal, Vol. 34 pp 1674–1686.

Schlaich J. and Robinson M., (1995). Principle of a

Solar Chimney: Solar Chimney, Axel Menges GmbH.
Situmbeko S. M., Inambao F. L., (2011). Mathematical Modelling and Simulation of Low Temperature Solar Thermal Energy Conversion Systems, Proceedings ISES Solar World Congress, Kassel, Germany.
Silva M R. et al, (2011). Interactive Tool to Teach Solar Parabolic Trough Concepts; Proceedings ISES, SWC, Kassel, German, September 2011.
Website:www.weather.com/weather/hourbyhour/graph/SFXX0011?begHour=2&begDay=95#hhView (accessed April 03, 2012).
Website: http://www.ienergyinc.com/(accessed November 5, 2013).
Website: www.nrel.gov/csp/troughnet/power_plant_ systems.htmlhttp://www.nrel.gov/csp/troughnet/power_plant_systems.html (accessed November 5, 2013).
Website: www.brightsourceenergy.com/technology (accessed November 5, 2013).
Website: www.:montaraventures.com/energy/wp-content/uploads/2008/05/rankine-cycle-diagram.jpg (accessed January 13, 2010).
Website: www.eng.usf.edu/~hchen4/Kalina%20Cycle.htm (accessed April 04, 2012).
Website: www.solardome.co.za/documents/file/25-solar-dome-sa-priclelist.html (accessed March 12, 2012).
Website:www.thermotechs.com/Downloads/Thermomax%20Handbook.pdf (accessed March 12, 2012).
Website: www.gaisma.com/en/location/durban.html (accessed March 12, 2012).

Received 23 May 2012; revised 4 October 2013

Modelling influence of temperature on daily peak electricity demand in South Africa

Delson Chikobvu
Department of Mathematical Statistics and Actuarial Science, University of the Free State, South Africa

Caston Sigauke
School of Statistics and Actuarial Science, University of the Witwatersrand, South Africa

Abstract
The paper discusses the modelling of the influence of temperature on average daily electricity demand in South Africa using a piecewise linear regression model and the generalized extreme value theory approach for the period - 2000 to 2010. Empirical results show that electricity demand in South Africa is highly sensitive to cold temperatures. Extreme low average daily temperatures of the order of 8.20C are very rare in South Africa. They only occur about 8 times in a year and result in huge increases in electricity demand.

Keywords: Extreme value theory, piecewise linear regression, regression splines, temperature

1. Introduction

Drivers of electricity demand are generally divided into economic factors, calendar effects, weather variables and lagged demand variables. Inclusion of these factors in electricity demand models improves the predictive power of the models and also enables system operators and load forecasters to have a better understanding of the factors that have a greater impact on electricity demand. Weather variables such as temperature, solar radiation, humidity, wind speed and rainfall are often used as explanatory variables in regression based load forecasting models. Most authors, however, use temperature as the main driver (Munoz *et al*., 2010).

The influence of temperature on daily electricity load forecasting has been studied extensively in the energy sector using classical time series, regression based methods including artificial neural networks (Miragedis *et al*., 2006; Hekkenberg *et al*., 2009; Psiloglou *et al*., 2009; Munoz *et al*., 2010; Pilli-Sihvola *et al*., 2010; among others). The paper discusses the modelling of the effect of average daily temperature on daily electricity demand in South Africa using a piecewise linear regression modelling framework and the generalized extreme value theory approach. A generalized extreme value distribution (GEVD) is fitted to the temperature data below the reference temperature. Extreme value theory (EVT) is a powerful and fairly robust framework for modelling the tail behaviour of a distribution (Gencay and Selcuk, 2004). Extreme value theory has been applied in various fields such as flood frequency analysis, environmental sciences, modelling extreme temperatures, finance and insurance including material and life sciences. The family of extreme value distributions is called the generalized extreme value distribution. GEVD consists of the Gumbel, Frechet and Weibull class distributions which are also known as the type I, II and III extreme value distributions respectively.

The rest of the paper is organized as follows. The models are discussed in Section 2. In Section 3 we briefly describe the data used. Empirical results are presented in Section 4 while Section 5 concludes.

2. The models

Our modelling approach is in two stages. A piecewise linear regression model is used to explore the effect of temperature on daily electricity demand. In stage two, we fit a generalized extreme value distribution to the temperature values below the reference temperature. The fitted distribution is then used to estimate extreme low temperatures and calculating the corresponding marginal increases of electricity demand.

2.1 Piecewise linear regression model

The piecewise linear regression model used for modelling the influence of temperature on electricity demand is given in equation (1).

$$ADED = \alpha_0 + \alpha_1 \max(0, t_h - ADT) + \alpha_2 \max(0, ADT - t_c) + \varepsilon_t \quad (1)$$

where ADED (Average Daily Electricity Demand), ADT (Average Daily Temperature), t_h and t_c are temperatures which separate summer and winter sensitive periods (hot and cold temperatures) from the weather neutral period respectively. The parameters to be estimated are α_0, α_1 and α_2 and ε_t is the error term with $\varepsilon_t \sim N(0, \sigma_t^2)$. A Multivariate Adaptive Regression Splines (MARS) algorithm developed by Friedman (1991) is used to estimate the two reference temperatures t_c and t_h which are 18^{0}C and 20^{0}C respectively and discussed in Chikobvu and Sigauke (2012).

2.2 Generalized extreme value distribution

The GEVD consists of the Gumbel, Frechet and Weibull class of distributions. The unified GEVD for modelling maxima is given by

$$G_\xi(x) = exp\left\{-\left[1 + \xi\left(\frac{x-\mu}{\sigma}\right)\right]^{-\frac{1}{\xi}}\right\}, \text{if } 1 + \xi\left(\frac{x-\mu}{\sigma}\right) > 0 \text{ and } \xi \neq 0 \quad (2)$$

where μ and σ are the location and scale parameters respectively. The shape parameter ξ also known as the extreme value index (EVI) determines the rate of tail decay. If $\xi > 0$, $G_\xi(x)$ belongs to the heavy-tailed Frechet class of distributions (Beirlant *et al.*, 2004). For $\xi < 0$ we have the short-tailed Weibull class and is bounded above by $\mu - \frac{\sigma}{\xi}$ (Beirlant *et al.*, 2004). If $\xi = 0$, $G_\xi(x)$ belongs to the light-tailed Gumbel class of distributions (Beirlant *et al.*, 2004).

In order to model minima we use the duality between the distributions for maxima and minima. If $M_n = \min\{x_1, x_2, \ldots, x_n\}$ where $x_i, i = 1,2, \ldots, n$ represents temperature, then $\widetilde{M}_n = \max\{-x_1, -x_2, \ldots, -x_n\}$. Extreme maxima theory and methods are then used to model extreme minima. The Maximum Likelihood (ML) method is used to estimate the parameters ξ, μ and σ. The survival distribution of the GEVD given in equation (2) is given by:

$$P(X > x) = 1 - G_\xi(x) = 1 - exp\left\{-\left[1 + \xi\left(\frac{x-\mu}{\sigma}\right)\right]^{-\frac{1}{\xi}}\right\}, \text{if } 1 + \xi\left(\frac{x-\mu}{\sigma}\right) > 0 \text{ and } \xi \neq 0 \quad (3)$$

If we let $p = P(X > x)$ and rearranging equation (3) to make x the subject we get the quantile function:

$$x_p = \mu + \frac{\sigma}{\xi}\left[\{-\ln(1-p)\}^{-\xi} - 1\right], \xi \neq 0 \quad (4)$$

Now as $p \to 0$ and $\xi < 0$ we get $x_p = \mu - \frac{\sigma}{\xi}$. The quantile function for the unified GEVD given in equation (4) is then used to estimate high quantiles and predicting the probability of exceedance levels.

3. Data

National daily electricity data for the industrial, commercial and domestic sectors of South Africa is used in this study. The data is from Eskom, South Africa's power utility company. Figure 1 shows that ADED data exhibits strong seasonality and has a positive upward trend.

Aggregated ADT from 32 meteorological stations of South Africa representing all provinces (regions) of the whole country is used in the analysis.[1]

Figure 2 shows that ADT has strong seasonality and is stationary. The minimum ADT and maximum ADT over the sampling period (2000-2010) are 7.5^{0}C and 26.1^{0}C respectively.

4. Empirical results and discussion

4.1 Piecewise linear regression model output

The model identifies the winter sensitive, weather neutral and summer sensitive periods. The model is not used for forecasting electricity demand but rather to explain the influence of temperature on electricity demand.

$$E(ADED = 23932 + 263 \max(0,22 - ADT) + 138 \max(0,ADT - 18) \quad (5)$$

The graphical plot of ADED against ADT is shown in Figure 3. The three demand-temperature equations are given in equations 6-8. If average daily temperature is less than or equal to 18^{0}C equation (5) reduces to

$$E(ADED = 23932 + 263 \max(0,22 - ADT) \quad (6)$$

That is, if the temperature decreases by 1^{0}C (e.g. from 18^{0}C to 17^{0}C) electricity demand will increase marginally by 263 MW. A fall in ADT of 1^{0}C (say, from 16^{0}C to 15^{0}C) would result in an increase of about 1.03% in electricity consumption.

If average daily temperature is greater than or equal to 22^{0}C equation (5) reduces to

$$E(ADED = 23932 + 138 \max(0,ADT - 18) \quad (7)$$

If temperature increases by 1^{0}C (e.g. from 22^{0}C to 23^{0}C) electricity demand will increase marginally by 138 MW. For a rise in average daily temperature of 1^{0}C (say, from 25^{0}C to 26^{0}C) would result in an increase of about 0.55% in electricity consumption.

For the average daily temperature between 18^{0}C and 22^{0}C we use the full model given in equation (5), i.e.

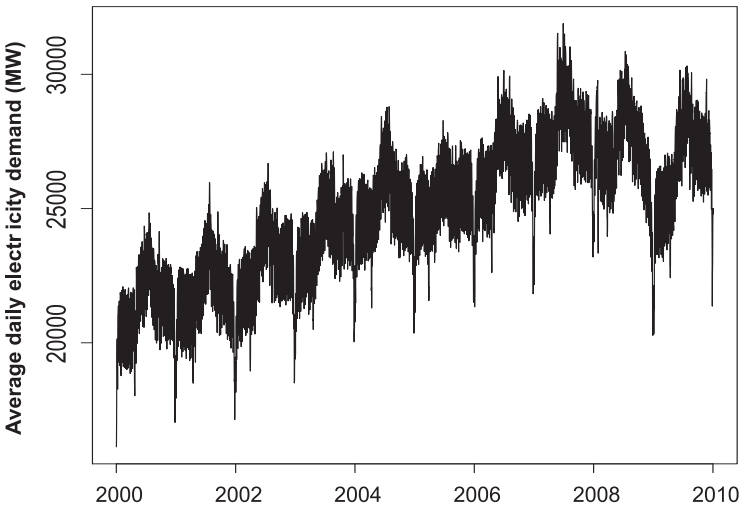

Figure 1: Average daily electricity demand (megawatts) from 2000-2010

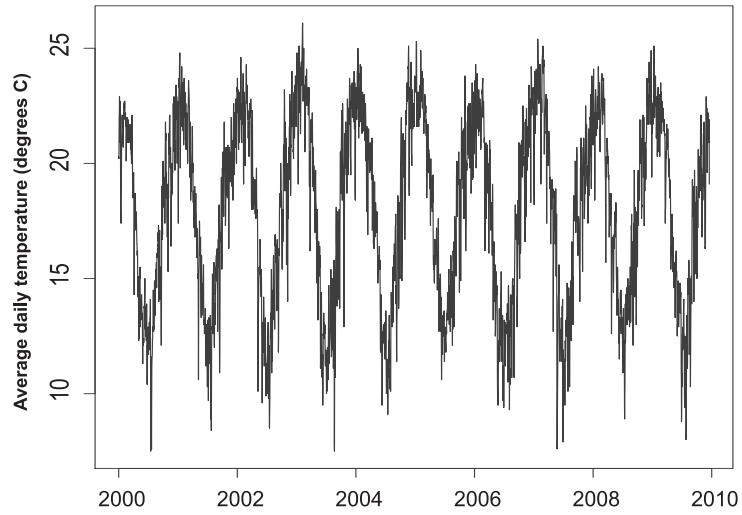

Figure 2: Time series plot of average temperature (degrees C)

$$E(ADED = 23932 + 263 \max(0,22 - ADT) + 138\max(0,ADT - 18) \quad (8)$$

If temperature decreases by 1^0C (e.g. from 22^0C to 21^0C) electricity demand will increase marginally by 125 MW. A decrease of ADT from 20^0C to 19^0C would result in an increase of about 0.51% in electricity consumption.

This analysis shows that electricity demand in South Africa is highly sensitive to cold temperature (see Figure 3). There is a non-linear relationship between temperature and electricity demand as shown in Figure 3. This non-linear relationship is modelled in literature using heating degree days (HDD) and cooling degree days (CDD). Modelling of this relationship between temperature and electricity demand is discussed in literature (Mirasgedis, 2006; Franco and Sanstad, 2008; Psilogu *et al.,* 2009; Munoz *et al.,* 2010; Pilli-Sihvola *et al.,* 2010; among others). HDD and CDD are calculated using the following functions:

$$HDD_t = \max(T_r - ADT,) \quad (9)$$

$$CDD_t = \max(ADT - T_r, 0) \quad (10)$$

where ADT is the average daily temperature at time and is the reference temperature.

In this paper a piecewise linear regression model is used with two reference temperature values which are estimated using the MARS algorithm (Friedman, 1991).

Figure 3 shows the plot of the model in equation (5). The piecewise linear regression plot separates the non-linear response of electricity demand to temperature into three regions: cold for temperatures lower than 18^0C, neutral for temperatures between 18^0C and 22^0C, and hot for temperatures above 22^0C.

There are other several methods of filtering data (i.e. removing both the trend and the calendar effects) which are discussed in literature (see Moral-Carcedo and Vic´ens-Otero, 2005; Munoz et *al.*, 2010; among others).

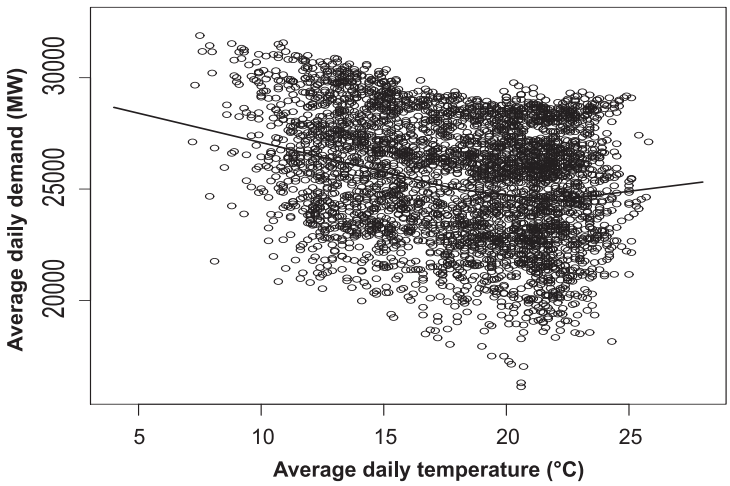

Figure 3: Scatter plot of ADED (seasonally adjusted) against ADT with the fitted piecewise regression line of equation (5)

4.2 Modelling the minimum daily temperature (tail quantile estimation)

In section 4.1 it was noted that demand of electricity is more sensitive to cold temperatures (less than 18^0C) than to hot temperatures (more than 22^0C). Modelling of extreme minimum temperatures is therefore important to load forecasters and system operators for planning, load flow analysis and scheduling of electricity. In this section, we estimate the extreme tail quantiles of ADT below 18^0C using the GEVD. The data is seasonally adjusted. There are 1649 observations below 18^0C. Figure 4 shows data for temperature below 18^0C.

4.3 Tail quantile estimation

We use the principle of duality between the distributions of minima and maxima as discussed in Section 2.2. Figure 5 shows the graph of $-x_i$, $i = 1, \ldots, n$ where x_i represents temperature below 18^0C. The R statistical package Ismev (Heffernan and Stephenson, 2013) is used to obtain the ML estimates. The estimates are given as (the standard errors are given in parentheses):

$$\hat{\xi} = -0.2004(0.01817),$$
$$\mu = -15.02544(0.05758) \text{ and}$$
$$\hat{\sigma} = 2.0800(0.04176)$$

The standard errors of the ML estimates of the parameters, are small. This shows that uncertainty about the parameters is small. These results show that the data can be modelled using a Weibull class of distributions, (since $\hat{\xi} < 0$) and the right endpoint is finite and is given by:

$$\mu - \frac{\sigma}{\xi} = -15.202544 - \frac{2.08}{-0.2004} = -4.646$$

This implies that for any degree decrease below 4.6^0C there won't be any further increase in electricity demand.

The quantile-quantile (QQ) and probability-probability (PP) plots given in Figure 6 show that a Weibull distribution is a good fit to the data. The return level estimates are inside the 95% confi-

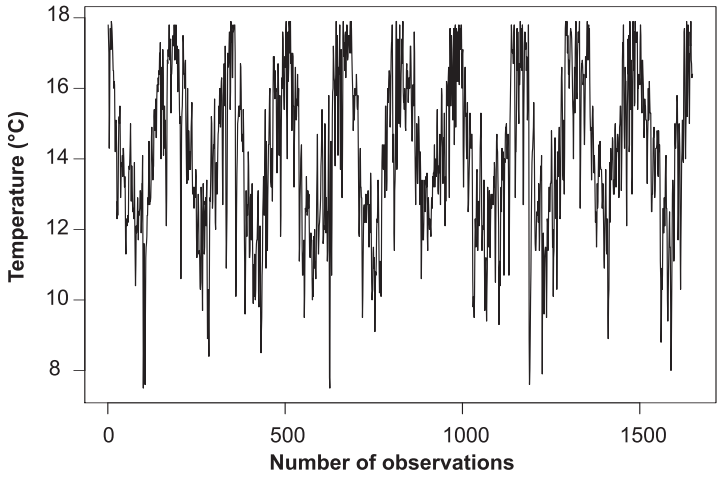

Figure 4: ADT below 18^0C (2000 to 2010)

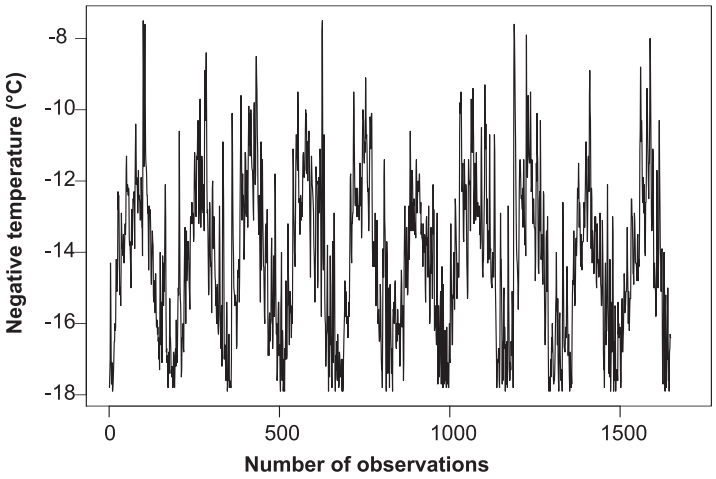

Figure 5: Inverted graph of Figure 4. Figure 4 is inverted so that we can use the duality between the distributions for maxima and minima

dence interval. This is an indication that the fitted distribution is capable of accurately predicting future return levels. We then use equation (4) to estimate the future return levels for different return periods. The return level is the quantile of the GEVD (Weibull distribution). For example, the 95th quantile is obtained as follows:

$$-x_{0.05} = -15.025 - \frac{2.08}{0.2004}[\{-\ln(0.95)\}^{0.2004} - 1]$$
$$= -10.369 \Rightarrow x_{0.05} = 10.369$$

The number of observations that are smaller than the estimated tail quantile ($x_{0.05}$ = 10.369) are then counted and found to be 78. For the observed number of exceedances, we get 0.05 × 1649 = 82.45 ≈ 82 where 1649 is the number of temperature values below 18^{0}C. The increase in electricity demand for a drop of temperature from 18^{0}C to $x_{0.05}$ = 10.4°C is given by (18 – 10.4) × 263 = 1998.8MW, where 263 is the marginal increase in demand for a decrease of 1^{0}C below 18^{0}C as discussed in Section 4.1. It should be noted that this

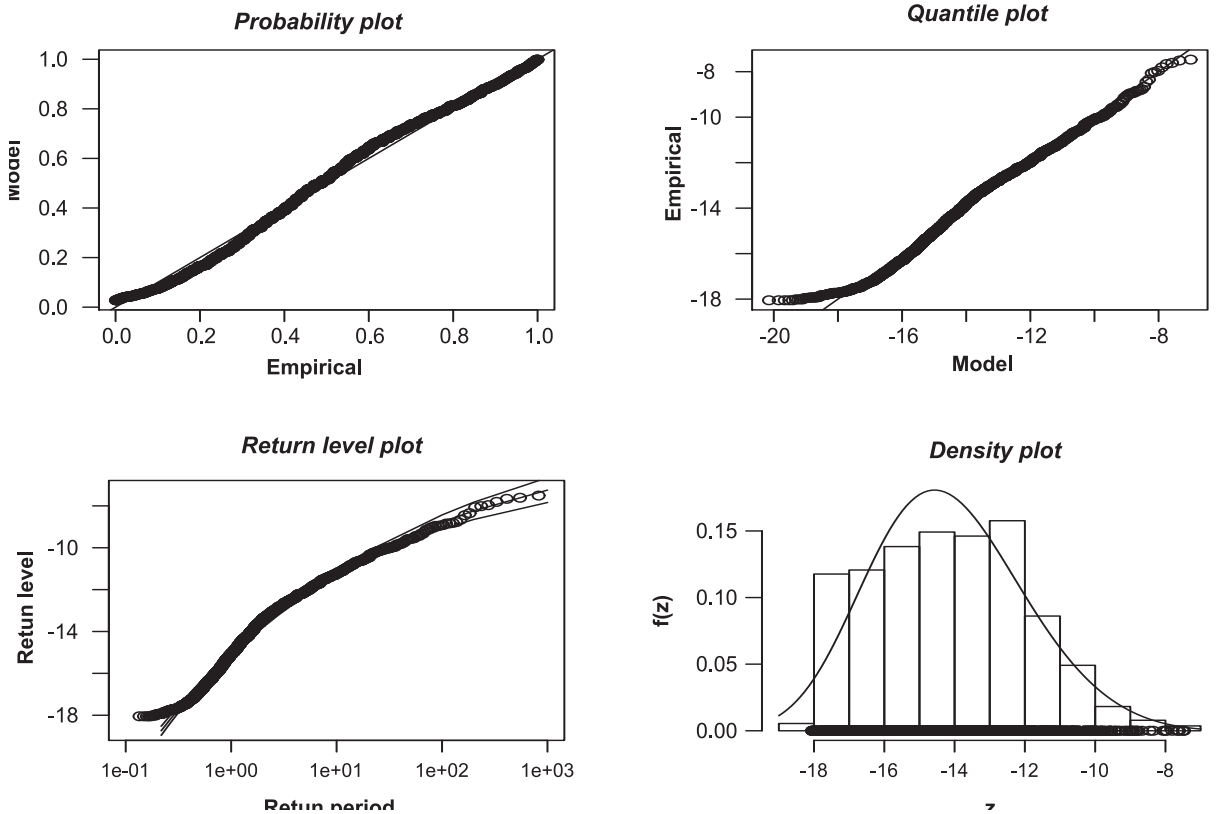

Figure 6: Diagnostic plots illustrating the fit of the data (temperature below 18^{0}C) to the GEVD, (a) Probability plot (top left panel), (b) Quantile plot (top right panel), (c) Return level plot (bottom left panel) and (d) Density plot (bottom right panel)

Table 1: In-sample evaluation of estimated tail quantiles at different probabilities (number of exceedances)

Quantiles	*Temp (xp)*	*Observed no. of exceedances*	*GEVD (no. of exceedances)*	*Marginal increase in demand (MW)*
90th	11.3^{0}C	164		159
95th	10.4^{0}C	82	78	236.7
99th	8.8^{0}C	16	12	420.8
99.5th	8.2^{0}C	8	8	157.8

Table 2: Monthly frequency of exceedances below $x_{0.05}$ = 10.4°C

Month	*Jan*	*Feb*	*Mar*	*Apr*	*May*	*Jun*	*Jul*	*Aug*	*Sep*	*Oct*	*Nov*	*Dec*
Freqency	0	0	0	0	11	16	45	6	0	0	0	0

increase in ADED for temperature decreases below 18^{0}C is bounded above. As temperature decreases below 18^{0}C, the increases in ADED reaches a certain maximum after which any further decrease in temperature will not have any effect on ADED. That is as temperature decreases people will switch on heating systems up to a point when all the heating systems are all switched on and no additional energy is consumed.

Table 1 presents a summary of the estimated tail quantiles at different tail probabilities. The tail quantiles (temperature) are given in column 2. The observed number of observations (temperature) that are smaller than the estimated tail quantiles are shown in column 3 while column 4 shows the corresponding number estimated using GEVD. In equation (5) it is given that for a degree decrease in temperature below 18^{0}C there will be a marginal increase in demand of 263 MW. For each of the estimated quantiles in column 2, column 5 shows the marginal increases from one quantile to the next, e.g. if temperature drops from 11.3^{0}C to 10.4^{0}C there will be an increase in demand of 263(11.3 – 10.4) = 236.7MW. Similarly, for a decrease from 10.4^{0}C to 8.8^{0}C the marginal increase will be 263(10.4 – 8.8) = 420.8MW. Extreme low average daily temperatures of the order of 8.2^{0}C are very rare in South Africa. This only occurs about 8 times in a year.

Table 2 given in the Appendix summarizes the temperature values at high quantiles and the corresponding marginal increases while Figure 7 shows that the marginal increases converge to 1.58 MW when temperature converges to 4.6^{0}C.

A summary of the monthly frequency of occurrence of temperature values below 12.4^{0}C (i.e. above the 95th quantile $-x_{0.05}$ = 10.369 is given in Table 2. Over the sampling period, i.e. years 2000 to 2010 the month of July has the highest number of days with temperature values below 10.4^{0}C. This is an indication that the month of July is the coldest month in South Africa and the winter period is from May to August of each year.

The bar chart of the monthly frequency of occurrence of exceedances is given in Figure 8.

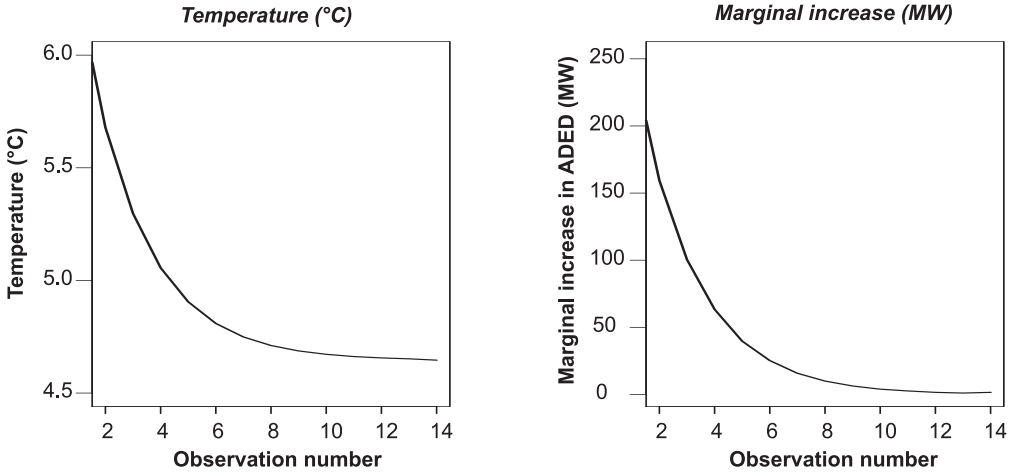

Figure 7: (a) Left panel shows that the gradual decrease in temperature converges to 4.6^{0}C and (b) Right panel shows that the marginal increases converge to 1.58MW when temperature converges to 4.6^{0}C

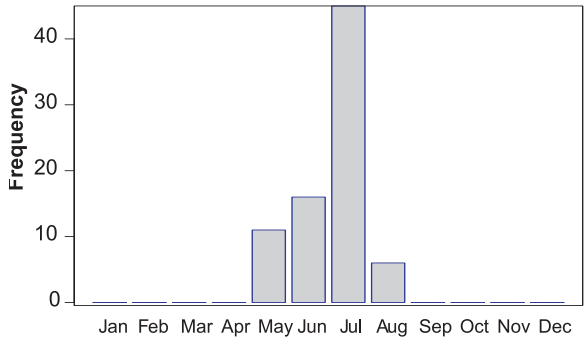

Figure 8: Bar chart of the monthly frequency of occurrence of exceedances ($x_{0.05}$ = 10.4). The exceedances are average daily temperature values below 10.4^{0}C

5. Conclusion

An analysis of the intensity and frequency of occurrence of extreme low temperatures is important for load forecasters in the electricity sector. In this paper, the modelling of the influence of temperature on average daily electricity demand in South Africa using a piecewise linear regression model and the extreme value theory modelling framework is discussed. The developed piecewise linear regression model is not meant for forecasting but to model the effect of temperature on electricity demand. The study establishes temperature as an important variable in explaining electricity demand. Empirical evidence from this study shows that for temperature values below 18^{0}C demand for electricity in South Africa increases significantly while for temperature values above 22^{0}C demand increases slightly. This analysis is important for decision makers in Eskom, South Africa's power utility company. Extreme low temperatures can be modelled by the Weibull class of distributions. Extreme low temperatures of the order of 6^{0}C are very rare in South Africa, but can cause huge increases in electricity demand. An investigation of expected cooler or warmer than typical years is important and helps in guiding planning to decision makers in the electricity sector.

Areas for future research would include a comparative analysis of the generalized extreme value distribution with a generalized Pareto distribution and a generalized single Pareto distribution in modelling extreme low temperatures in South Africa. These areas will be studied elsewhere.

Note

1. Average daily temperature for the whole country is usually built into the modelling as weighted average temperatures from different meteorological stations of a country. The weightings should reflect consumption of electricity of each region (province). Population figures are often used for estimating the weights. In this research, the weightings were not done since only aggregated average daily temperature was available.

Acknowledgments

The authors are grateful to Eskom for providing the data and to the numerous people who assisted in making comments on this paper.

References

Chikobvu, D. and Sigauke, C., (2012). A frequentist and Bayesian regression analysis to daily peak electricity load forecasting in South Africa. *African Journal of Business Management*, 6(40): 10524-10533.

ClimateTemp.info. (Accessed on 10 June 2012) www.climatetemp.info/south-africa/.

Franco, G. and Sanstad, A.H. (2008). Climate change and electricity demand in California. *Climatic Change*, 87 (Suppl 1): S139-S151.

Heffernan, J.E. and Stephenson, A.G. (2013). Ismev: R package version 1.39.

Hekkenberg, M., Benders, R.M.J., Moll, H.C. and

Appendix

Table 2: Evaluation of estimated tail quantiles using the GEVD quantile function

Observation number	1	2	3	4	5
Quantile	99.99th	99.999th	99.9999th	99.99999th	99.999999th
Temp (deg C)	6.285	5.679	5.297	5.056	4.905
Marginal increase (MW)	252.74	159.38	100.5	63.38	39.713
Observation number	6	7	8	9	10
Quantile	99.9999999th	99.99999999th	99.999999999th	99.9999999999th	99.99999999999th
Temp (deg C)	4.809	4.749	4.711	4.687	4.672
Marginal increase (MW)	25.248	15.78	9.994	6.312	3.945
Observation number	11	12	13	14	
Quantile	99.999999999999th	99.9999999999999th	99.99999999999999th	99.9999999 99999999th	
Temp (deg C)	4.662	4.656	4.652	4.646	
Marginal increase (MW)	2.63	1.578	1.052	1.578	

Schoot, A.J.M. (2009). Indications for a changing Electricity demand pattern: The temperature dependence of electricity demand in the Netherlands, *Energy Policy,* 37: 1542-1551.

Gencay, R. and Selcuk, F. (2004). Extreme value theory and value-at-risk: relative performance in emerging markets. *International Journal of Forecasting*, 20: 287-303.

Hyndman, R.J., Fan, S. (2010). Density forecasting for long-term peak electricity demand. *IEEE Transactions on Power Systems*, 25(2): 1142-1153.

Mirasgedis, S., Sarafidis, Y., Georgopoulou, E., Lalas, D.P., Mschovitis, M., Karagiannis, F. and Papakonstantinou, D. (2006). Models for mid-term electricity demand forecasting incorporating weather influences. *Energy*, 31: 208-227.

Moral-Carcedoa, J. and Vic´ens-Otero, J. (2005). Modelling the non-linear response of Spanish electricity demand to temperature variations. *Energy Economics*, 27, 477–494.

Munoz, A., Sanchez-Ubeda, E.F., Cruz, A. and Marin, J. (2010). Short-term forecasting in power systems: a guided tour. *Energy Systems*, 2: 129-160.

Pilli-Sihvola, K., Aatola, P., Ollikainen, M. and Tuomenvirta, H. (2010). Climate change and electricity consumption Witnessing increasing or decreasing use and costs, *Energy Policy*, 38(5), pp. 2409-2419.

Psiloglou, B.E., Giannakopoulos, C., Majithia, S. and Petrakis, M., (2009). Factors affecting electricity demand in Athens, Greece and London, UK: A comparative assessment. *Energy*, 34: 1855-1863.

SouthAfrica.info. (Accessed on 10 June 2012) southafrica.info/travel/advice/climate.htm.

www.ral.ucar.edu/˜ericg/softextreme.php.

Received 1 October 2012; revised 21 November 2013

Performance analysis of an air humidifier integrated gas turbine with film air cooling of turbine blade

Alok K Mahapatra
Department of Mechanical Engineering, Nalanda Institute of Technology, Bhubaneswar, India

B E Sanjay
Department of Mechanical Engineering, National Institute of Technology, Jamshedpur, India

Abstract
A computational analysis to investigate the effects of compressor pressure ratio, turbine inlet temperature, ambient relative humidity and ambient temperature on the performance parameters of an air cooled gas turbine cycle with evaporative cooling of inlet air has been presented. The blade cooling method selected is film cooling. The analysis indicates that the mass of coolant required for blade cooling is reduced with increase in temperature drop across the humidifier. Both decrease in ambient temperature and ambient relative humidity results in an increase in plant efficiency and plant specific work. The highest efficiency is obtained at a turbine inlet temperature of 1500 K for all range of ambient relative humidity and ambient temperature, beyond which it decreases. The compressor pressure ratio corresponding to the maximum plant specific work, however, varies with both ambient relative humidity and ambient temperature. The increase in specific work due to drop in ambient relative humidity is more pronounced at higher pressure ratios. Similarly, the increase in efficiency due to ambient temperature drop is prominent at higher turbine inlet temperatures. Finally, a design nomograph is presented to select the design parameters corresponding to best efficiency and specific work.

Keywords: inlet-air cooling, air-humidifier, gas turbine, evaporative cooling, parametric analysis, air-film blade cooling

Nomenclature

a = ratio of mass of coolant to mass of gas flow
a,b,c = constants
c_p = specific heat (kJ-kg^{-1}·K^{-1})
f_h = correction factor to account for vapor added in humidifier
F = factor
F_{sa} = correction factor to account actual blade surface
gt = gas turbine
h = specific enthalpy (kJ·kg^{-1})
ΔH_r = lower heating value (kJ.kg^{-1})
$\dot{m}$ = mass flow rate (kg·s^{-1})
Q = heat energy transfer (W)
r_p = cycle pressure ratio
R = gas constant (kJ-kg^{-1}·K^{-1})
p = total pressure (bar)
S = blade perimeter (m)
$\overline{St}$ = average Stanton number = $\dfrac{\overline{h}_g}{c_{p,g} \cdot \rho_g \cdot C_g}$
t = pitch of blade (m)
T = temperature (K)
TIT = turbine inlet temperature (K) = combustor exit temperature
W = specific work (kJ·kg^{-1})
t_a = air temperature (°C)

Greek symbols

ϕ = relative humidity (ratio)
ω = specific humidity (kg/kg)
α = gas flow discharge angle (degree)
ε = effectiveness (%) = $\dfrac{T_{c,e} - T_{c,i}}{T_b - T_{c,i}}$
η = efficiency (%)

Subscripts

a = air, ambient
av = average
b = blade
c = compressor
comb = combustor

dr = drop
e = exit
f = fuel
g = gas
alt = alternator
gt = gas turbine
h = humidifier
I = inlet, stage of compressor
in = inlet
inc = increase
j = coolant bleed points
net = difference between two values
p = pressure
plant = gas turbine plant
pt = polytropic
sat = saturation
vap = water vapor
v = volume ……..(m^3)
w = water

Acronym

AFC = Air film cooling
AHIGT = Air humidifier integrated gas turbine
C = Compressor
CC = Combustion chamber
GT = Gas turbine
RH = relative humidity (ratio)

1. Introduction

Gas turbines have gained widespread acceptance in the power generation, mechanical drive, and gas transmission markets. The gas turbine cycle burning natural gas (NG) as fuel, gives high efficiency, large output, and reduced emission. Major power plant equipment manufacturers are currently undertaking high profile development programs of gas turbines. The present state-of-the-art gas turbine plant (LMS100) employing an intercooled gas turbine, yields simple cycle thermal efficiency of the order of 47 per cent based on a lower heating value analysis. The efficiency of the gas turbine cycle has been improved mainly due to combination of many factors e.g. increased firing temperature, increased pressure ratio, improved component design, cooling and combustion technologies, and advanced materials and system integration (e.g. combined cycles, intercooling, recuperation, reheat, chemical recuperation) etc.

Wright and Gibbons (2007) have thoroughly reviewed the recent developments in gas turbine materials and technologies. Consequently, thermal efficiencies are currently very attractive, with simple cycle efficiencies ranging between 32% and 42 % and combined cycle efficiencies reaching the 60% mark. The efficiency of the gas turbine cycle has been improved mainly due to enhanced gas turbine performance through advancements in materials and cooling methods in recent years.

The two important methods of improving the gas turbine performance are by inlet air cooling and gas turbine blade cooling. The highest losses of power due to increase in the ambient air temperature in gas turbine power output usually coincide with periods of high electricity demand. A gas turbine loses approximately 7% of its nominal power when the intake temperature increases from 15 °C, ISO conditions, to 25 °C, and in cases such as in summer when the ambient temperature increases above 25 °C, the losses are still bigger, reaching even 15% of the power rating with 36 °C. By the addition of an air-cooling system at the compressor intake, the inlet air can be conditioned to lower temperatures than ambient, thus improving plant performance at high ambient temperatures. As the inlet air temperature drops, compressor work decreases and so the network and cycle efficiency increases. In addition, air density increases with drop in inlet temperature, which results in an increase in mass flow rate of air entering the compressor and so the power output is further enhanced.

De Lucia et al. (1995) have studied gas turbines with inlet air cooling and concluded that evaporative cooling could enhance the power produced by up to 4% per year. Hosseini et al., (2007) summarized that the output of a gas turbine of the Fars combined cycle power plant at 38 °C ambient temperature and 8% relative humidity is 11 MW more, and the temperature drop of the inlet air is about 19 ^{0}C with media evaporative cooling installations. Zadpoor and Nikooyan (2009) have concluded that evaporative inlet cooling systems do not work well in humid areas. Najjar (1996) analyzed that the addition of absorption inlet cooling improves the power output by about 21%, overall thermal efficiency by about 38 % and overall specific fuel consumption by 28%. Bassily (2001) carried out energy balance analysis of gas turbine cycles and reported that introducing indirect inlet air cooling, evaporative after cooling of the compressor discharge along with regeneration, intercooling, and reheat increase the performance significantly. Wang and Chiou (2004) calculated that the expected benefits from the inclusion of the inlet cooling feature is about 12% increase in power output and 5.16% increase in efficiency when the ambient temperature is cooled from 305 K to 283 K. Bassily (2001) presented the effect of evaporative inlet and after cooling on the performance of recuperated gas turbine cycle and showed that evaporative inlet cooling could boost the efficiency of the recuperated cycle by up to 3.2%. Alhazmy and Najjar (2004) have analysed the inlet air chilling using a cooling coil and observed that the cooling coil improves the turbine output by 10% during cold humid conditions and by 18% during hot humid conditions.

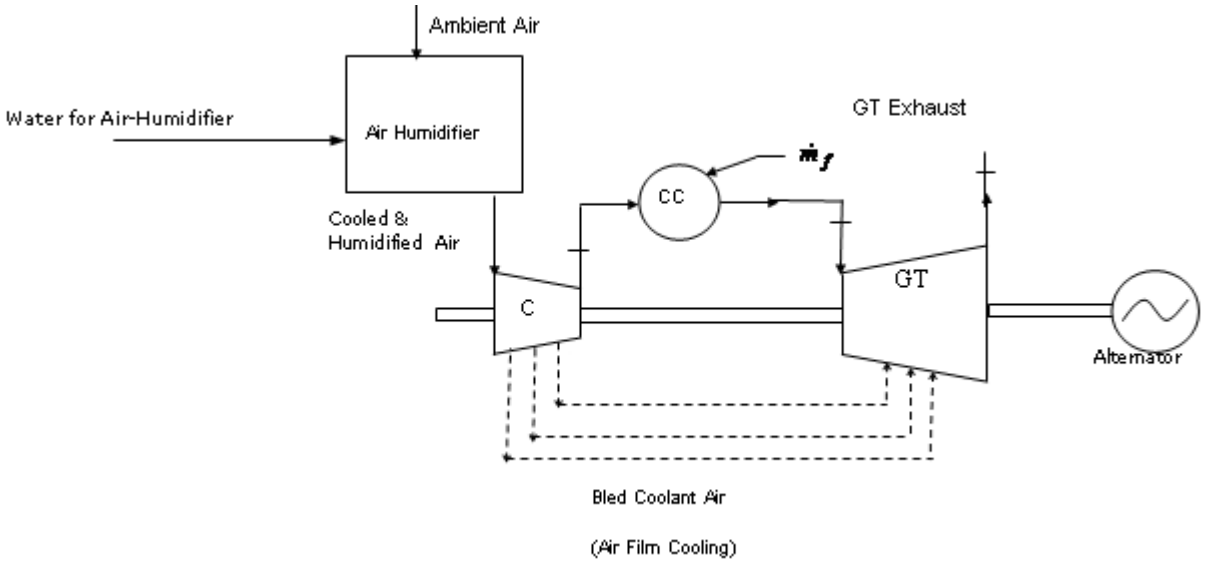

Figure 1: Schematic of an air humidifier integrated gas turbine

However, net power generated from the plant drops by 6.1% and 37.6%, respectively. Kakaras *et.al.,* (2004) presented a computer simulation of an inlet air cooling method and reported that the integration of absorption inlet cooling demonstrates higher power and efficiency compared to evaporative cooling for simple gas turbines.

The search for a better performance of gas turbine engines has also led to adoption of higher turbine inlet temperatures. However, the maximum value of TIT is restricted by metallurgical limits of turbine blade material, which should be kept at 1123 K in order to protect the blades from damage. The turbine inlet temperature TIT could be raised above this limit by using especial high temperature materials or cooling the hot turbine components with a suitable coolant. The objective of the blade cooling is to keep the blade temperature to a safe level, to ensure a long creep life, low oxidation rates, and low thermal stresses. The universal method of blade cooling is by air bled from compressor flowing through the internal passages in the blades.

Work in this area has been done by Louis *et al.,* (1983), Wu and Louis [1984], El-Masri (1986), El-Masri (1988), Briesh *et al,.* (1995), Bolland and Stadaas (1995), Bolland (1991), Chiesa and Macchi (2002),Dechamps (1998), and Sanjay *et al.,* (2007), Sanjay *et al.,* (2008), Sanjay *et al.,* (2009) and Sanjay (2011). Nevertheless, Horlock *et al.,* (2001) have argued that the efficiency benefits of higher temperatures may be more than offset by the increased losses associated with the cooling flow rates required. Also increasing TIT increases NO_x emission and so necessary control mechanism must be employed to keep this NO_x emission within permissible limits. This increase in coolant mass flow requirement and emission of NO_x gases with adoption of higher TIT can be substantially reduced by the integration of inlet air cooling systems to gas turbines and combined cycle plants. It is therefore interesting to investigate the effect of integration of inlet air cooling to cooled gas turbine based combined cycle plant

It is observed from a study in the cited literatures that none of the previous work has investigated the simultaneous effect of compressor inlet air-cooling and gas turbine blade cooling on the performance of a gas turbine cycle. It is interesting to note that the mass of coolant required for gas turbine blade cooling is a function of inlet air temperature and reduces with increase in temperature drop.

The present work is an attempt in this direction dealing with the combined effect of turbine blade cooling and evaporative inlet air-cooling on the performance of basic gas turbine cycle. The effects of compressor pressure ratio, turbine inlet temperature, ambient relative humidity and ambient temperature have been observed on the thermodynamic performance parameters of the cycle. Figure 1 shows the schematic diagram of a basic gas turbine cycle with inlet air humidifier and is being called air humidifier integrated gas turbine (AHIGT).

2. Modelling of governing equations

Parametric study of the combined cycle using different means of cooling has been carried out by modeling the various elements of a gas turbine cycle using the governing equations. The following are the modeling details of various elements.

2.1 Gas model

The specific heat of real gas varies with temperature and also with pressure at extreme high pressure levels. However, in the present model, it is assumed that specific heat of gas varies with temperature only and is given in the form of polynomials as fol-

lows:

$$c_p(T) = a + bT + cT^2 + dT^3 + ... \quad (1)$$

where a, b, c, and d are coefficient of polynomials, as taken from the work of Touloukian and Tadash (1970) and f_h is the humidity correction factor to account for the increase in specific humidity of ambient air across the air-humidifier:

$$f_h = 1 + 0.05\phi_{h,e} \quad (2)$$

where $\phi_{h,e}$ is the relative humidity at the outlet of humidifier.

Thus, the enthalpy of gas is expressed as:

$$h = \int_{T_a}^{T} c_p(T)dT \quad (3)$$

The enthalpy of ambient air entering the air-humidifier is assigned zero value. In the gas model, natural gas (NG) is the fuel used in combustors and the composition and physical properties (such as ,etc.) of burnt gas composition depend upon the composition of NG that may vary from well-to-well (i.e. the source of NG). For this thermodynamic study, the fuel composition is taken as CH_4 = 86.21 %, C_2H_6 = 7.20 %, and CO_2 = 5.56 %, and N_2 = 1.03 % by weight.

2.2 Humidifier model

Cooling in a hot, relatively dry climate can be accomplished by evaporative cooling. Evaporative cooling involves passing air across a spray of water or forcing air through a soaked pad that is kept replenished with water (Moran and Shapiro, 1995). Owing to the low humidity of entering air, a part of the water injected evaporates. The energy required for evaporation is provided by the air stream, which is undergoes a reduction in temperature.

The following assumptions are made in the humidifier model:

- The relative humidity at the humidifier outlet is 95%
- The pressure drop of air in the humidifier is 1% of the ambient air pressure.

Applying the mass balance equation across the humidifier control volume boundary gives

$$\omega_{a,e} = \omega_{a,i} + m_w \quad (4)$$

where ω is the specific humidity and is calculated at a certain temperature as

$$\omega = \frac{0.622 p_{vap}}{p - p_{vap}} \quad (5)$$

where $p_{vap} = \phi p_{sat}$ is the partial pressure of vapour, ϕ is the relative humidity and p_{sat} is the saturation pressure of air corresponding to the desired temperature.

The energy balance equation for the humidifier is given by

$$h_{a,e} = h_{a,i} + (\omega_{a,e} - \omega_{a,i})h_w \quad (6)$$

Where $h_{a,e}$ and $h_{a,i}$ are the enthalpy of moist air at outlet and inlet of the air humidifier respectively and are calculated as follows:

$$h_{a,e} = c_{p,a,in} t_{a,e} + (2500 + 1.88 t_{a,e})\omega_{a,e} \quad (7a)$$

$$h_{a,i} = c_{p,a,in} t_{a,i} + (2500 + 1.88 t_{a,i})\omega_{a,i} \quad (7b)$$

$$T_{a,e} = t_{a,e} + 273 \quad (7c)$$

The equations (4 – 7) can be solved to determine the value of $T_{a,e}$, $\omega_{a,e}$ and m_w.

2.3 Compressor model

The compressor used in a gas turbine power plant is of the axial flow type. The thermodynamic losses in an axial flow compressor are incorporated in the model by introducing the concept of polytropic efficiency. The temperature and pressure of air at any section of compressor are related by the expression:

$$\frac{dT}{T} = \left[\frac{R}{\eta_{pt,c} c_{p,c}}\right]\frac{dp}{p} \quad (8)$$

where $\eta_{pt,c}$ is the compressor polytropic efficiency and $c_{p,c}$ and R_c are the specific heat at constant pressure and the gas constant across the compressor respectively. R_c is given by

$$R_c = c_{p,c} - c_{v,c} \quad (9)$$

where

$$c_{p,c} = c_{p,a} + \omega_{at} c_{p,vap} \quad (10)$$

$$c_{v,c} = c_{v,a} + \omega_{at} c_{v,vap} \quad (11)$$

where $c_{p,a}$ and $c_{v,a}$ are the specific heats of air at constant pressure and at constant volume respectively, both in kJ/kg K, and are evaluated at the average temperature across the compressor from the following relations (Moran and Shapiro, 1995):

$$c_{p,a} = \frac{8.314}{28.97}\left(3.653 - 1.337\times10^{-3} T_{av} + 3.294\times10^{-6} T_{av}^2 - 1.913\times 10^{-9} T_{av}^3 + 2.763\times10^{-13} T_{av}^4\right) \quad (12)$$

$$c_{v,a} = c_{p,a} - 0.287 \quad (13)$$

where $c_{p,vap}$ and $c_{v,vap}$ are the specific heats of water-vapor at constant pressure and at constant volume respectively, both in kJ/kg K, and are evaluated at the average temperature across the compressor from the following relations (Moran and Shapiro, 1995):

$$c_{p,vap} = \frac{8.314}{18.02}\left(4.07 - 1.108\times10^{-3}T_{av} + 4.152\times10^{-6}T_{av}^{2} - 2.964\times10^{-9}T_{av}^{3} + 8.07\times10^{-13}T_{av}^{4}\right) \quad (14)$$

$$c_{v,vap} = c_{p,vap} - 0.4614 \quad (15)$$

The enthalpy at any polytropic stage of compressor may be calculated using equations (1) , (3), and (8).

Using mass and energy balance across control volume of compressor, the compressor work is calculated as follows:

$$\dot{m}_{c,i} = \dot{m}_{c,e} + \sum \dot{m}_{coolant,j} \quad (16)$$

$$W_c = \dot{m}_{c,e}h_{c,e} + \sum \dot{m}_{coolant,j}h_{coolant,j} - \dot{m}_{c,i}h_{c,i} \quad (17)$$

2.4 Combustor model

Losses inside the combustor, which arise due to incomplete combustion and pressure losses are taken into account by introducing the concept of combustion efficiency and percentage pressure drop of compressor exit pressure (Table 1). The mass and energy balances across the control volume of combustor yield the mass of fuel required to attain a specified exit temperature of combustor, which is taken as TIT, given by:

$$\dot{m}_e = \dot{m}_i + \dot{m}_f \quad (18)$$

$$\dot{m}_f \cdot \Delta H_r \cdot \eta_{comb} = \dot{m}_e \cdot h_e - \dot{m}_i \cdot h_i \quad (19)$$

2.5 Cooled gas turbine

Unlike steam turbine blading, gas turbine bladings need cooling. The objective of the blade cooling is to keep the "blade temperature to a safe level, to ensure a long creep life, low oxidation rates, and low thermal stresses. The universal method of blade cooling is by air bled from the compressor flowing through the internal passages in the blades. In the case of film cooling, the coolant exits from the leading edge of blade and a film is formed over the blade surface, which reduces the heat transfer from the hot gas to the blade surface.

In this work, the gas turbine blades have been modeled to be cooled by the air-film cooling (AFC) method. The cooling model used for cooled turbine is the refined version of that by Louis *et al.* The mass flow rate of coolant required in a blade row is expressed as (Sanjay, 2011):

$$a_{coolant} = \frac{\dot{m}_{coolant}}{\dot{m}_g} = \left[\frac{St_{in}\cdot c_{p,g}}{\varepsilon\cdot c_{p,coolant}}\right]\times\left[\frac{S_g\cdot F_{sa}}{t\cdot\cos\alpha}\right]\times\left[\frac{T_{g,i}-T_b}{T_b-T_{coolant,i}}\right] \quad (20)$$

where $S_g \cong 2c$, $S_g/t\cos\alpha = 3.0$, $F_{s,a} = 1.05$, $\alpha = 45°$ (for stator), $\alpha = 48°$ (for rotor), $St_{in} = 0.005$

Also blade coolant requirement is dependent on the temperature of coolant air at the bleed points, which in turn, is dependent upon the temperature of air at the compressor inlet. With a drop in temperature of air at the inlet of compressor achieved in the humidifier, there is a proportionate drop in the temperature of bled coolant due to more effective blade cooling achieved by lower temperature bled coolant and hence lesser coolant requirement. Also, as the mass of bled coolant is less, hence the quantum of pumping and mixing loss associated with the mixing of coolant stream with main gas stream is also less.

Figure 2 gives the details of expansion process for a cooled turbine stage. Process b_1-c_1 in Figure 2 depicts cooling due to heat transfer between hot gas and coolant, which takes place at constant pressure line due to which exergy decreases, while process c_1-d_1 depicts drop in temperature due to mixing of coolant with gas which is an irreversible process and also takes place along constant pressure line, which leads to drop in entropy. Process d_1-a_2 in the model denotes a process similar to throttling.

Table 1: Input data for analysis [21-24, 27]

Parameter	Symbol	Unit
Gas properties:	C_p=¦(T) Enthalpy h=óc_p(T) dT	kJ/kg K KJ/kg
Air-humidifier	Pressure drop across humidifier = 1 Wetted pad, cross flow type	% -
Compressor	Polytropic efficiency ($h_{p,c}$) =92.0 Mechanical efficiency(h_m) =98.5 Inlet plenum loss= 0.5% of entry pr.	% % bar
Combustor	Combustor efficiency (h_{comb}) =99.5 Pressure loss (p_{loss})=2.0% of entry pressure Lower heating value = 42.0	% bar MJ/kg
Gas turbine	Polytropic efficiency (h_{pt}) =92.0 Exhaust pressure=1.08 Exhaust hood loss=4 Turbine blade temp = 1123	% bar K K
Alternator	Alternator efficiency=98.5	%

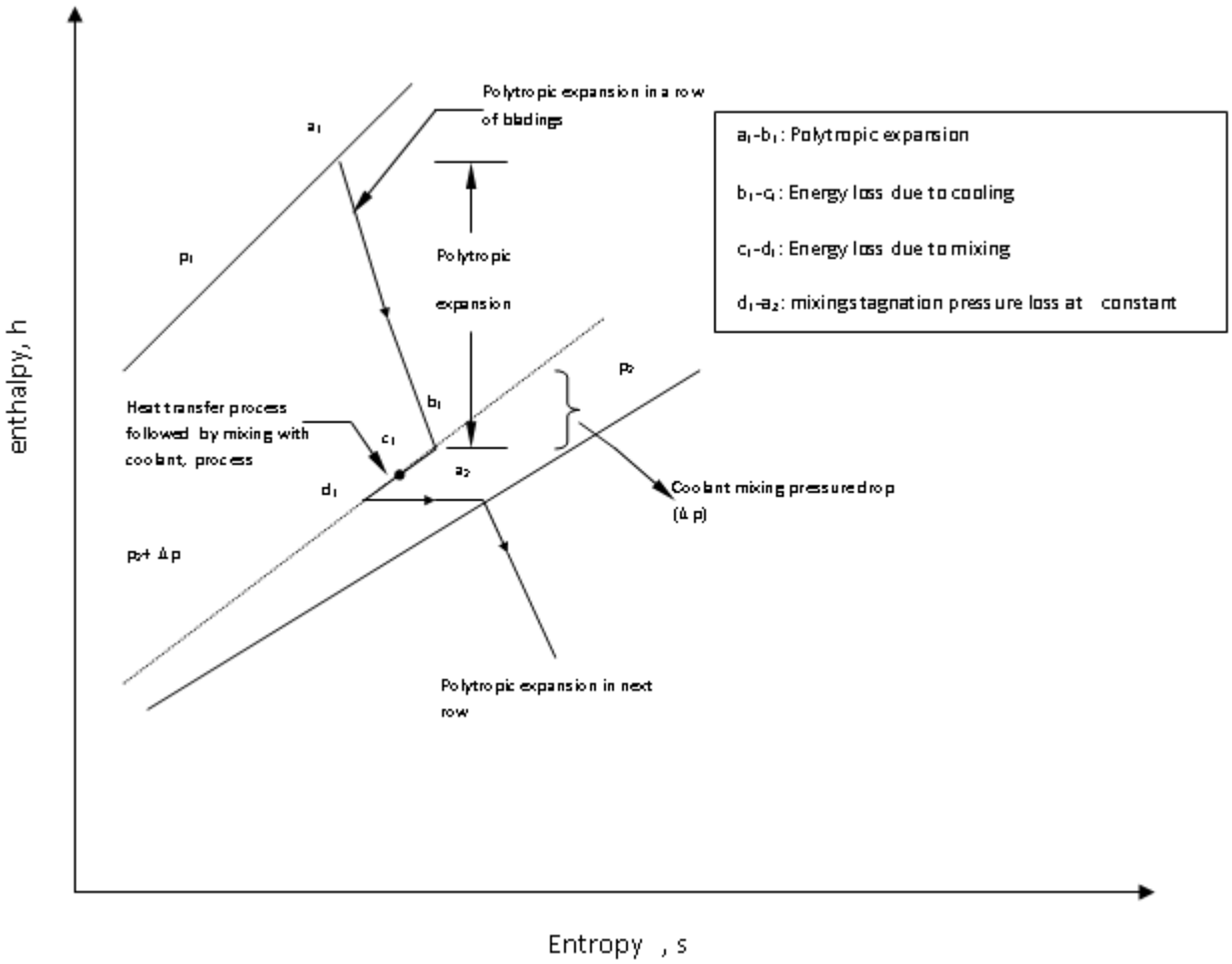

Figure 2: Expansion path in cooled gas turbine row

The deviation between actual and theoretical value is driven by the amount of coolant and coolant temperature used for cooling of blades and the actual value varies with blade cooling requirements. At TIT 1700K for air-film cooling, its maximum value is ±6% (Sanjay, 2011). Turbine work and exergy destruction are given by the mass, energy and exergy balance of gas turbine as under:

$$W_{gt} = \begin{matrix} \left[\dot{m}_{g,i} \cdot (h_{g,i} - h_{g,e})\right] + \\ \left[\sum \dot{m}_{coolant} \cdot (h_{coolant,i} - h_{coolant,e})\right] \end{matrix} \quad (21)$$

3. Performance parameters

The performance parameters $W_{gt,net}$, W_{plant}, and η_{plant} are expressed as follows:

$$W_{gt,net} = W_{gt} - \frac{|W_c|}{\eta_m} \quad (22)$$

$$W_{plant} = \left[W_{gt,net}\right] \cdot \eta_{alt} \quad (23)$$

$$\eta_{plant} = \frac{W_{plant}}{Q} = \frac{W_{plant}}{\dot{m}_f \cdot \Delta H_r} \quad (24)$$

Modeling of cycle components and governing equations developed for cycles proposed have been coded using C++ and results obtained. A flowchart of the programme code 'Simucomb' illustrating the method of solution is detailed in an earlier article (Sanjay 2011). The input data used in the analysis is given in Table 1.

4. Result and discussions

The influence of evaporative inlet air cooling on gas turbine performance has been shown through the performance curves, plotted using modeling, governing equations and input parameters (Table 1).

Fig. 3(a) shows the effect of inlet cooling on the variation of coolant mass required for blade cooling with respect to ambient temperature. It is evident from the results that the coolant mass required increases with increase in ambient temperature for both the cases. However, as the ambient temperature increases for a given RH, the effectiveness of the cooling is also increased due to a higher saturation pressure and, as a result, the increase in the mass of coolant required for turbine blade cooling is less for a given rise in temperature in case of inlet cooled gas turbine.

Figure 3(b) shows the effect of CIT on mass of blade coolant required and mass of fuel requirement for EVGT configuration. It is observed that as

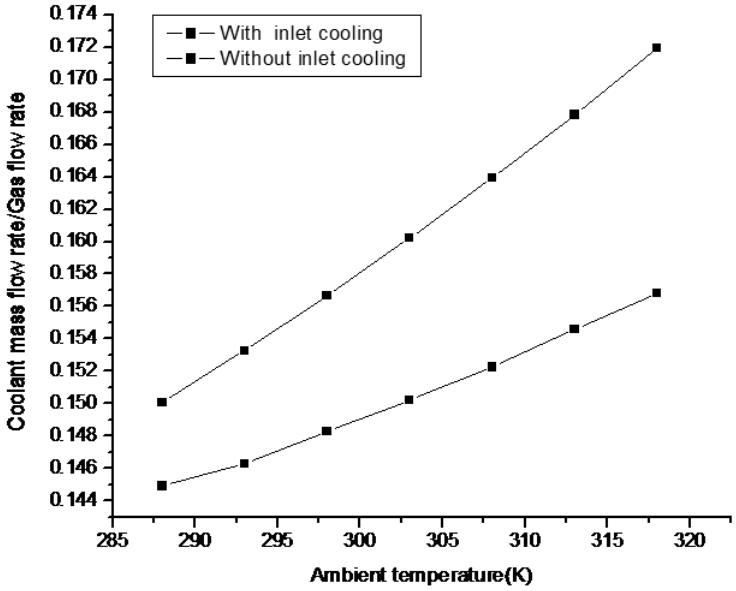

Figure 3(a): Effect of ambient temperature on coolant mass for basic and inlet cooled gas turbine

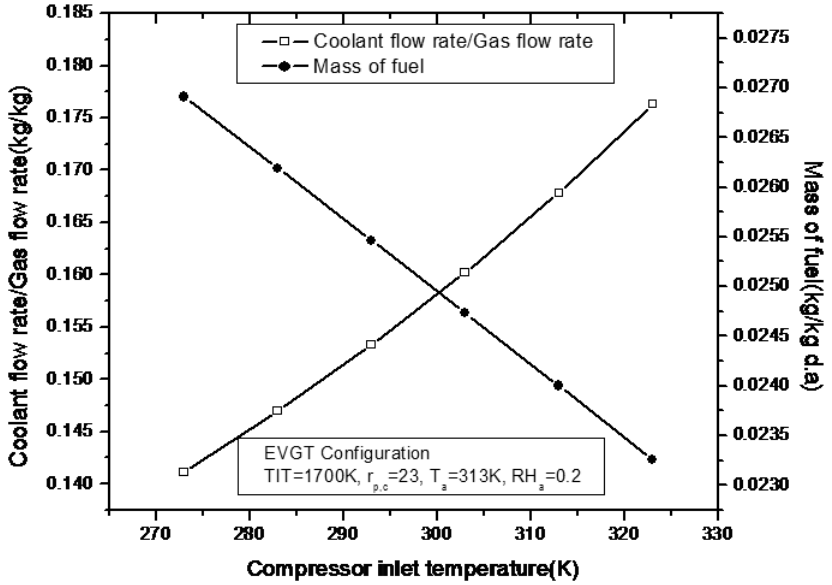

Figure 3(b): Effect of ambient temperature on coolant mass for basic and inlet cooled gas turbine

the CIT is reduced, and the blade coolant mass flow rate decreases. This is because, with a drop in temperature of air at the inlet of compressor, that is achieved in the refrigeration system, there is a proportionate drop in the temperature of bled coolant due to more effective blade cooling achieved by lower temperature bled coolant and, hence, lesser coolant requirement. However, due to the reduction in the CIT, the rise in temperature required to be achieved in the CC increases (for a given TIT). This requires a higher amount of heat to be supplied in the CC and so mass of fuel input increases.

Figure 4 shows the benefit of inlet cooled GT cycle over the basic GT cycle without inlet cooling in terms of enhancement in plant efficiency. It is observed that when the relative humidity is decreased for a given ambient temperature, the efficiency of inlet cooled GT cycle is increased due to higher drop in temperature achieved in the evaporator whereas the efficiency without inlet cooling almost remains unaltered. It can also be concluded from the results that for a given ambient relative humidity as the ambient temperature increases though the efficiency is reduced for both the cases the improvement in efficiency obtained due to inlet cooling is increased. This is due to the fact that at higher ambient temperature the difference between wet and dry bulb temperature is higher resulting in more effective cooling leading to larger temperature drop in the humidifier and lesser amount of coolant requirement as discussed for Figure 3(a).

Figure 5 shows the effect of TIT on plant efficiency at different ambient temperature. It is observed that the efficiency reduces with increase in

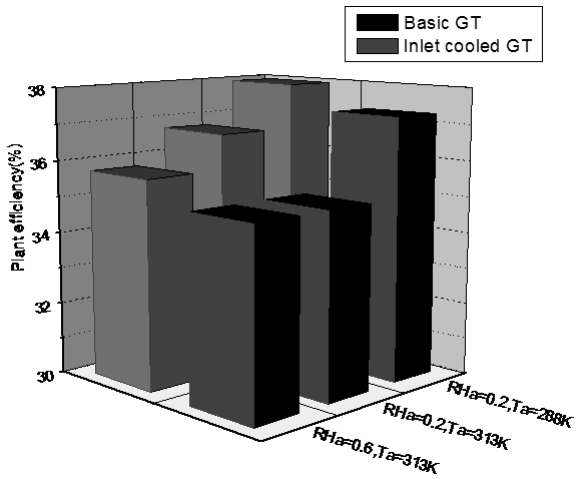

Figure 4: Effect of ambient condition on plant efficiency of gas turbine with and without inlet cooling

temperature. This is because at higher ambient temperature though the drop in temperature is higher owing to higher difference between WBT and DBT, the compressor inlet temperature is also high. A drop of 20° C at an ambient temperature of 318K results in a CIT of 298K against a CIT of 284K at an ambient temperature of 288K where the temperature drop is only 8°C. However, the reduction in efficiency at higher ambient temperature becomes less pronounced compared to basic gas turbine due to inlet cooling. It is also found from the results that the rate of increase in efficiency is higher at higher TIT. The inlet air cooling boosts the efficiency by 3. 51 % at a TIT of 1300K ($r_{p,c}$=25, RH_a=0. 2) when the ambient temperature drops by 30^0 C. This enhancement increases to 4. 22% for a TIT of 1800K at the same value of $r_{p,c}$, RH_a and ambient temperature drop. .

Figure 6 shows the variation of $r_{p,c}$ and increase in RH of air achieved in the humidifier on plant specific work. It is clearly seen that the specific work increases with increase in specific humidity of air achieved in the humidifier, the enhancement being higher at higher value of $r_{p,c}$. The specific work increases by 11. 62% at $r_{p,c}$=28 against an increase of 8. 4% at $r_{p,c}$=16 for same increase in RH of air achieved in the humidifier. The effect of variation of $r_{p,c}$ on turbine specific work suggests that specific work slightly increases with increase in pressure ratio for all range of specific humidity after which it decreases. It is also observed that the $r_{p,c}$ corresponding to maximum specific work increases with decrease in ambient relative humidity. This suggests that for a higher value of plant specific work there exists an optimum $r_{p,c}$ (for a given increase in RH achieved in the humidifier) and the $r_{p,c}$ needs to be chosen.

Figure 7 shows the variation of $r_{p,c}$ and T_a on specific fuel consumption and plant specific work of an AHIGT cycle. An increase in the specific work and decrease in specific fuel consumption is observed with decrease in T_a. This is because at higher temperature though the temperature drop in humidifier is higher, the compressor inlet temperature is also high. The specific fuel consumption decreases by 4. 29% at $r_{p,c}$=28 against a decrease of 3. 66% at $r_{p,c}$=16 for same range of ambient temperature drop. The effect of variation of $r_{p,c}$ on turbine specific work suggests that specific work increases with increase in pressure ratio for all range of ambient temperature after which it decreases. It is also observed that the $r_{p,c}$ corresponding to maximum specific work is higher at lower ambient temperature. This suggests that for a higher value of plant specific work there exist an optimum $r_{p,c}$ (cor-

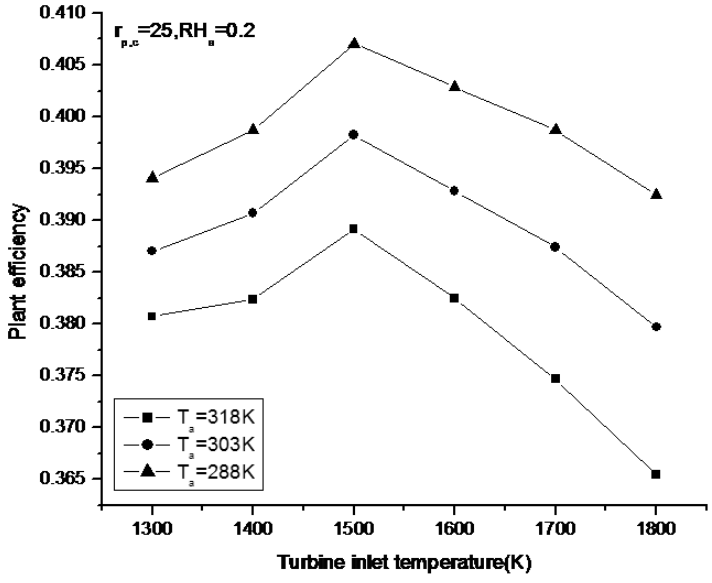

Figure 5: Effect of turbine inlet temperature on plant efficiency at different ambient temperature

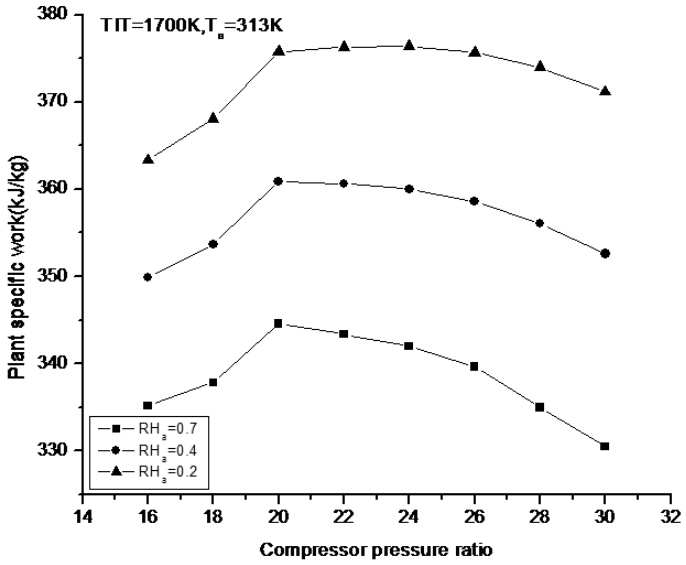

Figure 6: Effect of compression ratio on plant specific work at different ambient relative humidity

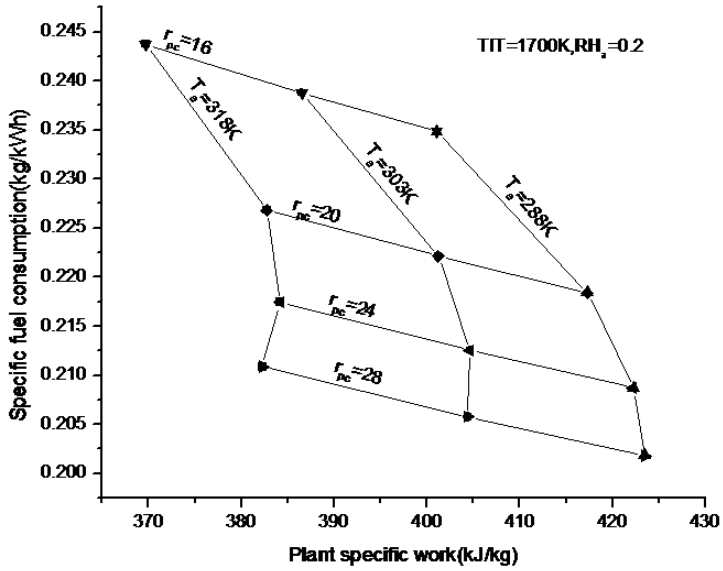

Figure 7: Specific fuel consumption versus plant specific work for different $r_{p,c}$ and T_a

responding to a given ambient temperature) and the same needs to be chosen as per discussions detailed in the previous section.

Figure 8 also called design nomogram, is helpful in selecting the design parameters such as $r_{p,c}$ TIT and cooling means for the best plant efficiency and specific work. The results show that for all pressure ratios, there exist an optimum TIT at which plant efficiency is the maximum. However, plant specific work continues to increase with increase in TIT and decreases with increase in $r_{p,c}$. The existence of optimum $r_{p,c}$ at any TIT with reference to the maximum plant efficiency is due to the combined effect of many factors. With increasing $r_{p,c}$ and TIT, the compressor work input, the fuel and coolant air requirements increase, however, the gas turbine work also increases but is restricted by the increasing pumping, cooling and mixing losses.

5. Conclusions

Based on the analysis of an air-humidifier-integrated-gas turbine cycle, the simultaneous integration of inlet air cooling and gas turbine blade cooling, the following conclusions can be deduced:

- The mass of coolant required for turbine blade cooling increases with increase in ambient temperature and ambient relative humidity for a gas turbine.
- The plant efficiency increases when inlet cooling using air-humidifier is integrated into a gas turbine plant.
- The enhancement in efficiency and specific work due to inlet-air cooling is higher at higher ambient temperature.
- The rate of increase in efficiency due to drop in ambient temperature is higher at higher value of TIT.

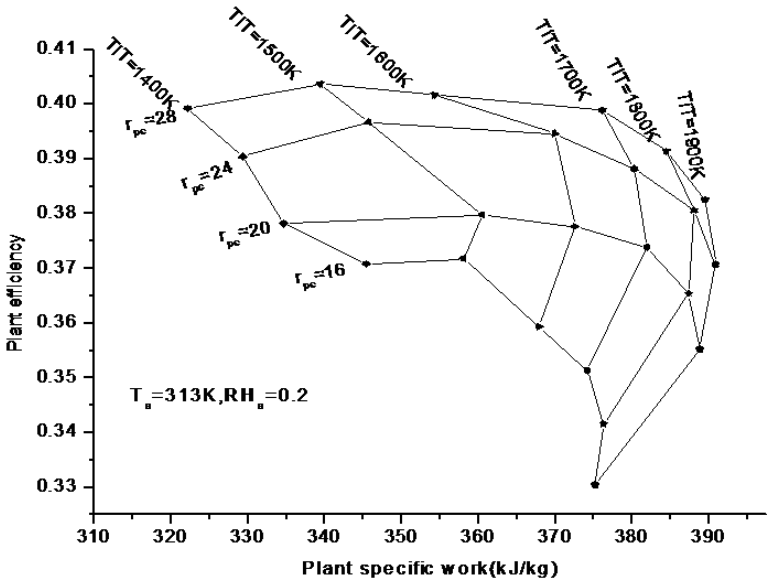

Figure 8: Plant efficiency versus plant specific work for different $r_{p,c}$ and TIT

- The plant specific work increases with increase in specific humidity of air achieved in the humidifier and this enhancement is higher at higher value of $r_{p,c.}$
- It is also observed that the $r_{p,c}$ corresponding to maximum specific work increases with decrease in ambient relative humidity.
- An increase in the specific work and decrease in specific fuel consumption is observed with decrease in ambient temperature due to integration with inlet air humidifier. It is also observed that the $r_{p,c}$ corresponding to maximum specific work is higher at lower ambient temperature.
- The design monogram shows that for all pressure ratios, there exists an optimum TIT at which plant efficiency is the maximum.

References

Alhazmy, M. M. , and Najjar, Y. S. H. (2004). Augmentation of gas turbine performance using air coolers. *App. Therm. Eng.* , 24, 415–429.

Basilly, A. M. (2001). Effects of evaporative inlet and after-cooling on the recuperated gas turbine cycle. *App. Therm. Eng.* , 21, 1875-1890.

Bassily, A. M, (2001). "Performance improvements of the intercooled reheat regenerative gas turbine cycles using indirect evaporative cooling of the inlet air and evaporative cooling of the compressor discharge, Proceedings of the Institution of Mechanical Engineers Part A, *Journal of Power And Energy,* Vol. 215, pp: 545-557.

Bolland, O. , and Stadaas, J. F. (1995). Comparative Evaluation of combined cycles and gas turbine systems with injections, steam injection and recuperation. ASME Journal of Engineering for Gas Turbines and Power, 117, 138-145.

Bolland, O. (1991). "A comparative evaluation of advanced combined cycle alternatives. " ASME Journal of Engineering for Gas Turbines and Power, 113, 190-197.

Briesh, M. S. , Bannister, R. L. , Diakunchak, I. S. , and Huber, D. J. (1995). A combined cycle designed to achieve greater than 60 percent efficiency. ASME Journal of Engineering for Gas Turbines and Power, 117, 734 -741.

Chiesa, Macchi. (2002). A thermodynamic analysis of different options to break 60 % electrical efficiency in combined cycle power plants. Proc. , ASME Turbo-Expo 2002, ASME, Amsterdam, GT-2002-30663.

Dechamps, P. J. (1998). Advanced combined cycle alternatives with latest gas turbines. ASME Journal of Engineering for Gas Turbines and Power, 120, 350-357.

Delucia, M. , Bronconi, R. , and Carnevale, E. (1994). Performance and economic enhancement of cogeneration gas turbines through compressor inlet air cooling. ASME Transactions Journal of Engineering for Gas Turbines and Power, 116, 360-365.

El-Masri, M. A. (1988). GASCAN - An interactive code for thermal analysis of gas turbine systems. ASME Transactions Journal of Engineering for Gas Turbines and Power, 110, 201-209.

El-Masri, M. A. (1986). On thermodynamic of gas turbines cycle – Part-2 – A model for expansion in cooled turbines. ASME Transactions Journal of Engineering for Gas Turbines and Power, 108, 151-159.

Gas Turbine World. (2010). Pequot Publishing Inc. Vol. 32(1).

Horlock, J. H. , Watson, D. T. , and Jones, V. (2001). Limitation on Gas turbine performance imposed by large turbine cooling flows. " ASME Journal of Engineering for Gas Turbines and Power, 123, 487-494.

Hosseini, R. , Beshkani, A. , and Soltani, M. (2007). Performance improvement of gas turbines of Fars (Iran) combined cycle power plant by intake air

cooling using a media evaporative cooler, Energy Conversion and Management, 48, 1055–1064.

Kakaras, E. , Doukelis, A. , and Karellas, S. , (2004). Compressor intake-air cooling in gas turbine plants", *Energy, 29*, 2347–2358.

Louis, J. F. , Hiraoka, K. , and El-Masri, M. A. (1983). A comparative study of influence of different means of turbine cooling on gas turbine performance. *Proc. , ASME Turbo-Expo 2002, ASME, Amsterdam, 83-GT-180*.

Data Series, IFI/PLENUNM, New York, Washington.

Moran, M. , and Shapiro, H. (1995). Fundamentals of Engineering Thermodynamics. *John Wiley*, New York.

Sanjay, B. E. , Singh, O. , and Prasad, B. N. (2007). Energy and Exergy Analysis of Steam Cooled Reheat Gas-Steam Combined Cycle. *App. Therm. Eng.* , 27, 2779–2790.

Sanjay, B. E. , Singh, O. , and Prasad, B. N. (2008). Influence of Different Means of Turbine Blade Cooling on the Thermodynamic Performance of Combined Cycle. " *App. Therm. Eng.* , 28, 2315-2326.

Sanjay, B. E. , Singh, O. , and Prasad, B. N. (2009). Comparative Performance Analysis of Cogeneration Gas Turbine Cycle for Different Blade Cooling Means. *Int. Journal of Thermal Sciences*, 48(7), 1432-1440.

Sanjay, B. E. (2011). "Investigation of effect of variation of cycle parameters on thermodynamic performance of gas/ steam combined cycle. " *Energy,* 36, 157-167.

Touloukian, Y. S. , and Tadash, M. (1970). Thermo-physical Properties of Matter. Vol. 6, The TPRC

Wang, F. J. , and Chiou, J. S. , (2004). Integration of steam injection and inlet air cooling for a gas turbine generation system, *Energy Conversion and Management*, 45, 15–26.

Wright, I. G. , and Gibbons, T. B. (2007). Recent developments in gas turbine materials and technology and their implications for syngas firing, *International Journal of Hydrogen Energy*, 32, 3610 – 3621.

Yousef S. H. Najjar (1996). Enhancement Of Performance Of Gas Turbine Engines By Inlet Air Cooling and Cogeneration System, *Applied Thermal Engineering*, Vol. 16, No. 2, pp. 163-173.

Zadpoor, A. A. , and Nikooyan, A. A. (2009). "Development of an Improved Desiccant-Based Evaporative Cooling System for Gas Turbines" , ASME *Journal of Engineering for Gas Turbines and Power,* 131, 034506.

Received 13 December 2011; revised 25 November 2013

Details of authors

Justin Beukes *B Com Rationum (Accounting and Economics) B Com (Hons) Com (Economics) M Com (Economics)*
E-mail: justinbeukes@gmail.com
Justin Beukes obtained his M Com in Economics, at the Nelson Mandela Metropolitan University in 2013. He is currently a junior economist in the private sector. His fields of interest include financial, resource and environmental economics.

Delson Chikobvu *PhD (Mathematical Statistics)*
Senior Lecturer: Mathematical Statistics and Actuarial Science, Department of Mathematical Statistics and Actuarial Science, University of the Free State P. O. Box 339 Bloemfontein 9300 South Africa
Tel: +27 51 401 2779
E-mail: Chikobvu@ufs.ac.za
Dr Delson Chikobvu is a Senior Lecturer: Mathematical Statistics and Actuarial Science, Department of Mathematical Statistics and Actuarial Science, University of the Free State.

Juliane Barbosa dos Santos *M Sc (Industrial Eng)*
Researcher: Sustainable Development, UNESP – Sao Paulo State University, School of Engineering at Bauru, Sao Paulo, ZIP CODE 17033360, Avenida Eng. L. Edmundo Carrijo Coube, 14-01, Bauru, Sao Paulo State, Brazil
Tel: +55 14 31036122
E-mail: julli_ane@hotmail.com
Juliane Barbosa dos Santos is a researcher with a Master's degree in Industrial Engineering. She is a researcher in the field of sustainability, energy management and environmental issues in Brazilian organizations.

Mario Du Preez *B Com (Economics) B Com Hon (Economics) M Com (Economics) PhD (Economics)*
Associate Professor: Economics, Department of Economics, School of Economics, Development Studies and Tourism, Nelson Mandela Metropolitan University
PO Box 77, Port Elizabeth, 6031, South Africa
Tel: +27 41 504 4815
E-mail: mario.dupreez@nmmu.ac.za
Mario Du Preez is an environmental economist with a PhD in environmental economics. Currently he is appointed as an associate professor in the Economics Department of the Nelson Mandela Metropolitan University. His research interests include non-market valuation, cost-benefit analysis and public choice theory.

Robert Huberts *PhD (Chem. Eng.)*
Senior Lecturer & Researcher, Department of Chemical Engineering Technology, Faculty of Engineering and the Built Environment, University of Johannesburg. PO Box 1701, Doornfontein, Johannesburg 2028
Tel: +27 11 559 6517
Fax: +27 11 559 6430
E-mail: roberth@uj.ac.za.
Robert Huberts holds a PhD in Chemical Engineering from the University of the Witwatersrand. He has worked at the Council for Mineral Technology (Mintek) for 12 years in the biotechnology research field. He worked in the IT industry and has been involved in small business. Since 2004, he has been a Senior Lecturer (and later postgraduate supervisor) in the Department of Chemical Engineering at the University of Johannesburg. His current research interests are in the areas of waste energy and biotechnology.

Freddie L. Inambao *MSc (Eng.), PhD (Technical Sciences) Senior Lecturer, Mechanical Engineering, University of KwaZulu-Natal, Durban, South Africa Tel: +27 (0) 31 260 8530 Fax: +27 (0) 260 3217 E-Mail: inambaof@ukzn.ac.za*
Dr Inambao is a Senior Lecturer at the University of KwaZulu-Natal. He has published papers in reputable Journals and presented papers at both National and International levels in the fields of Alternative and Renewable Energy, Energy Management and Internal Combustion Engines and related fields. Dr Inambao holds an MSc in Mechanical Engineering and PhD in Technical Sciences from Volgograd Polytechnic Institute.

Charbel José Chiappetta Jabbour *Ph D (Industrial Eng)*
Researcher: Sustainable Development, UNESP – Sao Paulo State University, School of Engineering at Bauru, Sao Paulo, ZIP CODE 17033360, Avenida Eng. L. Edmundo Carrijo Coube, 14-01, Bauru, Sao Paulo State, Brazil
Tel: +55 14 31036122
E-mail: prof.charbel@gmail.com or charbel@feb.unesp.br
Charbel José Chiappetta Jabbour is an Associate Professor of Sustainability and Industrial Engineering at UNESP – Sao Paulo State University. He is publishing in journals such as the Journal of Cleaner Production, International Journal of Sustainability in Higher Education, International Journal of Production Economics, and others. He is Editor in Chief of the Latin American Journal of Management for Sustainable Development and Deputy-Editor of the Brazilian Journal of Science and Technology.

Mahesh Kumar *B Tech. M.E. PhD*
Assistant Professor, Department of Mechanical Engineering, Guru Jambheshwar, University of Science & Technology, Hisar, India, 125001
Tel: 0941 693 5137 / 01662 263564
E-mail: mkshandilya1@gmail.com
Mahesh Kumar is an Assistant Professor, Department of Mechanical Engineering, Jambheshwar, University of Science & Technology, Hisar, India. He has previously published in this journal.

Golden Makaka *M Sc PhD (Applied Physics)*
Senior Lecturer (Renewable Energy), Physics Department, University of Fort Hare, Private Bag, X1314, Alice, 5700 South Africa
Tel: +27 (0)40 602 2207
Cell: +27 (0)71 8973 486
Dr Golden Makaka is a physicist with masters' degree in Applied Physics and a PhD in physics. He is currently a senior lecturer and a post graduate coordinator in the Physics Department at Fort Hare University. He specialized in renewable energy, energy efficiency and building physics. He is also a consultant in passive solar energy efficiency building design strategies in South Africa.

Sampson Mamphweli *PhD Physics, MenvSc, Mini-MBA*
Senior Researcher: (Renewable Energy), Institute of Technology, University of Fort Hare,
Tel: +27 4060 22311
Fax: +27 4065 30665
Mobile: +27 82 2140 367
Dr Sampson Mamphweli is a Senior Researcher at the Institute of Technology, University of Fort Hare, South Africa. He possesses a Doctor of Philosophy degree in Physics from the University of Fort Hare, and a Master of Environmental Sciences degree from the University of Venda, South Africa. He is also in possession of a Certificate in Financing Renewable Energy and Energy Efficiency from RENAC Renewables based in Germany. Dr Mamphweli also possesses the Green Power Mini-MBA from the Green Power Academy based in Britain. He is a recipient of the prestigious University of Fort Hare Vice Chancellor's Emerging Researcher medal for the year 2012. He conducts research on renewable energy technologies and their applications, and he is a respected authority in the biomass to energy field. He has published 18 scientific papers in peer-reviewed journals and conference proceedings including two book chapters. Dr Mamphweli reviews papers for publication in several journals in the engineering and renewable energy fields of study. His current area of research interest includes biomass gasification for electricity generation, biogas digesters, co-gasification of coal and biomass for electricity generation as well as solar energy technologies.

Sherpherd Misi
Department of Civil Engineering University of Zimbabwe, P. O. Box MP167, Mount Pleasant, Harare, Zimbabwe
Tel: +263 7721 00941
Fax: +263 430 3280
E-mail: senmisi@yahoo.co.uk
He holds a PhD in Renewable Energy (Biomass), an M Sc in Renewable Energy Engineering, and a B Sc (Hons) in Civil Engineering. He is a Lecturer in the Faculty of Engineering, University of Zimbabwe.

Alok Ku Mohapatra *B E (Mech) M.Tech (CIM) PhD (Thermal Eng.)*
Professor: Department of Mechanical Engineering
Principal: Nalanda Institute of Technology, Bhubaneswar. Odisha, India-754005
E-mail: m.alokkumar@gmail.com
Dr. Alok ku Mohapatra has an M.Tech in Computer Integrated Manufacturing from the Indian Institute of Technology, Madras, and a PhD in Thermal Engineering from the National Institute of Technology, Jamshedpur. He has more than 13 years of teaching and research experience in various reputed engineering colleges across India.
Currently, he is appointed as the Principal at the Nalanda Institute of Technology, Bhubaneswar, India, in addition to the position of Professor and Head of the Mechanical Engineering Department. His research interest includes energy and exergy analysis of gas turbines and combined cycle plant including cogeneration, trigeneration and polygenation systems.

Patrick Mukumba
Physics Department, University of Fort Hare, Private Bag, X1314, Alice, 5700
Cell: +27 71 5056 937
Fax: +27 40 653 0665
E-mail: patrickmukumba@gmail.com
Patrick Mukumba is a PhD candidate (Renewable Energy) in the Physics Department at the University of Fort Hare (UFH). He holds an M Sc in Renewable Energy Engineering (University of Zimbabwe), a BSc Ed (Hons) in Physics with Bindura University of Science Education (Zimbabwe) and a Diploma in Education (Science) with Belvedere Technical Teachers' College (Zimbabwe), His research work is on biomass and biogas.

Edison Muzenda *PhD (Chem. Eng.)*
Associate Professor: Environmental and Process Systems Engineering Research Group, Department of Chemical Engineering Technology, Faculty of Engineering and the Built Environment, University of Johannesburg., PO Box 1701, Doornfontein, Johannesburg 2028
Tel: +27 11 559 6817
Fax: +2711559 6430
E-mail: emuzenda@uj.ac.za.
Edison Muzenda is an Associate Professor, Research and Postgraduate Coordinator as well as Head of the Environmental and Process Systems Engineering Research Group in the Department of Chemical Engineering at the University of Johannesburg. He holds a B Sc Hons (Zimbabwe, 1994) and a PhD in Chemical Engineering (Birmingham, 2000). He has more than 15 years' experience in academia. Prof Edison's teaching interests and experience are in unit operations, multi-stage separation processes, environmental engineering, chemical engineering thermodynamics, entrepreneurship skills, professional engineering skills, research methodology as well as process economics, management and optimization. He is a recipient of several awards and scholarships for academic excellence. His research interests are in waste water treatment, gas scrubbing, environment, waste minimization and utilization, energy as well as phase equilibrium measurement and computation. He has published more than 85 international peer reviewed and refereed scientific papers in journals, conferences and books.

Prof Edison has supervised over 18 postgraduate students as well as more than 130 Honours and B Tech research students. He serves as reviewer for a number of reputable international conferences and journals. He has also chaired several sessions at International Conferences. Edison is an associate member of the Institution of Chemical Engineers (AMIChemE), a member of the International Association of Engineers (IAENG); associate member of Water Institute of Southern Africa (WISA) and member of the International Scientific Committee of the World Academy of Science, Engineering and Technology (WASET) as well a member of the Scientific Technical Committee and Editorial Board of the Planetary Scientific Research Centre. Prof Edison is recognized in Marquis Who's Who 2012 as an Engineering Educator.

Tsietsi J Pilusa *Masters (Chem. Eng.)*
Department of Mechanical Engineering Science, University of Johannesburg, PO Box 17011, Doornfontein, Johannesburg 2028
Tel: +2710 210 4800
Fax: +2710 210, 4800
E-mail: pilusat@webmail.co.za
Tsietsi Pilusa holds a Master's degree in Chemical Engineering from the University of Johannesburg. He has more than 7 years' experience in mining, metallurgy and waste management industries. He is an associate member of the South African Institute of Mining and Metallurgy (SAIMM) and is a registered member of South African Institute of Chemical Engineers (SAIChe). He is also registered with the Engineering Council of South Africa (ECSA) as candidate Technologist. His main areas of research are in alternative fuels, waste to energy, environmental pollution and waste management. His research involves classifications of industrial wastes, energy recovery, beneficiations processes and energy utilization mechanisms.

B E Sanjay *B E (Mech) M.Tech (Design) PhD (Mechanical Eng.)*
Professor: Department of Mechanical Engineering, National Institute of Technology, Jamshedpur, India - 831014
E-mail: ritsanjay@yahoo.com
Prof. Sanjay is a graduate of Mechanical Engineering with a Masters and PhD in Mechanical Engineering. He has over 20 years of professional experience with over 13 years devoted to imparting Engineering education at the highest level. He has over a score of publications in the world's leading journals in the area of Mechanical Engineering and Engineering Education. His j-index and h-10 index are currently four and with around a hundred citations. He is also the co-author of numerous books on thermal and mechanical engineering. He is presently working as Professor of Mechanical Engineering at the National Institute of Technology, Jamshedpur, India. He also has over five years of industrial experience in inspection of rotating and reciprocating machines as well as pressure vessels. He is Level-II in Ultra-sonic and radiographic testing as well as a certified welding inspector. His research interest includes energy and exergy analysis of gas turbines and combined cycle plant including cogeneration, green energy systems.

Caston Sigauke *M Sc (Operations Research)*
Lecturer: Operations Research and Statistics, School of Mathematical and Computer Sciences and Department of Statistics and Operations Research, University of Limpopo, Turfloop, Campus, Private Bag X 1106, Sovenga 0727 South Africa
Tel: +27 (0) 15 268 2188
Fax: +27 (0) 15 268 3487
Cell: +27 835 255 684
E-mails: caston.sigauke@ul.ac.za and csigauke@gmail.com
Caston Sigauke is a Lecturer in Operations Research and Statistics, School of Mathematical and Computer Sciences and the Department of Statistics and Operations Research, University of Limpopo, Turfloop, Campus. He is undertaking a PhD in Statistics with the University of the Free State.

Nishant Singh *B Eng (Mech) M Tech (Mech Eng)*
Assistant Professor: Mechanical Engineering, Hindustan College of Science and Technology, NH-2, Agra-Delhi Highway, Farah, Mathura, Uttar Pradesh, India
Tel: +9199 9758 2969
E-mail: nishant.singh78@gmail.com
Nishant Singh is a mechanical engineer with a Master's degree in Mechanical Engineering, and is pursuing a PhD in Optimization Techniques. Since 2005 he has been involved in teaching and research. He taught various subjects like kinematics of machines and dynamics of machines.
Currently he is assistant professor in the Mechanical Engineering Department of Hindustan College of Science and Technology, Mathura. He is also serving as visiting faculty to the Excel Institute of Management & Technology, Mathura, India.

Yashvir Singh *B Eng (Mech) M Tech (Mech Eng)*
Assistant Professor: Mechanical Engineering, University of Petroleum and Energy Studies Energy Acres, P.O. Bidholi, Via Premnagar, Dehradun, India
Tel: +9197 6099 5818
Fax: +911 3527 7609 0/95
E-mail: yashvirsingh21@gmail.com
Yashvir Singh is a mechanical engineer with Master's degree in Mechanical Engineering, and is pursuing a PhD in alternative fuels. Since 2007 he has been involved in teaching and research. He taught various subjects related to alternate fuels used in internal combustion engines.
Currently he is appointed as assistant professor in the Mechanical Engineering Department of the University of Petroleum and Energy Studies, Dehradun. He is also serving as a visiting faculty to the Apex Institute of Technology, Bilaspur, India.

Shadreck M Situmbeko *B Eng. (Mech), M Sc (Eng. Design)*
University of Kwazulu-Natal, Mechanical Engineering, Durban, South Africa
Tel 27 (0) 31 260 8530
Fax 27 (0) 31 2603217
Cell 27 710570753; 267 72952615
E-Mail: ssitumbeko@yahoo.com; 209542168@stu.ukzn.ac.za
Shadreck Situmbeko is a Mechanical Engineer with a master's degree in engineering design and currently pursuing a PhD in Mechanical Engineering. He has lectured at University of Botswana in the department of Industrial Design and Technology for 9 years from 2004. Previously he worked as Chief Engineer Energy and Chief Engineer Projects with RIPCO(B), Botswana (1996-2003). He has undertaken a number of renewable energy projects and consultancies and has authored a number of peer reviewed conference papers and journal papers.

Ernest E van Dyk *BSc (Physics and Applied Mathematics) BScHons (Physics) MSc (Physics) PhD (Physics) Pr.Nat.Sci.*
Professor of Physics, Nelson Mandela Metropolitan University (NMMU)
Director: Centre for Energy Research, NMMU
Head of Department: Physics, NMMU
Centre for Energy Research, PO Box 77000, Nelson Mandela Metropolitan University, Port Elizabeth, 6031
Tel: +27 41 504 2259
Fax: +27 41 504 1959
E-mail: ernest.vandyk@nmmu.ac.za
Web: http://energy.nmmu.ac.za
Ernest van Dyk obtained his PhD in Physics at the University of Port Elizabeth in 1994. He teaches Physics at the NMMU and is also Director of the Centre for Energy Research (CER) at the NMMU since 2006. The CER is involved with several renewable energy research projects for industry and government agencies. He is currently also the Physics Head of Department.
Prof van Dyk's research interests are in the field of Solar Energy, specialising in Photovoltaics and Solar Thermal research. He has supervised 16 MSc and 7 PhD student projects to completion and is currently supervising 1 MSc students and 6 PhD students. He has published forty-seven scientific journal articles in the field of Photovoltaics and has authored or co-authored 37 international conference papers and 117 national conference presentations. Prof van Dyk has a passion for teaching Physics and researching Renewable Energy Technologies.

Index to Volume 24: February–November 2013

Authors / Title index

Subject index